SOLAR MAXIMUM MISSION

X-RAY POLYCHROMATOR

USER'S GUIDE

Lockheed Palo Alto Research Labs.
Lockheed Missile & Space Corp.

Mullard Space Science Laboratory
University College London

Space & Astrophysics Division
Appleton Laboratory

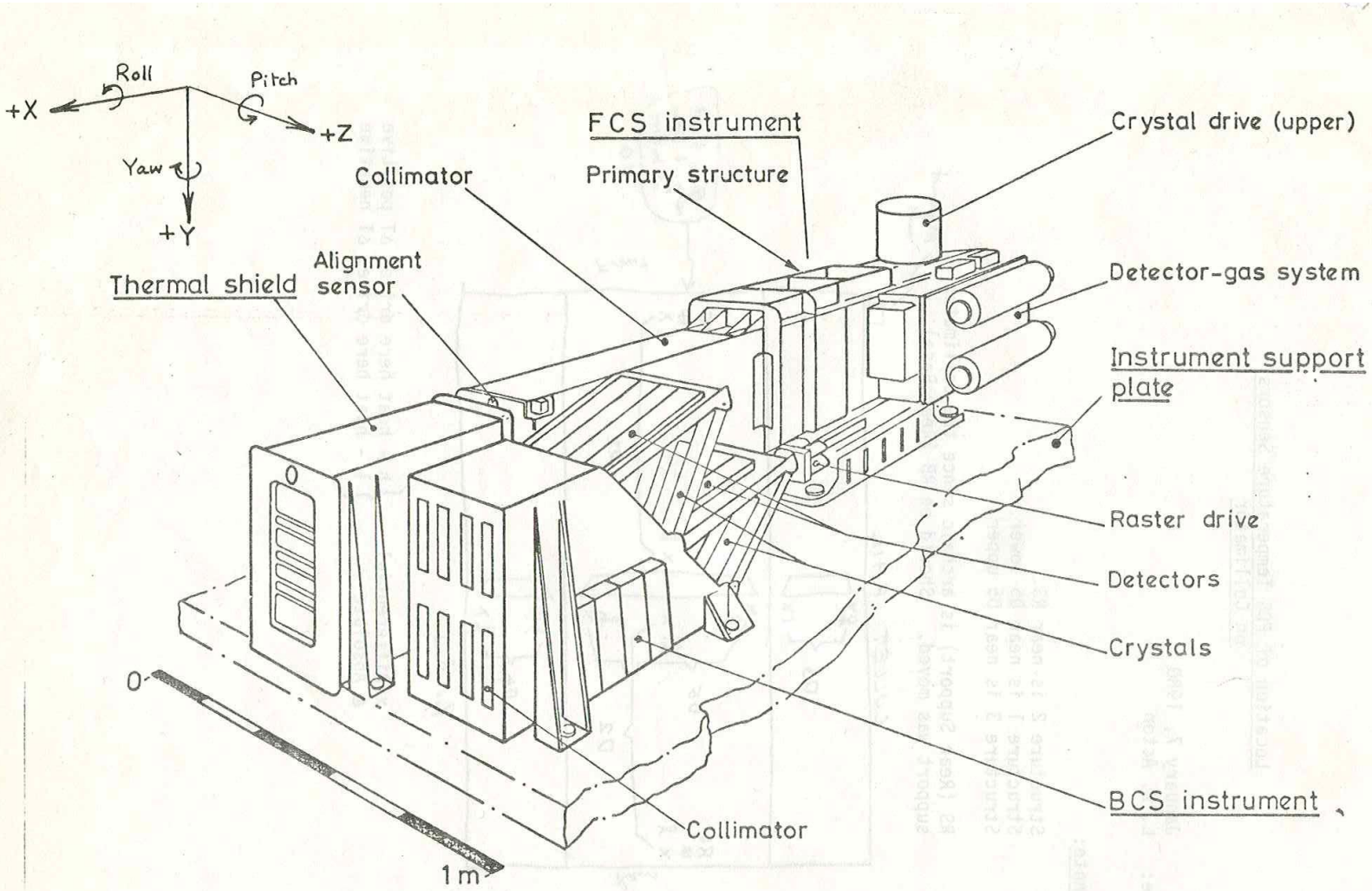

X-ray polychromator

Location of FCS Temperature Sensors on Collimator

Date: January 7, 1980
Source: L. W. Acton

Also note:

Structure 2 is near RS.
Structure 1 is near D5 lower.
Structure 3 is near D5 upper.

RS (Rear Support) is archaic since the collimator support was moved. Should be RB (Rear Base).

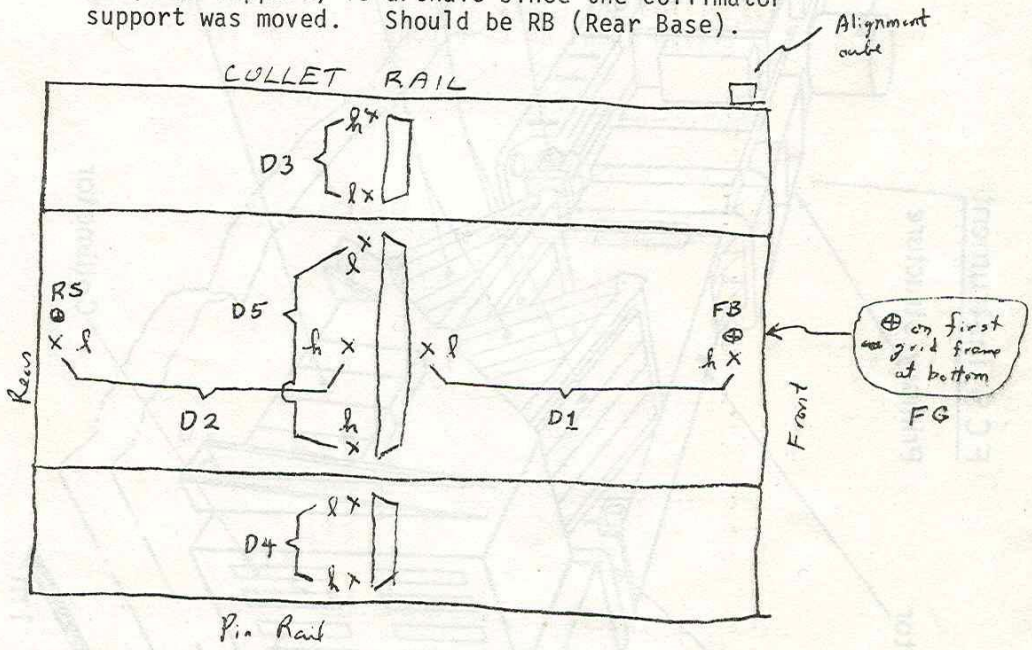

x Differential
⊕ Absolute

h - heat here drives ΔT positive
l - heat here drives ΔT negative

HOME-POSITION WAVELENGTHS AND WAVELENGTH RANGES OF FCS CRYSTALS

Date: December 28, 1979

Sources: 'Wavelength Data Requested for XRP' (Note, B.C. Fawcett, 13-i-79)
'FCS Crystal Calibration Date' (B.J. Keut, 1-ii-79)
Computer listings giving FCS λ's for crystal shaft rotation. (B.J. Kent)

Wavelengths (λ) are in Å. 'Extended range' is from one crystal drive 'stop' to another. (At each end there is a reduction in sensitivity, and at the long-wavelength end there is an extra background count rate due to the calibration sources.)

CRYSTAL	2d(Å) (15°C)	HOME POSITION λ*	HOME POSITION θ_o	NORMAL RANGE λ's for $\theta_o-16°$	NORMAL RANGE λ's for $\theta_o+12°$	EXTENDED RANGE λ's for $\theta_o-17°.1$	EXTENDED RANGE λ's for $\theta_o+21°.2$
KAP (001)	26.6224	18.9689	45°.5275 (4400)	13.100	22.426	12.660	24.409
Beryl (10$\bar{1}$0)	15.9625	13.447	57.4671	10.562	14.936	10.334	15.635
ADP (101)	10.6405	9.169	59.5365	7.327	10.090	7.180	10.497
Qu (10$\bar{1}$0)	8.5091	6.649	51.4038	4.929	7.607	4.796	8.116
Qu (10$\bar{1}$1)	6.6859	5.039	48.9198	3.633	5.842	3.526	6.284
Ge (220)	4.0003	3.173	52.4921	2.379	3.610	2.318	3.838
Ge (422)	2.3095	1.85035	53.2450	1.398	2.097	1.363	2.224

* Wavelengths from Fawcett Note

θ_o = corrected Bragg angle for Home Position
= $\sin^{-1}(\lambda/2d)$ + refractive index correction

FCS WAVELENGTH RANGES IN TERMS OF CRYSTAL DRIVE ADDRESSES

Date: February 11, 1980

Sources: a) Note by John Firth (Feb. 1980)
b) Computer print-out of FCS λ's and crystal address (B.J. Kent)

Of the two Baldwin encoder units A and B, one will be prime (A). Baldwin addresses are in octal. Step number is decimal number of steps from the minimum position of the 'normal' range (Θ_0 - 16° where Θ_0 = Home Position angle).

	Step No.	System A	System B
Launch Position*	5824	14242	14327
Minimum Position	-401	∿00121	∿00175
Maximum Position	13771	∿33535	∿33621
Cal. sources exposed at	10800	∿26000	∿26000
Normal scan range†	0 10195	742 24665	1020 24743

NOTES

* Variations expected with spacecraft orientation and zero g field.

† Corresponding to (Θ_0 - 16°, Θ_0 + 12°).

- Launch position has been set at or near Home Position.
- Low addresses correspond to short wavelengths.
- Increasing addresses are for a clockwise rotation, viewed along +Y axis, of crystal shaft.

FCS CRYSTAL DRIVE

Date: December 31, 1979

Sources: XRP Phase II Report 'FCS Motions and Timings' (C.J. Wolfson, December 1978).

Total angular range: 38^{o} ($\theta_o - 17^{o}$ to $\theta_o + 21^{o}$) (θ_o = home position angle).

Normal angular range: 28^{o} ($\theta_o - 16^{o}$ to $\theta_o + 12^{o}$)

Shaft step = 9.889 arcsec = 0.002747 degrees.

Types of scan

Under normal microprocessor control, spectroscopic and integral scan modes are possible.

Spectroscopic scans. A new address is given to the crystal drive system, and the shaft races to this position with these characteristics:

Maximum acceleration: 5.15 rad/sec^2 = 1.062 x 10^9 arcsec/sec^2
Maximum slew rate = 0.07 rad/sec = 14000 arcsec/sec
Time taken to attain full speed ≃ 14 msec (i.e. much smaller than FCS data-gather interval, 1DGI = 256 msec)
∿ 98 arcsec of rotation traversed when full speed attained .
For minimum (10 arcsec) move, time ≃ 6 msec.
At maximum slew rate, the crystal shaft could traverse its full normal operating range (28^{o}) in 7.0 sec.

Integral scans. The microprocessor program defines one of five rotation speeds and a duration of motion. Thus, a series of evenly spaced 10-arcsec steps is performed; the rates are:-

Rate 1	= 2 steps/DGI	= 7.8125	steps/sec
2	= 4 "	= 15.625	" "
3	= 8 "	= 31.25	" "
4	= 16 "	= 62.5	" "
5	= 32 "	= 125	" "

(Note 1 step = 9.889 arcsec.)

FCS DETECTORS - WINDOWS AND GAS FILLINGS

Date: February 11, 1980

Source: XRP "Solar Physics" paper
L. W. Acton notes on FCS Sensitivity (March 14, 1979)

Detector	Home Position Ion (λ)	Gas*	Gas Depth (cm)	Window† Material	Window thickness (10^{-4} cm)
1	OVIII(18.97Å)	Pr	2.5	P	2
2	NeIX(13.45)	Pr	2.5	P	2
3	MgXI(9.17)	Pr	2.5	P	6
4	SiXIII(6.65)	Pr	2.5	P	10
5	SXV(5.04)	X	2.0	Be	75
6	CaXIX(3.17)	X	2.0	Be	125
7	FeXXV(1.85)	X	2.0	Be	125

* Gas: Pr = Propane; X = 0.97 Xenon/0.03 carbon dioxide.
All at pressure = 900 Torr.

† Window material: P = carbon-coated polypropylene on nickel mesh;
Be = Beryllium.

ESTIMATED COSMIC RAY BACKGROUND RATES FOR FCS DETECTORS

Date: February 11, 1980

Source: "Solar Physics" paper (revised July 21, 1979 version)

Channel*	Background Rate	
	cts./sec.	cts./DGI
OVIII	0.9	0.23
NeIX	0.6	0.15
MgXI	0.6	0.15
SiXIII	0.9	0.23
SXV	0.6	0.15
CaXIX	1.0	0.26
FeXXV	1.7	0.44

* identified by home position ion

ESTIMATED COSMIC RAY BACKGROUND RATES FOR BCS DETECTORS

Date: March 30, 1979

Source: C. G. Rapley Note

Detector		Background Rate (cts./sec.)
1	CaXIX	0.6
2	FeKα Hi	1.1
3	FeKα lo	1.1
4	FeXXV Lo	1.3
5	FeXXV Hi I	1.0
6	FeXXV Hi II	1.1
7	FeXXV Hi III	1.0
8	FeXXVI	1.3

FCS COLLIMATOR CALIBRATION

Date: February 11, 1980

Source: G. Joki information to L.W. Acton, April 23, 1979

X-ray calibrations of the FCS collimator were carried out using Cu Kα collimated X-rays incident on the crystals with and without the collimator. Each crystal has associated with it a 'module' in the collimator, large-area crystals having large modules (LM1-LM4), small-area crystals small modules (SM1-SM3). The following values of peak transmission and collimator FWHM are averaged from values taken in various positions across each entrance aperture. The collimator FWHM was found to be the same, to within measurement errors, in orthogonal directions.

For a pyramidal field-of-view profile, the average transmission is 1/3 the peak value.

MODULE	CRYSTAL	λ (Å)	PEAK TRANS.	COLLIMATOR EQUIV. WIDTH (arcsec)		½ PIXELACH FWHM	
LM1	KAP	21.6	.18	16.1			
		19.0	.18	15.7	→	0,523	①
		15.0	.18	15.1			
LM3	Beryl	13.5	.17	15.2	→	0,507	②
LM2	ADP	9.2	.19	13.9	→	0,463	③
LM4	$Q10\bar{1}0$	6.6	.17	14.1	→	0,470	④
SM1	$Q10\bar{1}1$	5.0	.16	12.7	→	0,423	⑤
SM2	Ge220	3.2	.15	12.0	→	0,400	⑥
SM3	Ge422	1.85	.14	15.1	→	0,503	⑦
		1.78	.14	13.7			

X-RAY TRANSMISSION OF FCS THERMAL FILTER ASSEMBLY

Date: February 22, 1980

Sources: (1) L. W. Acton notes on FCS Sensitivity (March 14, 1979), based on G. Joki note, Feb. 27, 1979).
(2) "Measured X-ray transmission of FCS thermal filters," note by M. Kayat (July 20, 1979).

The curves should theoretical transmissions of the thermal filter assembly for the scaled detectors (those using the crystals Q $10\bar{1}1$, Ge 220, Ge 422) and the thin-window detectors (crystals KAP, Beryl, ADP, $Q10\bar{1}0$). The broken curve is the transmission for 100 Å layers of oxide on each surface of the filters.

Measured points by M. Kayat indicate that the theoretical curve for the thin-window detectors should be raised by a factor of about 1.15. These values are used in the FCS Sensitivity a few pages hence. The theoretical curve for the sealed detectors is used without correction.

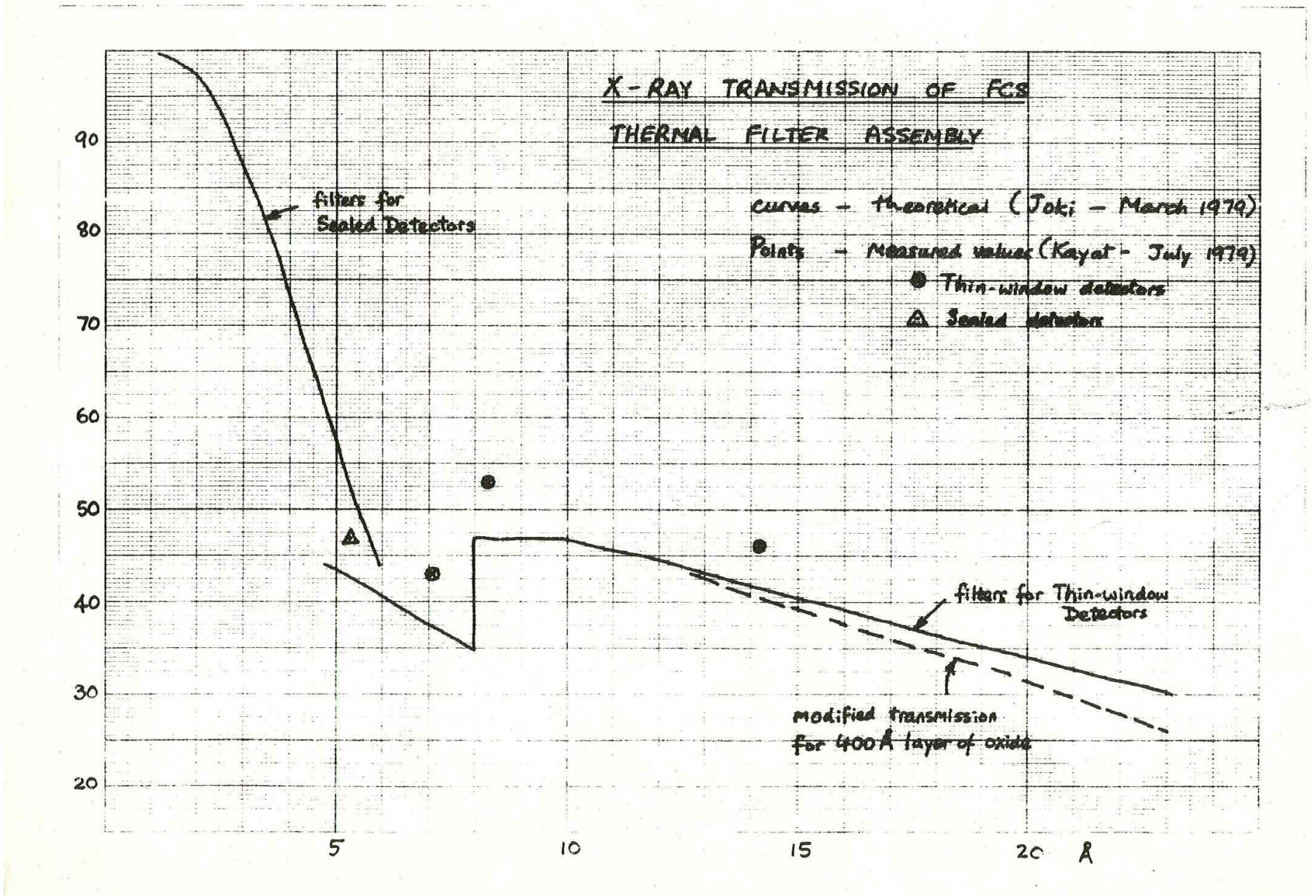
X-RAY TRANSMISSION OF FCS
THERMAL FILTER ASSEMBLY
curves - theoretical (Toki - March 1979)
Points - Measured values (Kayat - July 1979)
Thin-window detectors
Sealed detectors
filters for Sealed Detectors
filters for Thin-window Detectors
modified transmission for 1400 Å layer of oxide
90
80
70
60
50
40
30
20
5
10
15
20
Å

FCS RASTER STEP SIZE

Date: February 11, 1980

Source: Information from R. Turner (January 1980)

The table indicates values of raster step sizes (arcsec) for the cams specified and over the ranges that are shown in the diagram (a plot of angular displacement vs. no. of camsteps).

Cam	7' range	3½' A range	3½' B range	Extreme range
YA	4.68	4.57	4.79	4.88
YB	4.79	4.57	5.0	4.96
ZA	4.93	5.0	4.86	4.95
ZB	4.93	5.0	4.86	4.92

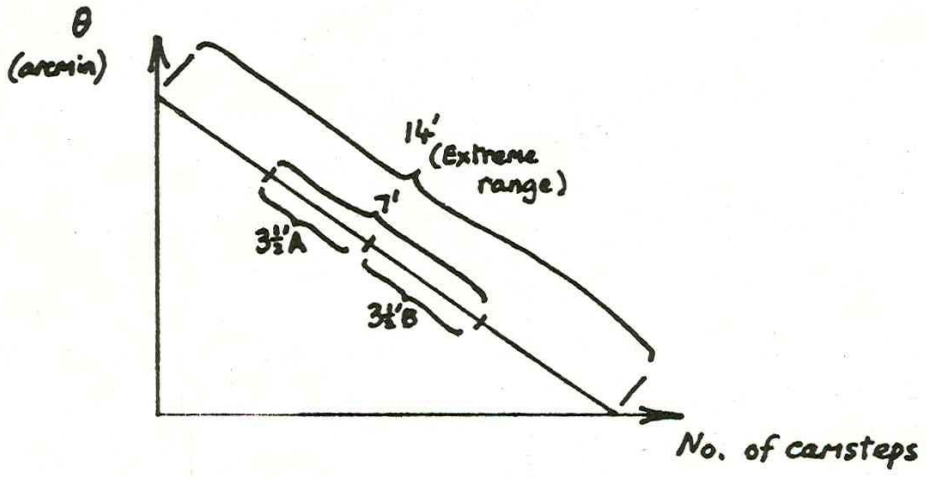

FCS RASTER LINEARITY AND DISTORTIONS

Date: February 12, 1980

Source: "Analysis of the XRP Raster Mechanism,' D. Simpson (June 1979)

Figures 1 and 2 show measurements and computer model results of the FCS raster linearity using the two raster cams that will be prime (cam 2 = Z_A, cam 4 = Y_A). The vertical scale is angular displacement (arcmin), the horizontal number of raster motor steps.

Figure 3 shows the raster pattern formed by driving cams 2 and 4. The field of view is shown looking forwards with the +y axis pointing downwards (see XRP diagram with coordinate system). The horizontal and extreme left-hand vertical scale are angular displacements in arcmins. θ_2 and θ_4 are cam rotation angle in degrees.

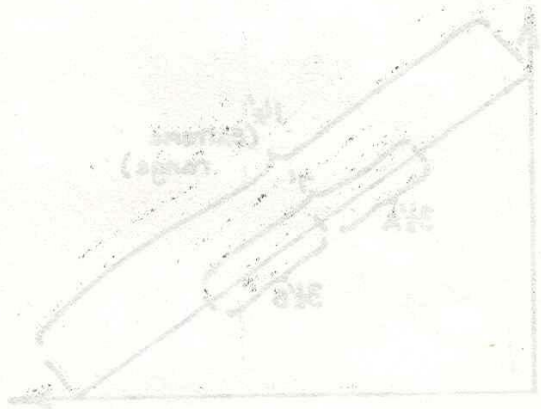

Fig.1

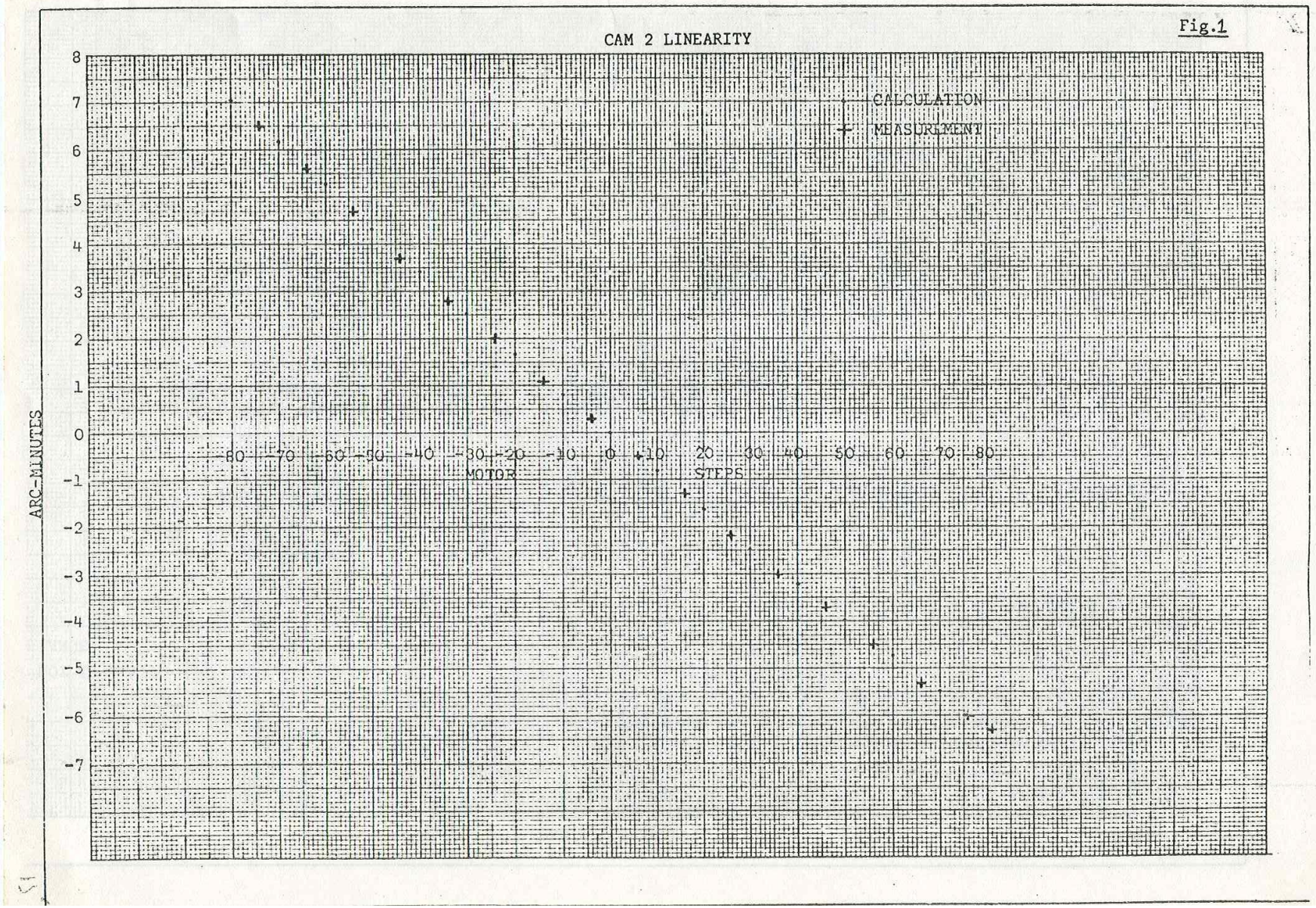
CAM 2 LINEARITY
CALCULATION
MEASUREMENT
ARC-MINUTES
8
7
6
5
4
3
2
1
0
-1
-2
-3
-4
-5
-6
-7
-80 -70 -60 -50 -40 -30 -20 -10 0 +10 20 30 40 50 60 70 80
MOTOR STEPS

CAM 4 LINEARITY

Fig.2

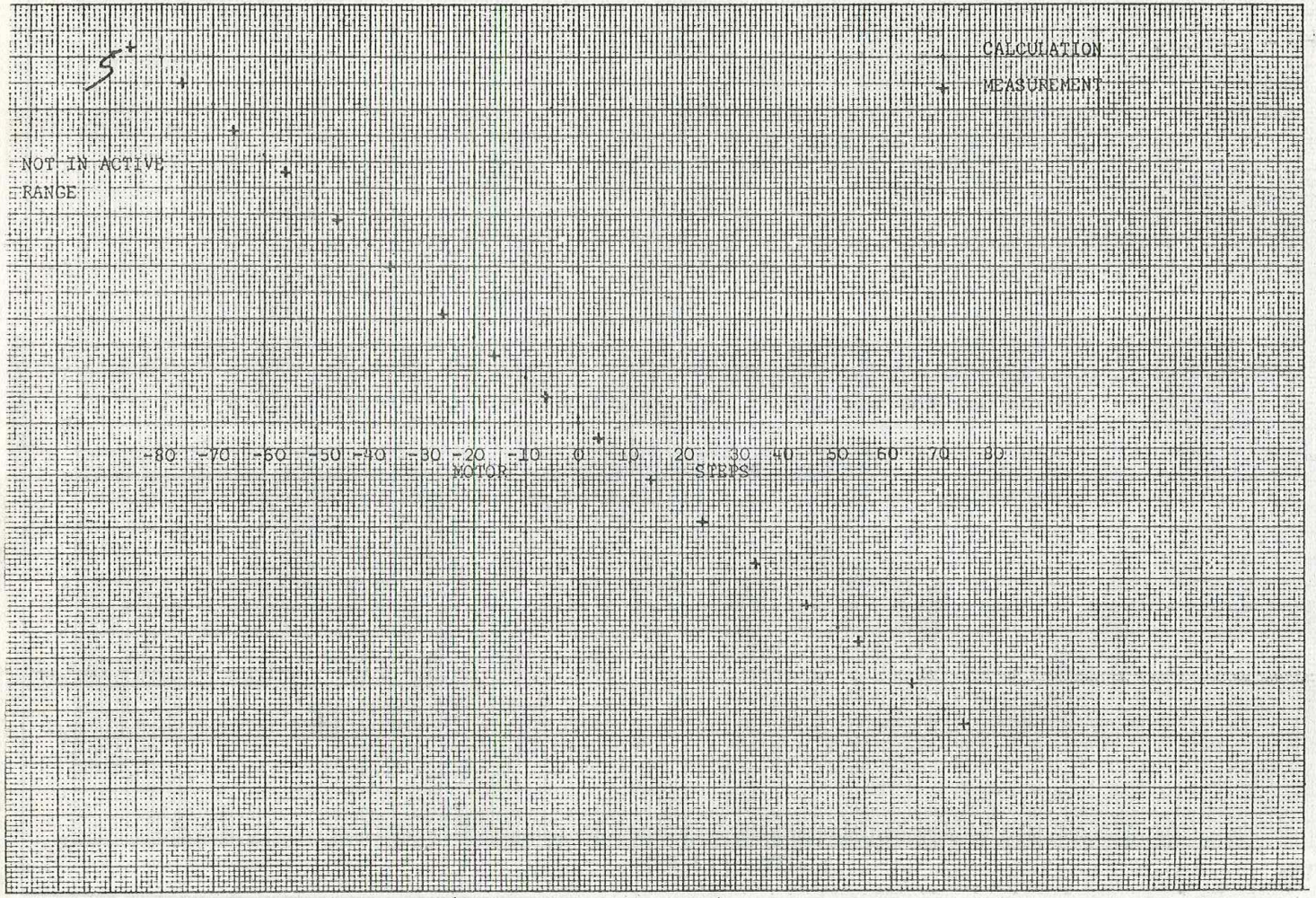

Fig 3 – RASTERING WITH CAMS 2 AND 4

LOOKING FORWARD

+y downwards

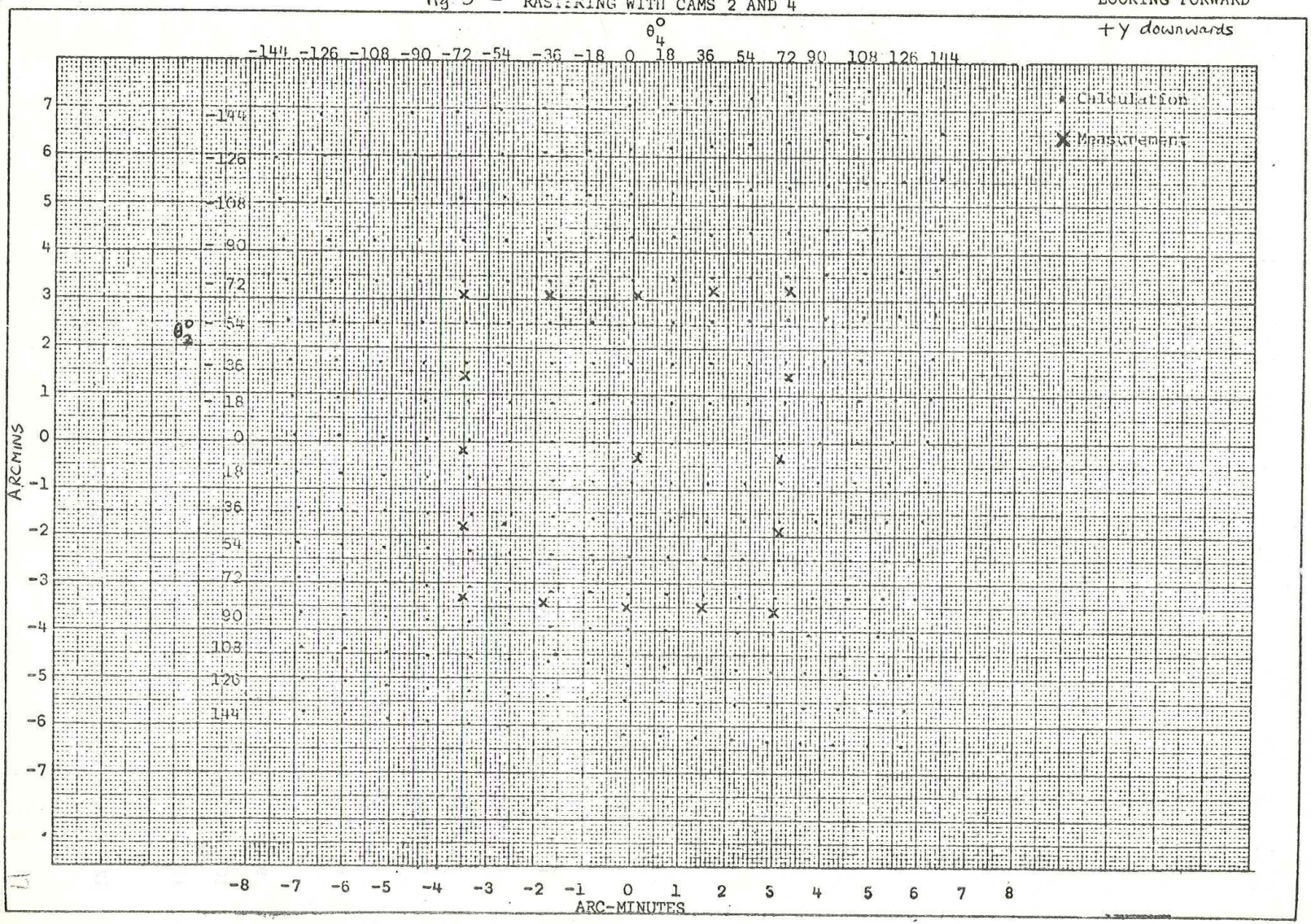

FCS CRYSTAL CALIBRATION DATA

Date: Feb. 1, 1979.

Compiler: B. J. Kent

Crystal Rocking Curves, Reflectivities and Refractive-Index Corrections

The results of the NBS work on the F.C.S. crystals are contained in a computer programme, written by Tony Burek, from which various parameters may be extracted. To use this programme a crystal channel is selected and the wavelength at which the information is required is specified. Then using data from the NBS measurements the programme computes the following.

1. Bragg angle in decimal degrees.
2. Peak reflectivity for flight crystal as a percentage.
3. Theoretical peak reflectivity.
4. Integrated reflectivity in radians.
5. Single crystal rocking curve FWHM in arc sec., for flight crystal, taking deviations from flatness into account and assuming an unpolarised input beam.
6. Theoretical cyrstal rocking curve, flat, perfect crystal.
7. Crystal resolving power actual and theoretical.
8. The correction to the Bragg angle due to the refractive index of the crystal in arc sec from Bragg angle.
9. The position of the peak of the rocking curve in arc sec. from Bragg angle.
10. Theoretical crystal value for position of rocking curve peak.
11. The position of the centroid of the rocking curve in arc sec. from Bragg angle.
12. Theoretical crystal value for the position of the rocking curve centroid.

Since this programme is rather large for the 11/34 ARD computer, running it tends to be a somewhat special event. For this reason in order to have some information available in a rather more accessible form, for general use, I have plotted graphs of some of the more important crystal parameters given by the programme.

Figures 1 A-G

For each crystal over its operating wavelength range are plotted:-

1. Single crystal rocking curve FWHM, actual and theory.
2. Peak reflectivity actual and theory.
3. Integrated reflectivity.

On each graph the home position is indicated by a dotted line.

Figures 2 A-C

The refractive index/flatness correction is plotted against wavelength. This correction is given for both the peak position and centroid position.

The correction is applied to the Bragg law formula.

$$n\lambda = 2d \sin \theta_B ,$$

for a spectral line wavelength λ in the n th order having a Bragg angle θ_B (measured from the crystal plane) as follows:-

$$\theta = \theta_B + \text{correction}.$$

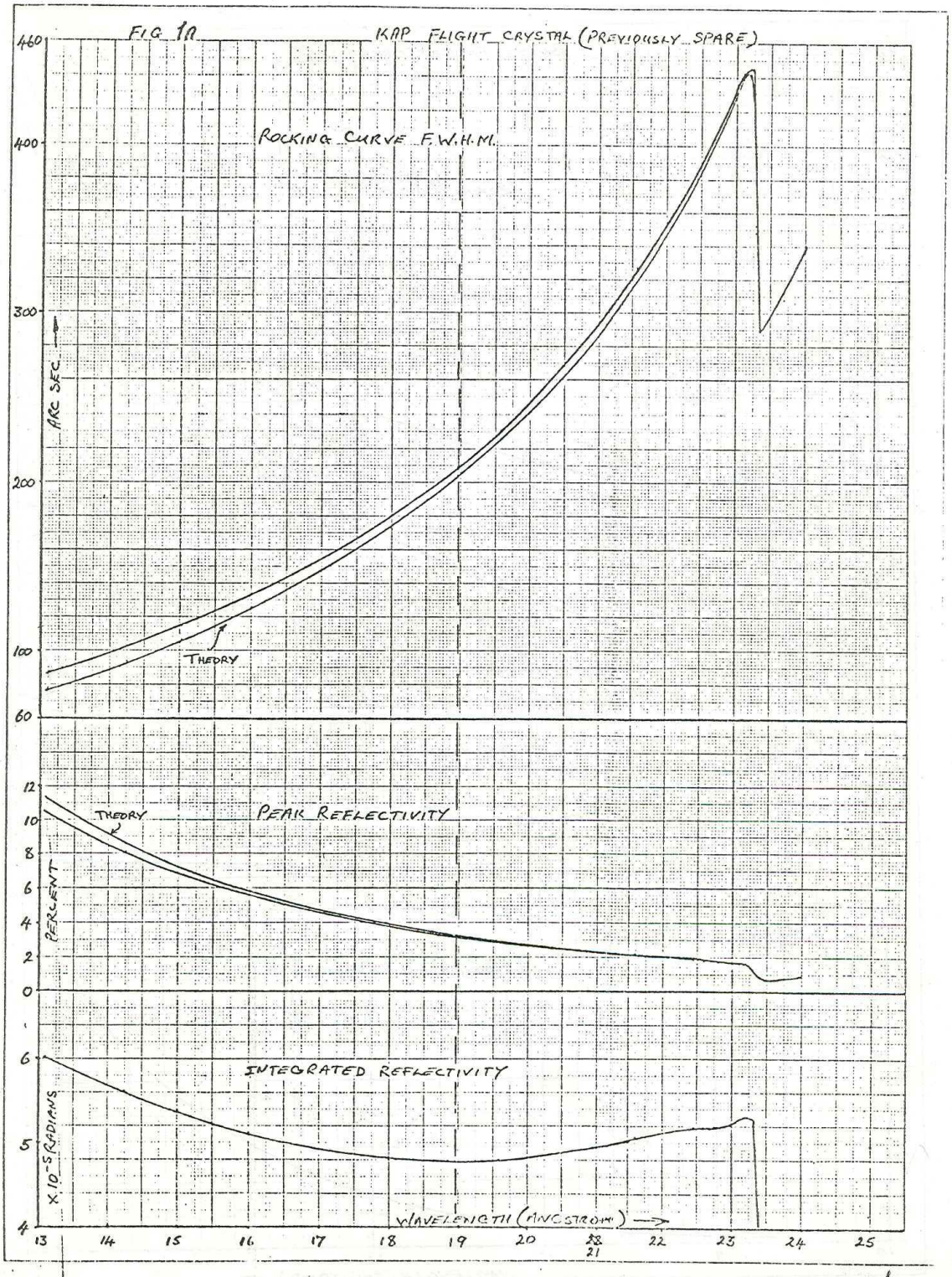
FIG 1A
IKAP FLIGHT CRYSTAL (PREVIOUSLY SPARE)
ROCKING CURVE F.W.H.M.
ARC SEC.
460
400
300
200
100
60
THEORY
PEAK REFLECTIVITY
THEORY
PERCENT
12
10
8
6
4
2
0
INTEGRATED REFLECTIVITY
X 10⁻⁵ RADIANS
6
5
4
WAVELENGTH (ANGSTROM)
13
14
15
16
17
18
19
20
21
22
23
24
25

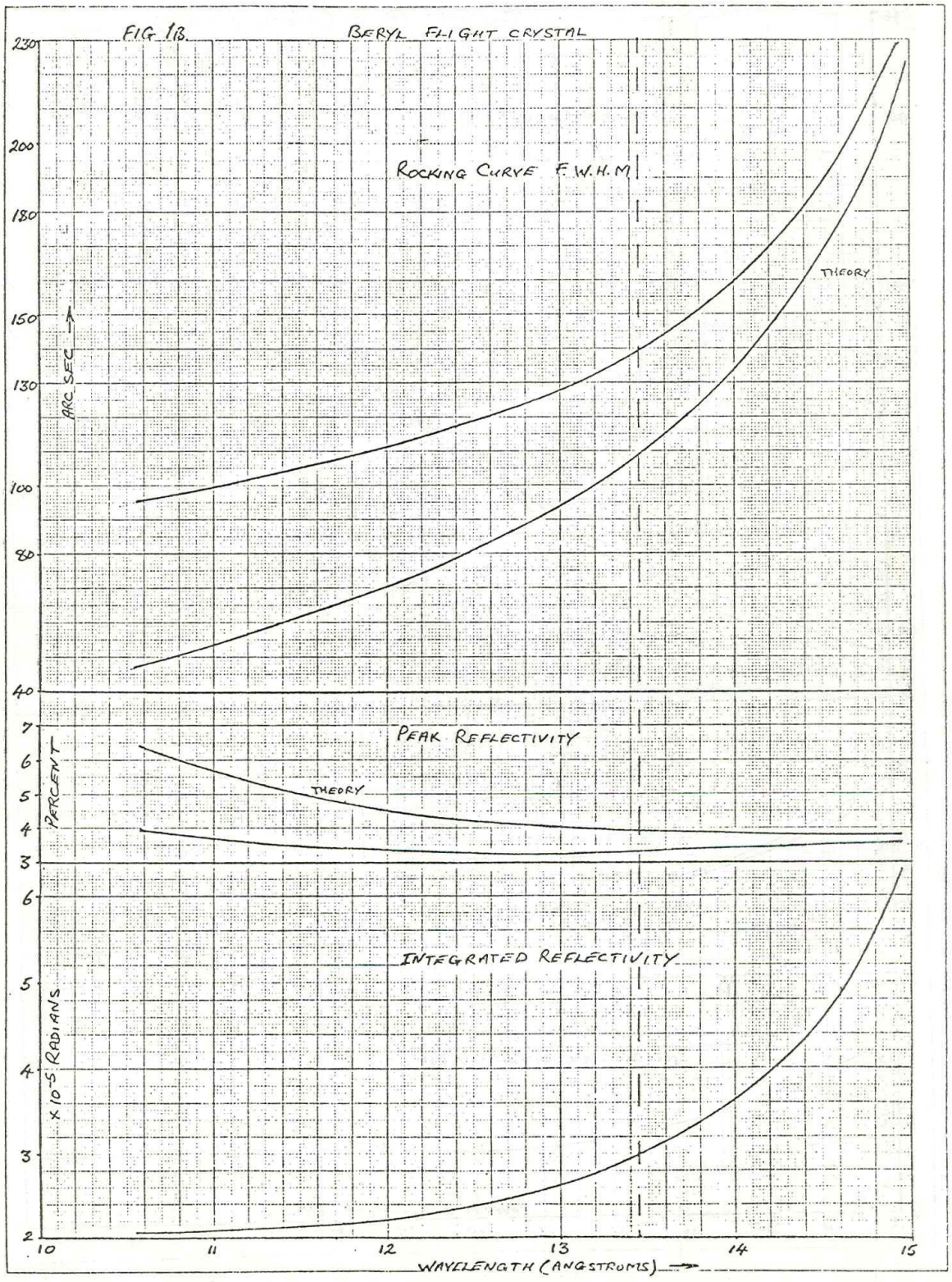
FIG 18.
BERYL FLIGHT CRYSTAL
ROCKING CURVE F.W.H.M
ARC SEC
THEORY
PEAK REFLECTIVITY
PERCENT
THEORY
INTEGRATED REFLECTIVITY
X 10⁻⁵ RADIANS
WAVELENGTH (ANGSTROMS)

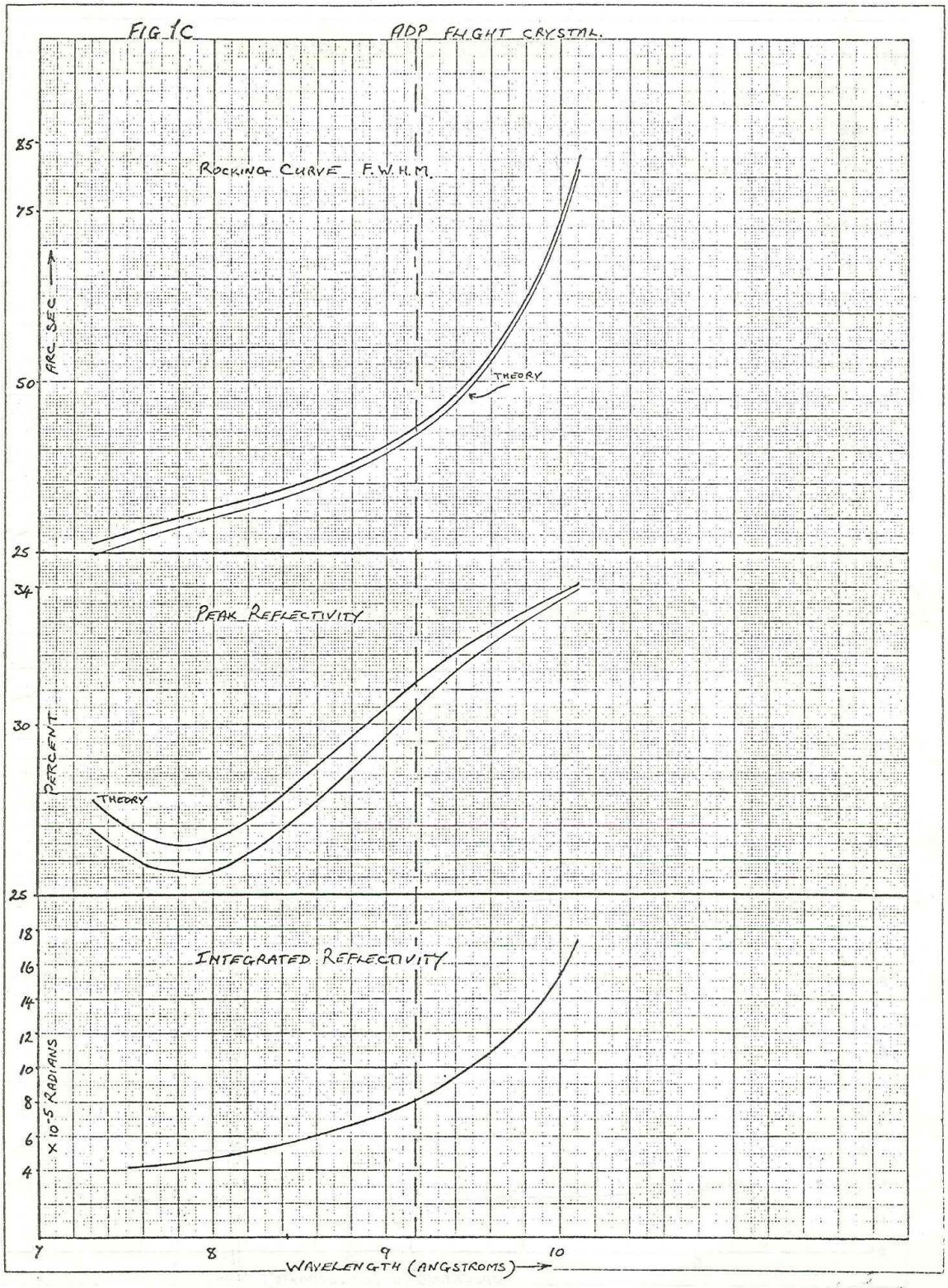
FIG 1C
ADP FLIGHT CRYSTAL.
ROCKING CURVE F.W.H.M.
ARC SEC
85
75
50
25
THEORY
PEAK REFLECTIVITY
PERCENT
34
30
25
THEORY
INTEGRATED REFLECTIVITY
X 10⁻⁵ RADIANS
18
16
14
12
10
8
6
4
7
8
9
10
WAVELENGTH (ANGSTROMS)

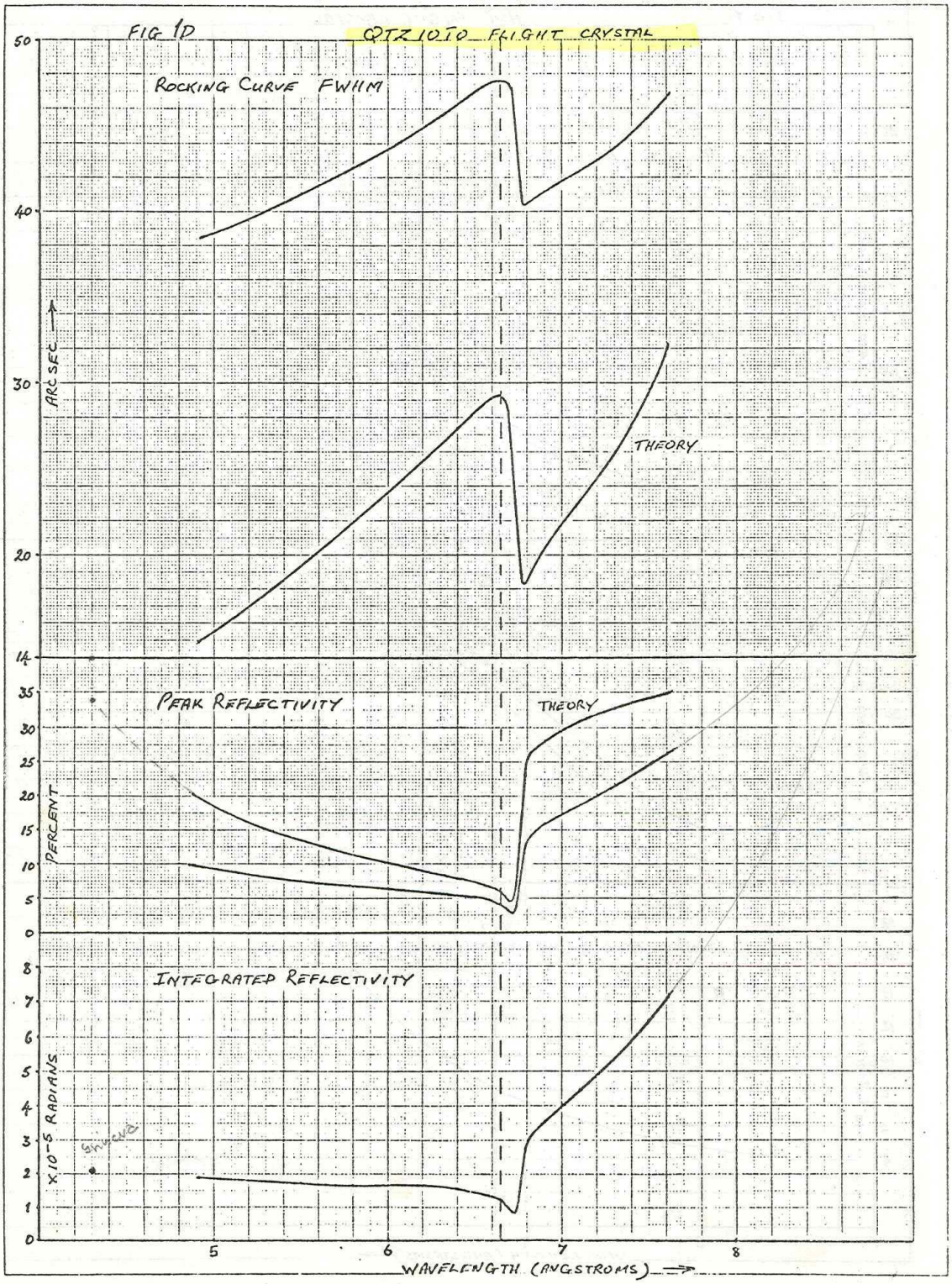
FIG 1D
QTZ 1010 FLIGHT CRYSTAL
ROCKING CURVE FWHM
ARC SEC
50
40
30
20
14
THEORY
PEAK REFLECTIVITY
THEORY
PERCENT
35
30
25
20
15
10
5
0
INTEGRATED REFLECTIVITY
X 10⁻⁵ RADIANS
8
7
6
5
4
3
2
1
0
Shaved
5
6
7
8
WAVELENGTH (ANGSTROMS)

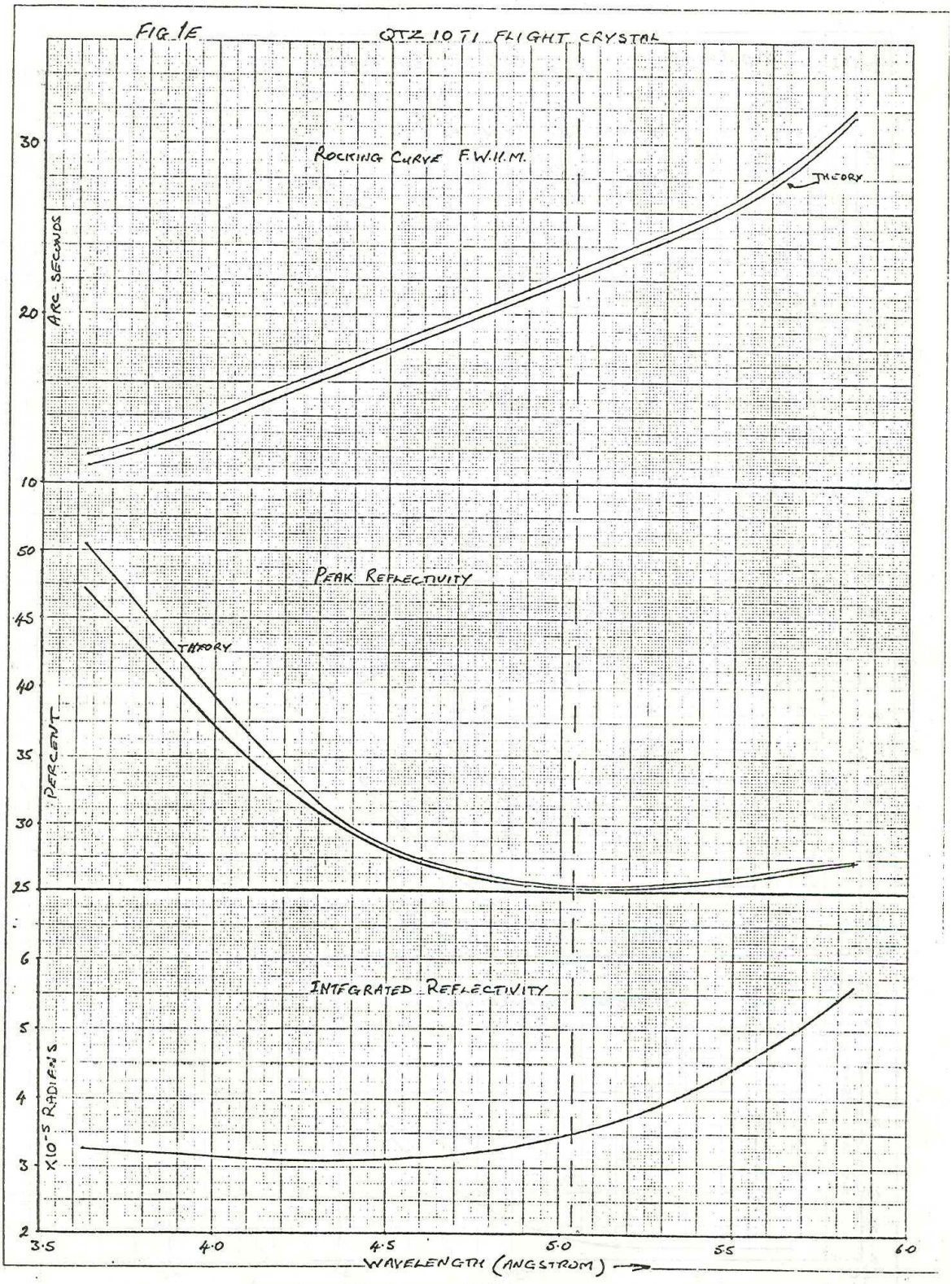
FIG 1E
QTZ 10 T1 FLIGHT CRYSTAL
ROCKING CURVE F.W.H.M.
THEORY
ARC SECONDS
30
20
10
PEAK REFLECTIVITY
THEORY
PERCENT
50
45
40
35
30
25
INTEGRATED REFLECTIVITY
X10⁻⁵ RADIANS
6
5
4
3
2
3.5
4.0
4.5
5.0
5.5
6.0
WAVELENGTH (ANGSTROM)

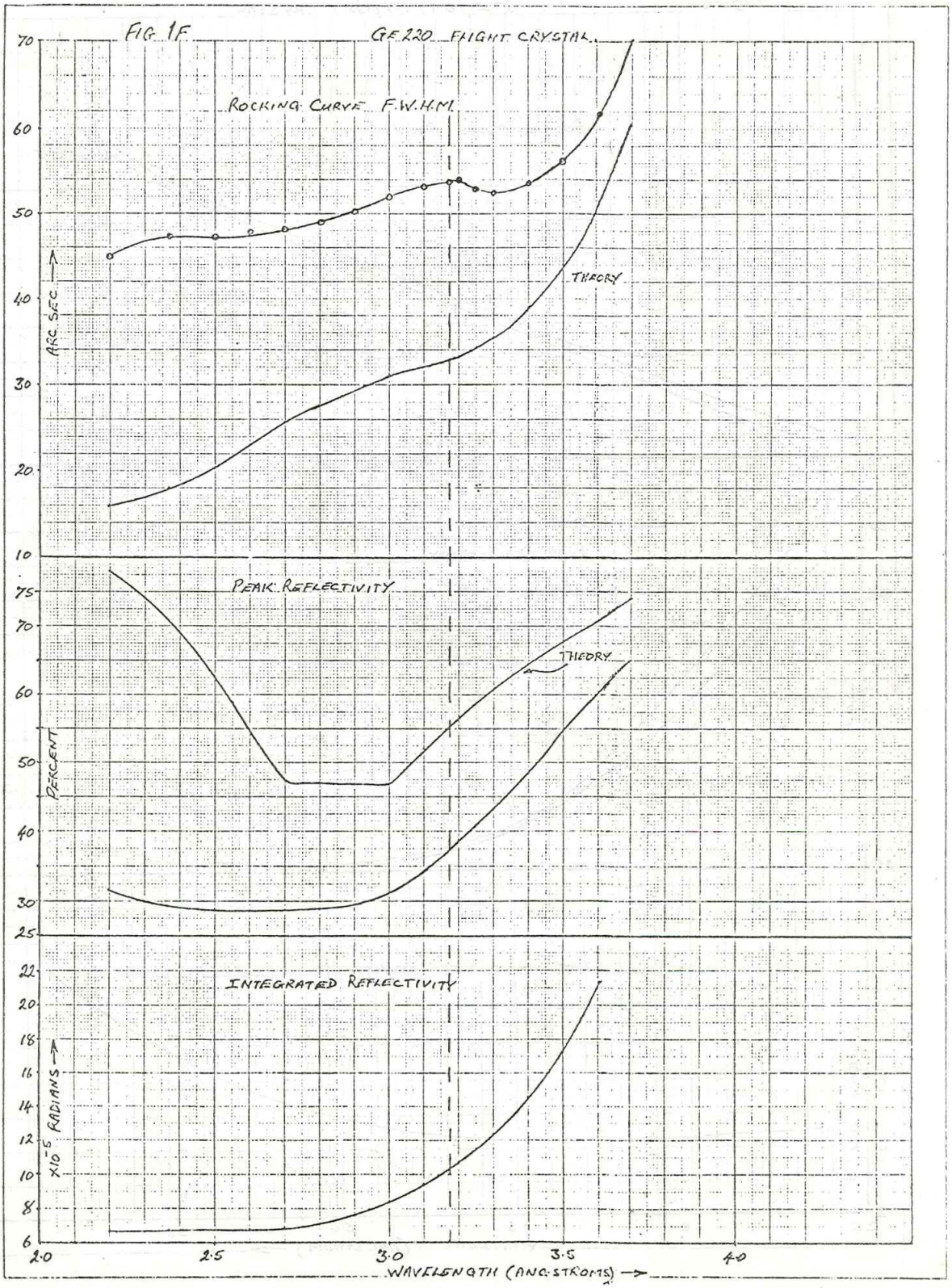
FIG. 1F
GE 220 FLIGHT CRYSTAL
ROCKING CURVE F.W.H.M.
THEORY
ARC SEC →
PEAK REFLECTIVITY
THEORY
PERCENT
INTEGRATED REFLECTIVITY
X10⁻⁵ RADIANS →
WAVELENGTH (ANGSTROMS) →

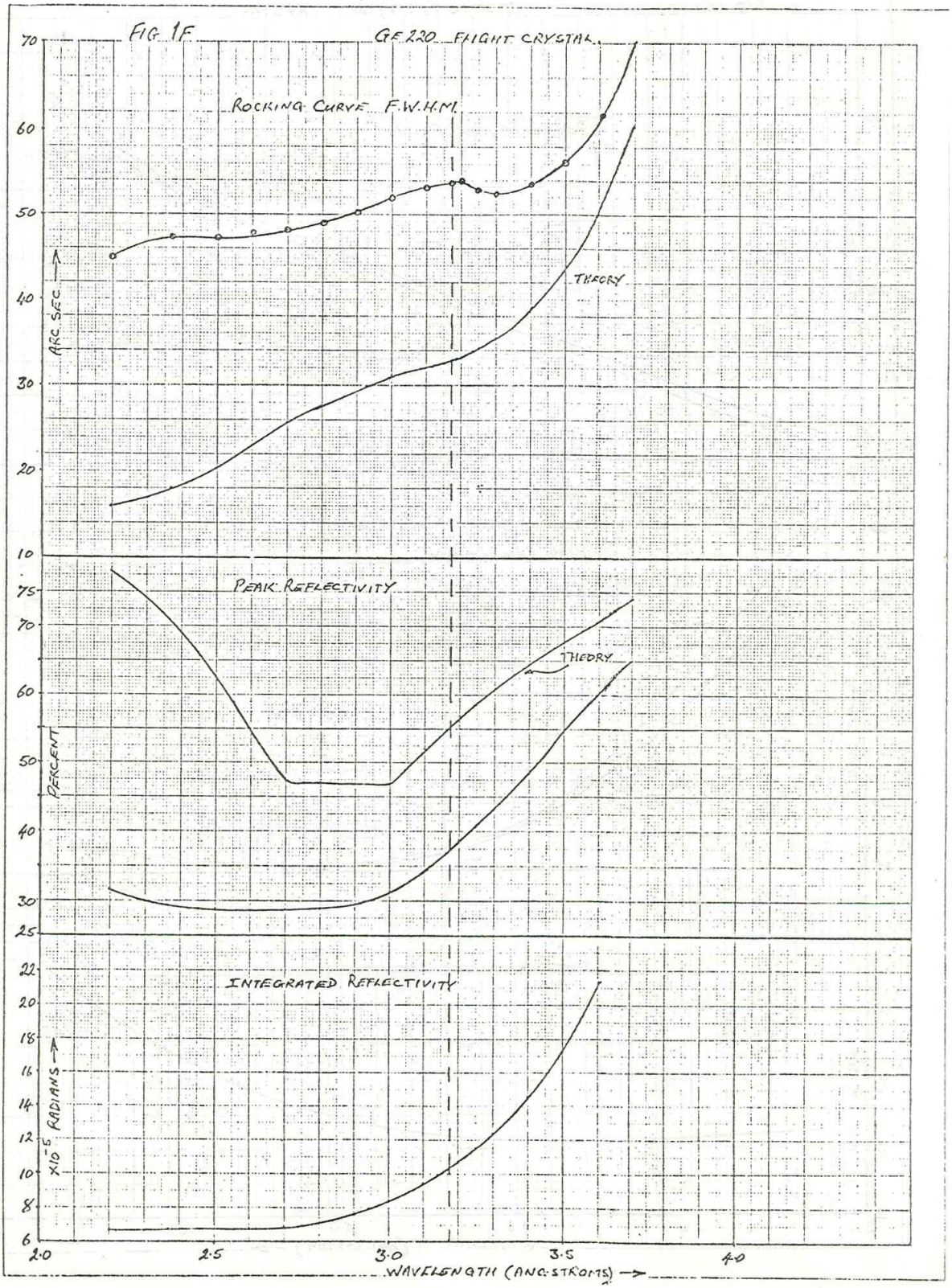
FIG 1F
GE 220 FLIGHT CRYSTAL
ROCKING CURVE F.W.H.M.
ARC SEC →
THEORY
PEAK REFLECTIVITY
PERCENT
THEORY
INTEGRATED REFLECTIVITY
X10⁻⁵ RADIANS →
WAVELENGTH (ANGSTROMS) →
70
60
50
40
30
20
10
75
70
60
50
40
30
25
22
20
18
16
14
12
10
8
6
2.0
2.5
3.0
3.5
4.0

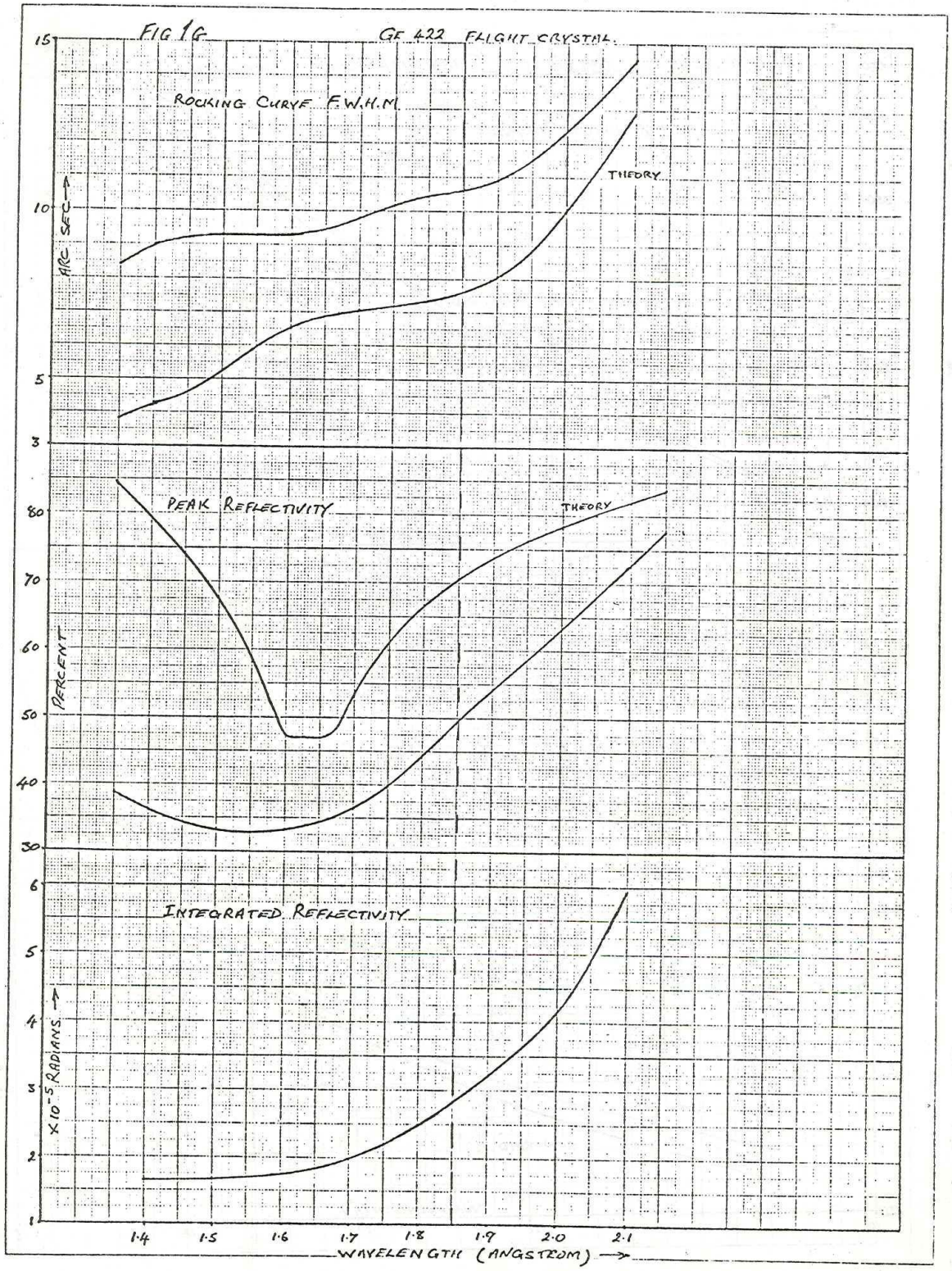
FIG 1G
GE 422 FLIGHT CRYSTAL.
ROCKING CURVE F.W.H.M.
THEORY
ARC SEC →
15
10
5
3
PEAK REFLECTIVITY
THEORY
PERCENT
80
70
60
50
40
30
INTEGRATED REFLECTIVITY
X 10⁻⁵ RADIANS →
6
5
4
3
2
1
1·4
1·5
1·6
1·7
1·8
1·9
2·0
2·1
WAVELENGTH (ANGSTROM) →

FIG 2a

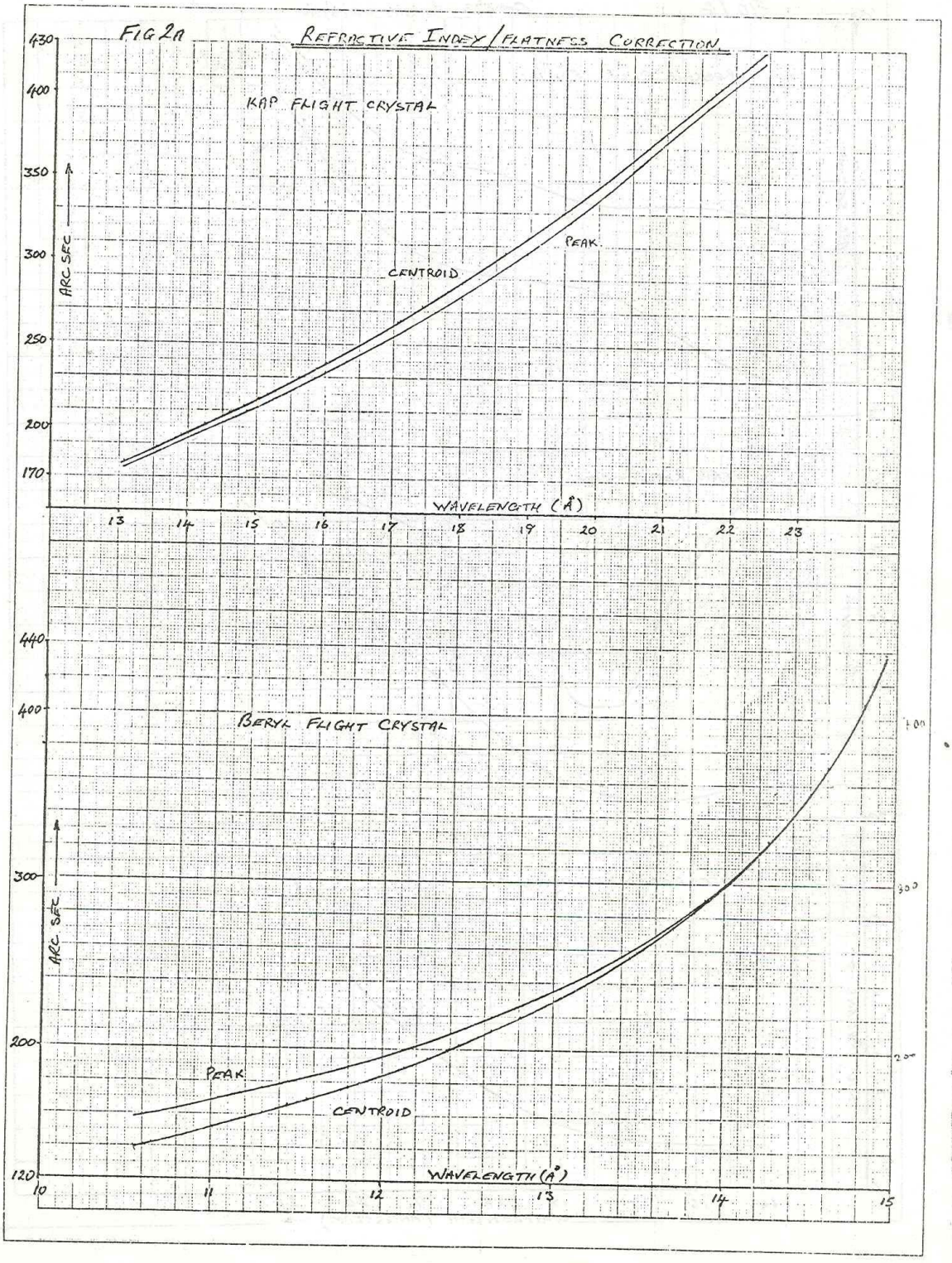
REFRACTIVE INDEX / FLATNESS CORRECTION
KAP FLIGHT CRYSTAL
ARC SEC
CENTROID
PEAK
WAVELENGTH (Å)
BERYL FLIGHT CRYSTAL
ARC SEC
PEAK
CENTROID
WAVELENGTH (Å)

FIG 2B

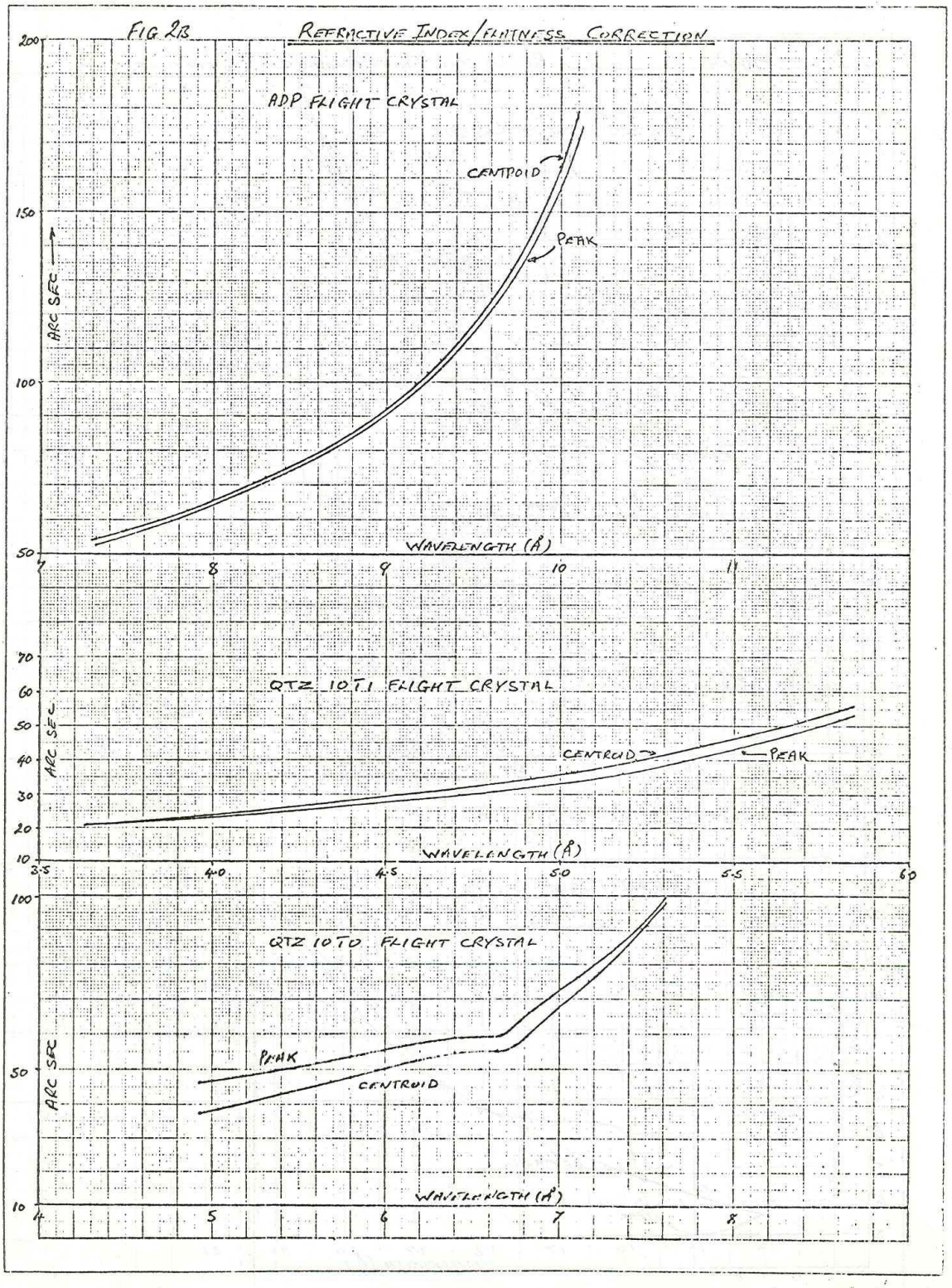
REFRACTIVE INDEX/FLATNESS CORRECTION
ADP FLIGHT CRYSTAL
CENTROID
PEAK
ARC SEC
WAVELENGTH (Å)
200
150
100
50
7
8
9
10
11
QTZ 10.1.1 FLIGHT CRYSTAL
70
60
50
40
30
20
10
3.5
4.0
4.5
5.0
5.5
6.0
QTZ 10.1.0 FLIGHT CRYSTAL
100
50
10
4
5
6
7
8

FIG. 2c

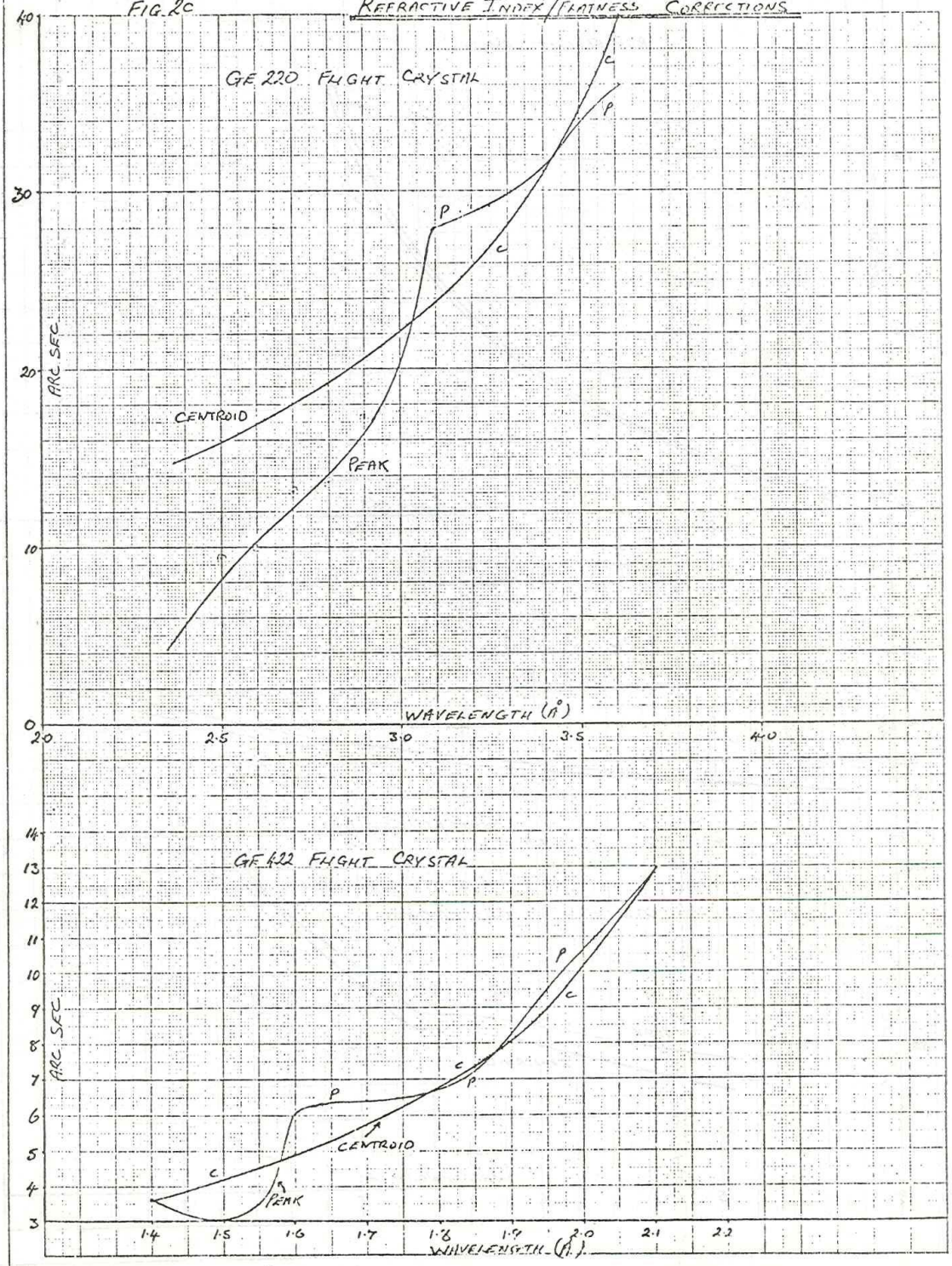
REFRACTIVE INDEX / FLATNESS CORRECTIONS
GE 220 FLIGHT CRYSTAL
ARC SEC
CENTROID
PEAK
WAVELENGTH (Å)
GE 422 FLIGHT CRYSTAL
ARC SEC
CENTROID
PEAK
WAVELENGTH (Å)

ADDENDUM TO 'FCS CRYSTAL CALIBRATION DATA'

Date: December 31, 1979

Source: Letter from A.J. Burek (National Bureau of Standards) to C.J. Wolfson, October 12, 1979.

Owing to the presence of the Si K edge at 6.738 Å in the Qu $10\bar{1}0$ crystal (H.P. line: Si XIII res. line), values of peak and integrated reflectivities, rocking curves and refractive-index corrections will show sharp variations near this wavelength. The figure on the following page shows unreduced laboratory measurements of relative intensities. Burek estimates that the integrated reflectivity at 6.738 Å has an upper limit of 4×10^{-6} (lower limit indeterminate because of background). Solar SiXIII lines plus SiXII satellites will be affected, especially SiXII satellite q ($1s^2 2s\ ^2S_{\frac{1}{2}} - 1s2s2p(^1P)^2P_{3/2}$; λ 6.719 Å) which falls close to the intensity minimum, and the SiXIII intercombination line ($1s^2\ ^1So - 1s2p\ ^1P_1$; λ 6.688 Å) which is near the strong resonance at 6.705 Å.

In the figure, the data are not reduced to the shape of the source continuum, but all the structure apart from the tungsten Mβ line (6.754 Å) is due to the crystal.

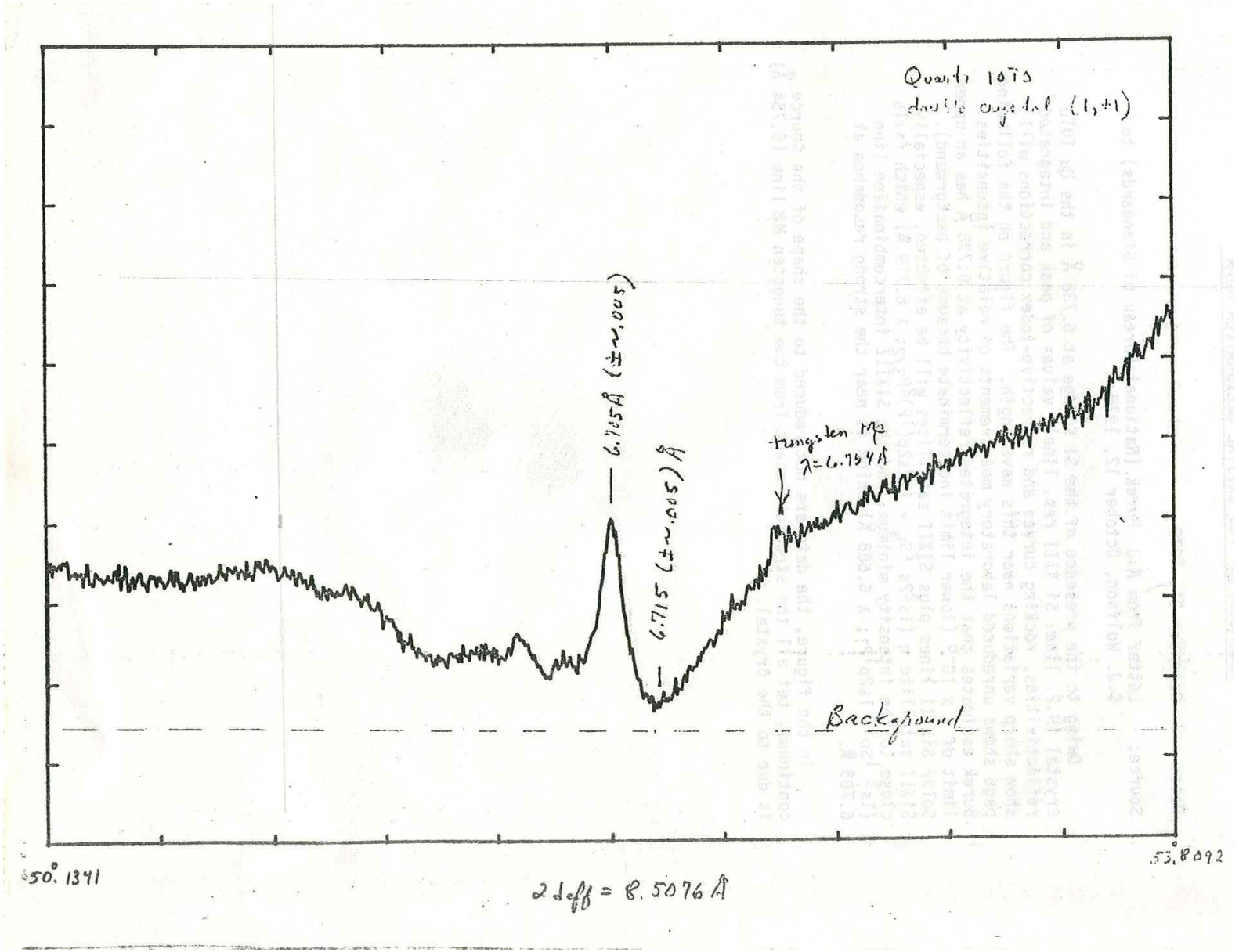
Quartz 10T5
double crystal (1,+1)
6.765Å (±~.005)
6.715 (±~.005) Å
tungsten Kα
λ=6.754Å
Background
50°.1341
53°.8092
2 d_ff = 8.5076 Å

FCS ALIGNMENT SENSOR

Date: February 11, 1980

Sources: Phase II XRP Report (December 1976)
Information from K. T. Strong

The FCS alignment sensor consists of a 19 mm lens mounted on the collimator front grid assembly with a co-aligned detector mask 1 m behind it on the rear-most grid assembly. The detector mask consists of four square apertures equi-spaced around a circle that approximates the image of the Sun formed by the lens. There is a separate photosensor behind each aperture. A fifth, circular aperture lies at the mask centre, forming the basis for the primary alignment of the system; the optical axis is expected to be within ±2" arc of X-ray optical axis.

Square hole dimensions: 0.0127 x 0.0127 cm, providing angular resolution of 27" arc.

Square hole separation (centre-centre): 0.9322 cm.

Mean solar diameter: 0.9302 cm (corresponding to 31'59" arc).

Circular aperture diameter: 0.076 cm.

Solar diameter required to fit square-hole separation: 32' 02".

There is also a 100 Å bandpass filter, centered on 6500 Å, in the thermal filter structure, passing sunlight to the FCS alignment sensor.

XRP FLAT CRYSTAL SPECTROMETER

INSTRUMENT MODES

This document describes FCS instrument modes which have been used in SMM Joint Observing Sequences (JOS's). It brings earlier versions (in June 1979 and October 1979) up to date. As before, both raster motions and spectroscopic modes are described. In this document, however, mode identifications (UMMID's - Unique Mission Mode Identifications) are specified, these being the numbers actually specified in command generation.

K. J. H. PHILLIPS

J. H. PARKINSON

J. W. LEIBACHER

February 1980

RASTER SIZES AND SHAPES

In principle any raster size (in 5" arc steps up to 7' arc square) and any raster shape are possible, but various limits on this flexibility have been imposed (a) to reduce the number of parameters stored by the on-board microprocessor, (b) to simplify the flight and ground software.

Under normal operating conditions the coordinate system is ($\pm$y, $\pm$z), with +z pointing towards celestial N, +y towards E. (astronomically speaking, increasing R.A.).

The following constraints on rasters are those known about to date, and are incorporated in this document whereever applicable:-

(1) Raster shapes will be single rectangles or squares (i.e. no compound shapes such as 'T' shapes) or else will consist of single lines (in y or z).

(2) In the FCS data stream, an identifying code consisting of an 8-bit number N (so N $<$ 256) serves to specify the raster, defined by its y and z dimensions and the step size (Δy and Δz) in each dimension. Thus up to 2^8 = 256 possible combinations of (y,z,Δy,Δz) are allowed.

Of these 256 combinations, some 200 have now been selected which have dimensions expected to be commonly used during the Mission. The tables on the following pages specify these raster patterns, each with a UMMID. Note that so far almost all rasters have Δy = Δz.

(3) Equal dwell times Δt per raster element ('pixel'). Although Δt = 0.256 sec. (= 1 'data gathering interval,' DGI) is possible, the minimum dwell time is being set at Δt = 1.024 sec. (= 4 DGI) to avoid resonant frequencies in the rastering mechanism.

(4) All rasters will be traced out in the same sense:

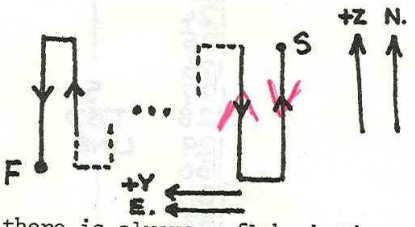

S = Start

F = Finishing Point

Thus there is always a flyback time at the completion of a raster before a new one can be performed.

UMMID's FOR RASTERS

UMMID	Y	Z	ΔY	ΔZ
0	NO MOTION			
1	20"	20"	5"	5"
2	30"	30"	5"	5"
3	1'	1'	5"	5"
4	7'	7'	10"	10"
5	7'	7'	15"	15"
6	7'	7'	20"	20"
7	1'	4'	10"	20"
8	4'	1'	20"	10"
9	2'	LINE	5"	—
10	LINE	2'	—	5"
11	1'	1'	5"	5"
12	5'	2'	15"	15"
13	5'	5'	5'	5'
⋮	TBD			
63				
64				
65	LINE	20"	10"	10"
66	|	30"	|	|
67	|	1'	|	|
68	|	2'	|	|
69	|	3'	|	|
70	|	4'	|	|
71	LINE	5'	|	|
72	20"	LINE	|	|
73	|	20"	|	|
74	|	30"	|	|
75	|	1'	|	|
76	|	2'	|	|
77	|	3'	|	|
78	|	4'	|	|
79	20"	5'	|	|
80	30"	LINE	|	|
81	|	20"	|	|
82	|	30"	|	|
83	|	1'	|	|
84	|	2'	|	|
85	|	3'	|	|
86	|	4'	|	|
87	30"	5'	|	|
88	1'	LINE	|	|
89	|	20"	|	|
90	|	30"	|	|
91	|	1'	|	|
92	|	2'	|	|
93	|	3'	|	|
94	|	4'	|	|
95	1'	5'	10"	10"

UMMID	Y	Z	ΔY
96	2'	LINE	10"
97	|	20"	|
98	|	30"	|
99	|	1'	|
100	|	2'	|
101	|	3'	|
102	|	4'	|
103	2'	5'	|
104	3'	LINE	|
105	|	20"	|
106	|	30"	|
107	|	1'	|
108	|	2'	|
109	|	3'	|
110	|	4'	|
111	3'	5'	|
112	4'	LINE	|
113	|	20"	|
114	|	30"	|
115	|	1'	|
116	|	2'	|
117	|	3'	|
118	|	4'	|
119	4'	5'	|
120	5'	LINE	|
121	|	20"	|
122	|	30"	|
123	|	1'	|
124	|	2'	|
125	|	3'	|
126	|	4'	|
127	5'	5'	10"
128	TBD		
129	LINE	20"	15"
130	|	30"	|
131	|	1'	|
132	|	2'	|
133	|	3'	|
134	|	4'	|
135	LINE	5'	|
136	20"	LINE	|
137	|	20"	|
138	|	30"	|
139	|	1'	|
140	|	2'	|
141	|	3'	|
142	|	4'	|
143	20"	5'	15"

UMMID	Y	Z	ΔY
144	30"	LINE	15"
145		20"	
146		30"	
147		1'	
148		2'	
149		3'	
150		4'	
151	30"	5'	
152	1'	LINE	
153		20"	
154		30"	
155		1'	
156		2'	
157		3'	
158		4'	
159	1'	5'	
160	2'	LINE	
161		20"	
162		30"	
163		1'	
164		2'	
165		3'	
166		4'	
167	2'	5'	
168	3'	LINE	
169		20"	
170		30"	
171		1'	
172		2'	
173		3'	
174		4'	
175	3'	5'	
176	4'	LINE	
177		20"	
178		30"	
179		1'	
180		2'	
181		3'	
182		4'	
183	4'	5'	
184	5'	LINE	
185		20"	
186		30"	
187		1'	
188		2'	
189		3'	
190		4'	
191	5'	5'	15"
192	TBD		

UMMID	Y	Z	ΔY
193	LINE	20"	20"
194		30"	
195		1'	
196		2'	
197		3'	
198		4'	
199	LINE	5'	
200	20"	LINE	
201		20"	
202		30"	
203		1'	
204		2'	
205		3'	
206		4'	
207	20"	5'	
208	30"	LINE	
209		20"	
210		30"	
211		1'	
212		2'	
213		3'	
214		4'	
215	30"	5'	
216	1'	LINE	
217		20"	
218		30"	
219		1'	
220		2'	
221		3'	
222		4'	
223	1'	5'	
224	2'	LINE	
225		20"	
226		30"	
227		1'	
228		2'	
229		3'	
230		4'	
231	2'	5'	
232	3'	LINE	
233		20"	
234		30"	
235		1'	
236		2'	
237		3'	
238		4'	
239	3'	5"	20"

UMMID	Y	Z	ΔY
240	4'	LINE	20"
241	|	20"	|
242	|	30"	|
243	|	1'	|
244	|	2'	|
245	|	3'	|
246	|	4'	|
247	4'	5'	|
248	5'	LINE	|
249	|	20"	|
250	|	30"	|
251	|	1'	|
252	|	2'	|
253	|	3'	|
254	|	4'	|
255	5'	5'	20"

COMBINED RASTER AND CRYSTAL MOTIONS

The table on p.5 defines the types of combined raster and crystal motion which are envisaged for normal FCS operating. The exact details of the spectroscopic motions are described fully on p.6 et seq., where spectroscopic and integral scans are also defined.

NOTES: (1) spectroscopic motions are performed once completely for each raster element, i.e. the rastering motion forms the 'outer loop' in the modes of type 4, 5, 6, and 7.Also in these mode types spectroscopic motions cannot be repeated for each raster element.

(2) Flight and ground software demands that the minimum duration of a combined raster and crystal motion is 9 DGI = 2.304 sec.

(3) There is a maximum dwell of 255 DGI at any location in a raster.

DEFINITION OF FCS MODE TYPES DESCRIBING RASTER AND CRYSTAL MOTIONS

UMMID	Mode Name	Comments
0	Nothing Moves (NM)	
1	Raster (R)	Crystals fixed.
2	Spectroscopic Scans (SS)	Raster fixed. Series of λ positions, dwell at each of which constant. SS always in same direction, so flyback between repeats.
3	Integral Scans (IS)	Raster fixed. Scans at selected rate for selected time. IS always in same direction, so flyback between repeats.
4	Spectroscopic Scan in Raster (SSR)	Like 2 but within a raster.
5	Integral Scan in Raster (ISR)	Like 4 but integral scan.
6	Multiple Spectroscopic Scans (MSS)	Raster fixed. Scan one λ range, go to new range, scan that range, etc. Dwell at each point of a λ range is constant.
7	Multiple Integral Scans (MIS)	As 3 but integral scans.
8	Multiple Spectroscopic Scans in Raster (MSSR)	Like 3 but within a raster.
9	Multiple Integral Scans in Raster (MISR)	Like 5 but integral scans

(b) SPECTROSCOPY MODES

The spectroscopy modes described in the following pages have been formulated to examine several questions related to atomic physics. Particular areas of interest are:-

a. line ratios to determine densities (or place limits on densities) and temperatures;

b. satellite lines near He-like ion lines;

c. Doppler shifts in line emission due to moving (particularly flare-accelerated) material;

d. temperature-dependent emission measure function from line fluxes; and

e. surveys of the spectrum in flare and non-flare conditions.

Where necessary, diagrams showing the positions of lines and the ranges of the intended wavelength scans are included in the mode description. Wavelengths of lines have been obtained from a note by B Fawcett and K Phillips (dated October 1979), drawing on several sources.

Wavelength scans are performed by crystal motions in two ways. With spectroscopic scans, the crystal shaft on which the seven FCS crystals are mounted is rotated in a step fashion such that one wavelength is observed at a time; the angular interval between two positions can be any multiple of 9.889" arc, the smallest step size. The shaft may remain at a single spectral location for multiples of 0.256 sec, though data are gathered each 0.256 sec = 1 Data Gathering Interval (DGI). With integral scans, the crystal shaft rotates uniformly over a range, data being collected as before, each DGI. There are certain permissible integral scan rates:

Rate	1	=	2	steps/DGI	=	7.8125	steps/sec
	2	=	4	" "	=	15.625	" "
	3	=	8	" "	=	31.25	" "
	4	=	16	" "	=	62.5	" "
	5	=	32	" "	=	125	" "

Faster scanning rates are not in practice possible. For instrumental reasons, integral scans can only be performed in the increasing θ direction, and so, when the scanning of a line profile is complete, the crystal shaft must be relocated to the initial position to repeat the scan; a definite 'flyback' time is thus required. Though the same hardware restriction does not apply to spectroscopic scans, both flight and ground software is facilitated by introducing it, so flyback times must be included for these also. In addition, when two or more lines are being scanned (multiple integral or spectroscopic scans), definite 'skip' times (again integral multiples of DGIs) are required to go from one line to another. In the mode descriptions, scan, skip and flyback times are indicated (units of DGI), values being obtained from John Sherman's document ('Timing Conventions for FCS Crystal Motions', 10 April 1979), based on studies by

C. J. Wolfson of experimental data ('FCS Crystal Drive Response Calibration Status'. 22 January 1979).

There is a maximum of 4096 types of spectroscopic motions, these being defined by a 12-bit number in the FCS telemetry.

With multiple integral or spectroscopic scans a single value for the integral scan rate or the dwell time at each point must be used. There is a maximum duration of 255 DGI for an integral scan, and a maximum 'dwell' at any wavelength in a spectroscopic scan of 255 DGI.

Scan rates across spectral lines are decided by expected count rates. These are derived using:

a. calculated FCS sensitivities and count rates in a note by K. Phillips (23 March 1979);

b. line fluxes from R. Mewe (Solar Phys. 22, 459, 1972).

A comparison of the sensitivity values with a calculation by Loren Acton suggests that the total count values, as obtained in integral scans, are good to about 50%. The same comparison has shown that the peak count rates are less accurate; revised values will be inserted as soon as possible. Present values are calculated from total count rates using line widths which are a combination of instrumental profile (rocking curve) and thermal widths. Mewe's line fluxes are sufficiently accurate in most cases, though there is an anomaly with the 12.38Å Fe XXI line (see mode 3B). Two assumptions in the derivation of these count rates should be borne in mind:

a. The active region emission measure = 10^{47} cm^{-3} in a 10" x 10" arc area (roughly the collimator field-of-view); flare emission measure = 10^{49} cm^{-3} (point source), value typical of rather a large flare.

b. In general, lines are emitted at the temperature of maximum G(T), the function $(n_{ion}/n_{element})$ x collisional excitation rate. However, active region ions with G(T)'s peaking at $T > 6.3 \times 10^6$K are assumed to emit at 6.3×10^6K.

Crystal shaft positions are defined in terms of crystal steps from a minimum position. This is a departure from the June 1979 document in which crystal angles from the Home Position were specified. One unit represents one crystal shaft step (9.889" arc). According to this scheme, the Home Position is at step no. 5825. Other step numbers have been determined from runs of a computer programme written by Barry Kent.

Some details remain to be specified in Sections 5 and 6. These modes generally have low priority or await atomic data (eg. wavelengths of the Ly α satellites.

WAVELENGTHS OF LINES NEAR FCS HOME POSITION

Using information from B. J. Kent and B. C. Fawcett, the FCS home position wavelength settings are given in the table below. The wavelengths selected are close approximations to published data. Calculated wavelengths are also available :

(a) G. W. Erickson (J. Phys. Chem. Ref. Data 6, 831, 1977) for hydrogenic ions;

(b) A. M. Ermolaev and M. Jones (J. Phys. B 6, 1, 1973) for He-like ions;

both of which include relativistic, mass and quantum electrodynamic effects on energy levels. The calculated wavelengths of the H. P. lines, also given below, agree quite well except for Ca XIX R, for which the difference (0.004 Å) is large compared with the expected line width (0.002 Å), calculated as a Voigt profile convolution of thermal Doppler broadening ($T = 20 \times 10^6 K$) and crystal rocking curve. In Figure 1 the line wavelengths as given by these calculations are plotted together with the intercombination and forbidden lines (also from Ermolaev and Jones) and three satellite lines due to the Li-like stage (from Gabriel, M. N. 160, 99, 1972 and Bely-Dubau et al, M.N. 186, 405, 1979). Voigt profiles are superimposed, with temperatures equal to that of maximum G (T) or 20×10^6 K, whichever is the smaller.

In Figure 2 the line positions are re-plotted with the resonance lines aligned with the home position. It is this figure which has been used to set wavelength ranges over which the FCS should scan in the spectroscopy modes. One small division = 100" of crystal shaft rotation angle ≈ 10 spectrometer steps. Line intensities are very roughly indicated.

FCS HOME POSITION LINE WAVELENGTHS

CRYSTAL	LINE*	WAVELENGTH SET AT (Å)	CALCULATED WAVELENGTH (Å)	FWHM VOIGT PROFILE (Å)
KAP (001)	O VIII Lα	18.9689	18.9689	0.0371
Beryl ($10\bar{1}0$)	Ne IX R	13.447	13.447	0.0176
ADP (101)	Mg XI R	9.169	9.169	0.0048
Quartz ($10\bar{1}0$)	Si XIII R	6.649	6.648	0.0038
Quartz ($10\bar{1}1$)	S XV R	5.039	5.038	0.0025
Ge (220)	Ca XIX R	3.173	3.177	0.0020
Ge (422)	Fe XXV R	1.85035	1.8502	0.0009

* R = resonance line $1^1S - 2^1P$

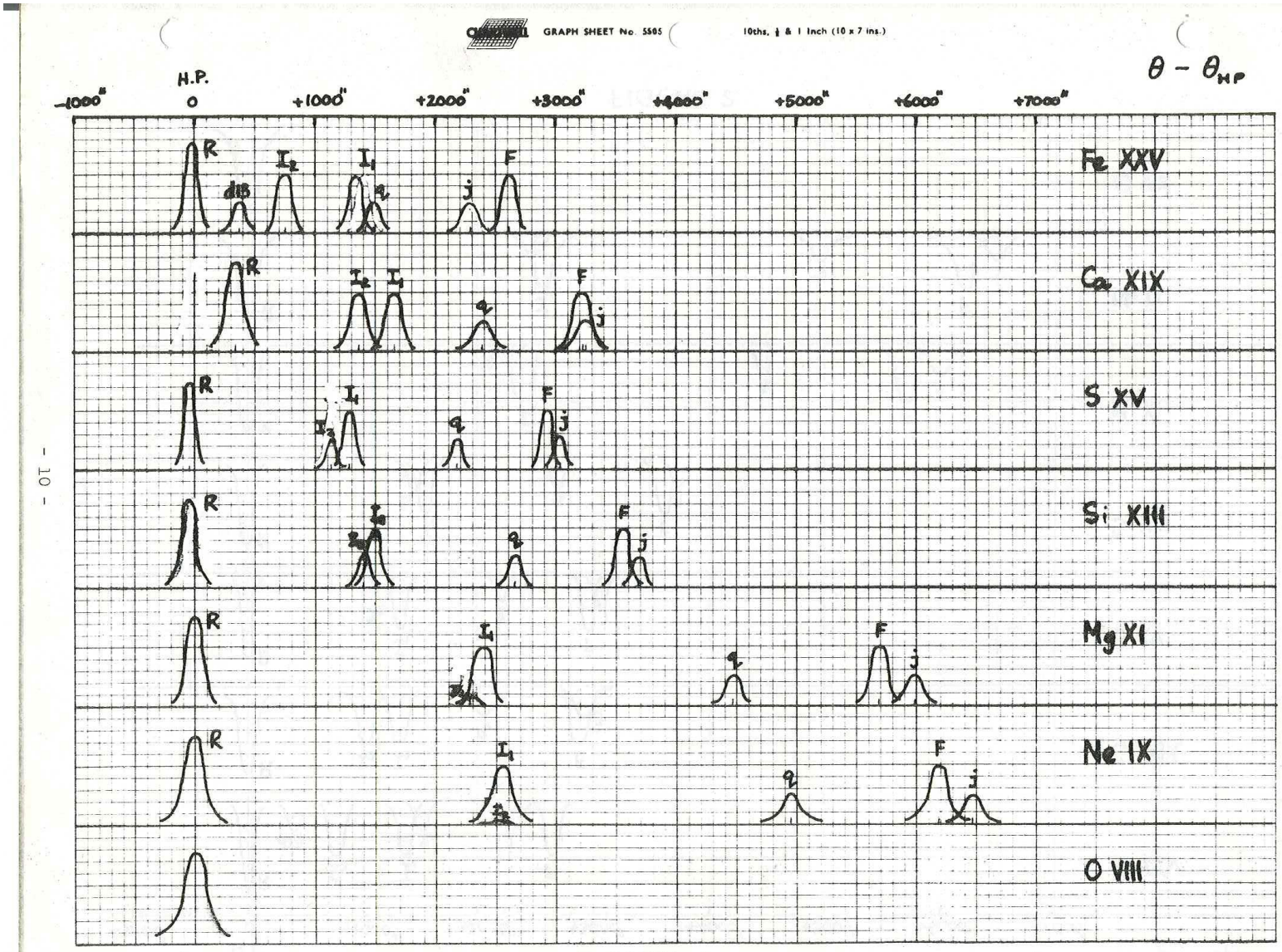
GRAPH SHEET No. 5505
10ths, ½ & 1 Inch (10 x 7 ins.)
H.P.
θ − θHP
−1000"
0
+1000"
+2000"
+3000"
+4000"
+5000"
+6000"
+7000"
Fe XXV
Ca XIX
S XV
Si XIII
Mg XI
Ne IX
O VIII
R
F
I1
I2
I3
dB
j
q

FIGURE 1

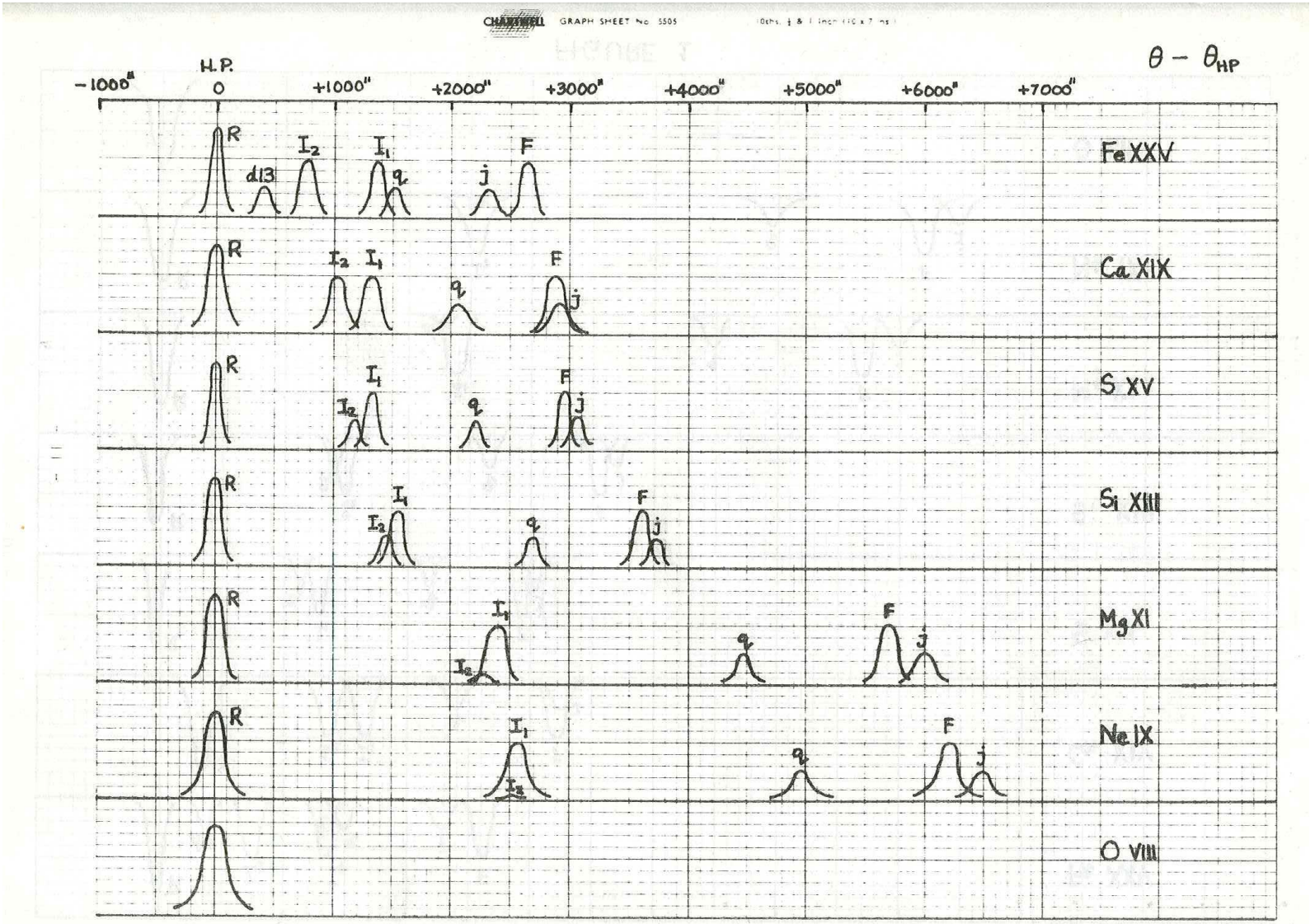
CHANNELL GRAPH SHEET No. 5505
H.P.
θ − θHP
−1000"
0
+1000"
+2000"
+3000"
+4000"
+5000"
+6000"
+7000"
R
d13
I2
I1
q
j
F
Fe XXV
Ca XIX
S XV
Si XIII
Mg XI
Ne IX
O VIII

FIGURE 2

CONVENTIONS USED IN SPECTROSCOPY MODES

In compiling these instrument modes we have adopted several conventions.

1) For Si XIII and high He-like ions the quadrupole intersystem line, I_2, has been included.

2) Wavelengths are taken from the references of p8; however a small uncertainty has been allowed in the wavelength of some lines (e.g. He-like satellite lines).

3) For single active region lines scans extend from one FWHM on one side of the zero velocity wavelength to one FWHM on the other side. Scans have been rounded to an integer number of DGI's or steps.

4) For single flare lines scans extend from $-(600\ \text{km s}^{-1} + 1\ \text{FWHM})$ to $+(100\ \text{km s}^{-1} + \text{FWHM})$.

5) Step numbers refer to B. Kent's computer programme output.

6) UMMID's are used to identify spectroscopy modes as with raster-crystal motions and raster sizes, and are indicated by a 3-field number in square brackets [ ]. The first field indicates general wavelength location (1 = home position, 2 = OVII resonance line, 3 = other); the second whether spectroscopic (0) or integral (1) scan; the third a sequence number.

SPECTROSCOPY MODES

0 SINGLE LINE MODE

0A HOME POSITION [UMMID: 1.0.1]

Crystals fixed at Home Position ($\theta = \theta_H$; step no. 5825)
Peak counts/DGI:

Flare: Ne IX = 6120; Mg XI = 9570; Si XIII = 3320;
S XV = 1620; Ca XIX = 510; Fe XXV = 1540.

Active Region: O VIII = 470; Ne IX = 61; Mg XI = 96;
Si XIII = 18; S XV = 2.

0B O VII POSITION [2.0.1]

Crystals fixed with KAP crystal at O VII resonance line peak (21.602Å; step no. 9040).

Peak counts/DGI for active region: 174.
(It requires 15 DGI = 3.84 sec to skip and stabilise from HP to O VII 21.60Å.)

0C HOME POSITION INTEGRAL SCAN [1.1.1]

Integral scan at rate 3 (80"/DGI) over ± 120" about HP (steps 5813-5837).
Time taken: 3 DGI + 1 DGI flyback = 4 DGI = 1.024 sec.
Total integrated counts:

Flare: Ne IX = 14700; Mg XI = 17700; Si XIII = 5400;
S XV = 1940; Ca XIX = 1060; Fe XXV = 2410.

Active Region: O VIII = 1350; Ne IX = 147; Mg XI = 177;
Si XIII = 29; S XV = 2.

0D O VII INTEGRAL SCAN [2.1.1]

Integral scan at rate 3 (80"/DGI) over ± 120" about O VII resonance line, 21.602Å (step 9040).
Time taken: 3 DGI + 1 DGI flyback = 4 DGI = 1.024 sec.
Total integrated counts for active region: 756.

0E O VII FORBIDDEN LINE INTEGRAL SCAN [2.1.2]

As 0D, but over forbidden line of O VII (22.098Å): steps 9712-9736.
Time taken: 3 DGI + 1 DGI flyback = 4 DGI = 1.024 sec.

0F Fe XVII 15.012Å LINE [3.0.4]

Crystals fixed with KAP crystal at peak of FeXVII 15.012Å line (step no. 1769).

0G FeXVII 15.012Å LINE (INTEGRAL SCAN) [3.1.6]

Integral scan at rate 3 (80"/DGI) over ±120" about FeXVII 15.012Å line (steps 1757-1781). Time taken: 3DGI + 1 DGI flyback = 4 DGI = 1.024 sec.

1. He DENSITY MODE

1A. ACTIVE REGION, ZERO VELOCITY, INTEGRAL SCANS [1.1.2]

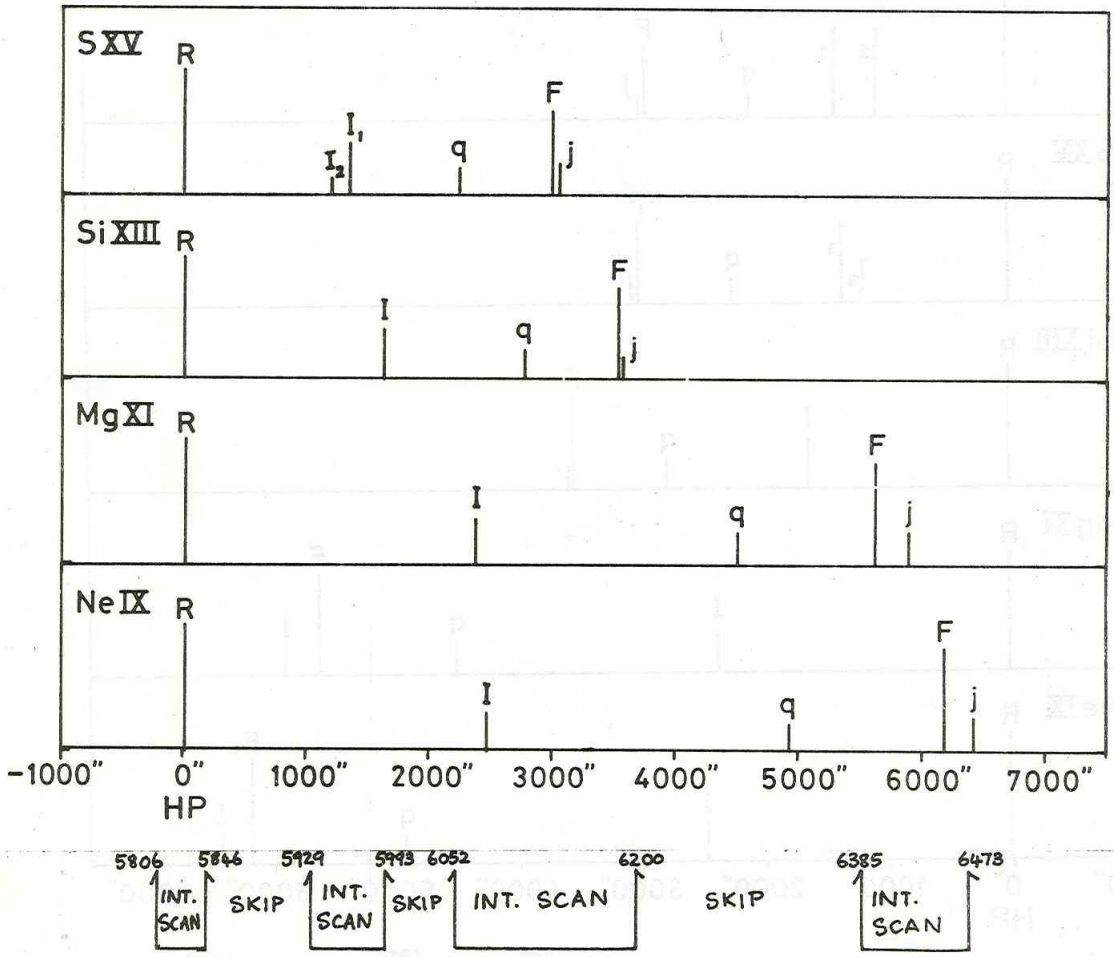

DGI: 10 2 16 2 37 2 22 ⟹ 91

+ 5 flyback
= 96 DGI

With Rate 2 (40"/DGI), total time = 96 DGI
= 24.58 sec.

Integrated counts over entire line for resonance lines of:

S XV = 4; Si XIII = 58; Mg XI = 354; Ne IX = 294.

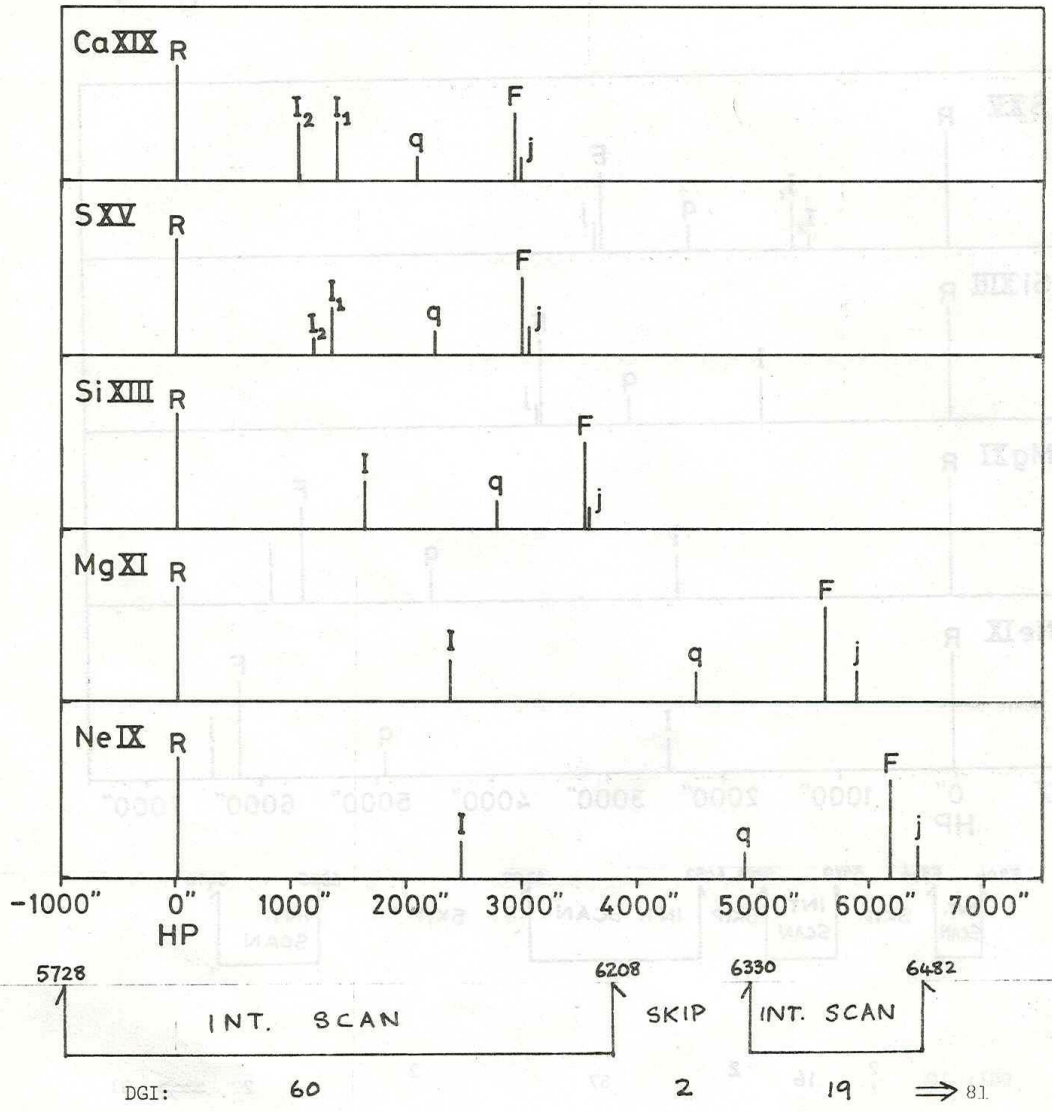

With Rate 3 (80"/DGI), total time = 86 DGI
= 22.02 sec.

Integrated counts in resonance lines of:

Ca = 1060; S XV = 1940; Si XIII = 5400; Mg XI = 17700;
Ne IX = 14700.

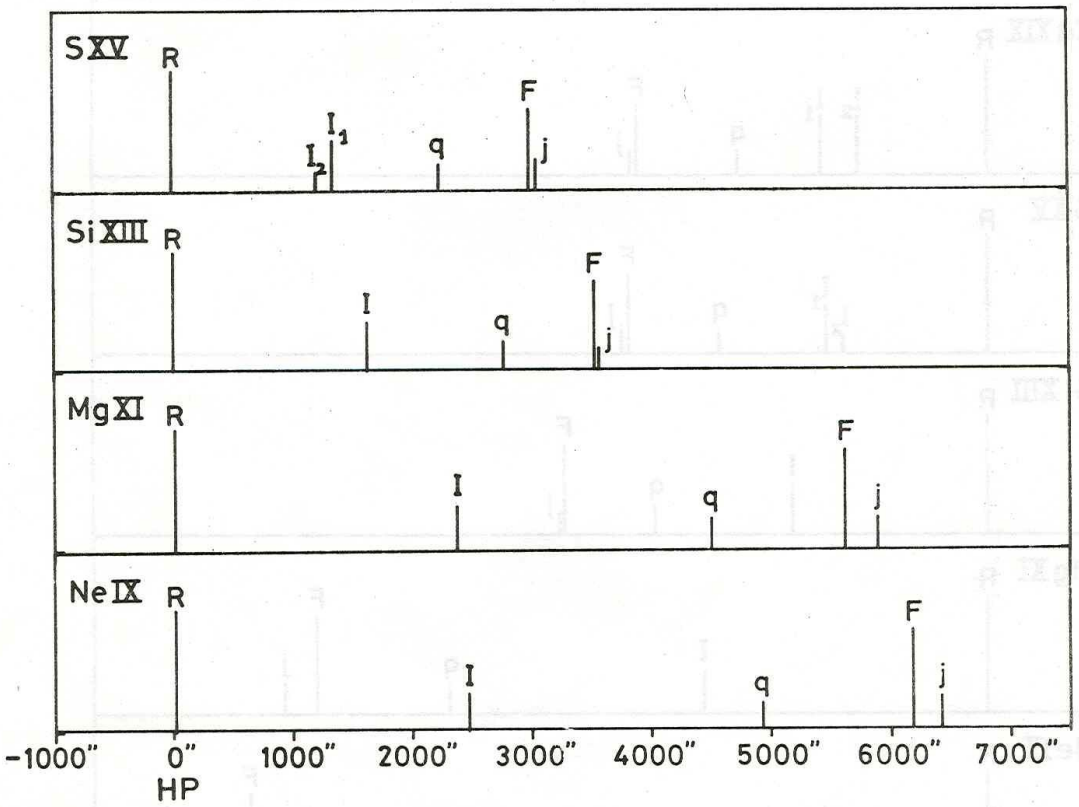

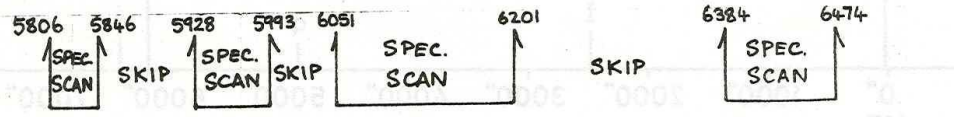

DGI: 9 2 14 2 31 2 19 ⇒ 79

+ 5 flyback
= 84

With 50" steps, total time = 84 DGI
= 21.50 sec.

Counts/DGI at peak of resonance lines of:

S XV = 2; Si XIII = 18; Mg XI = 96; Ne IX = 61.

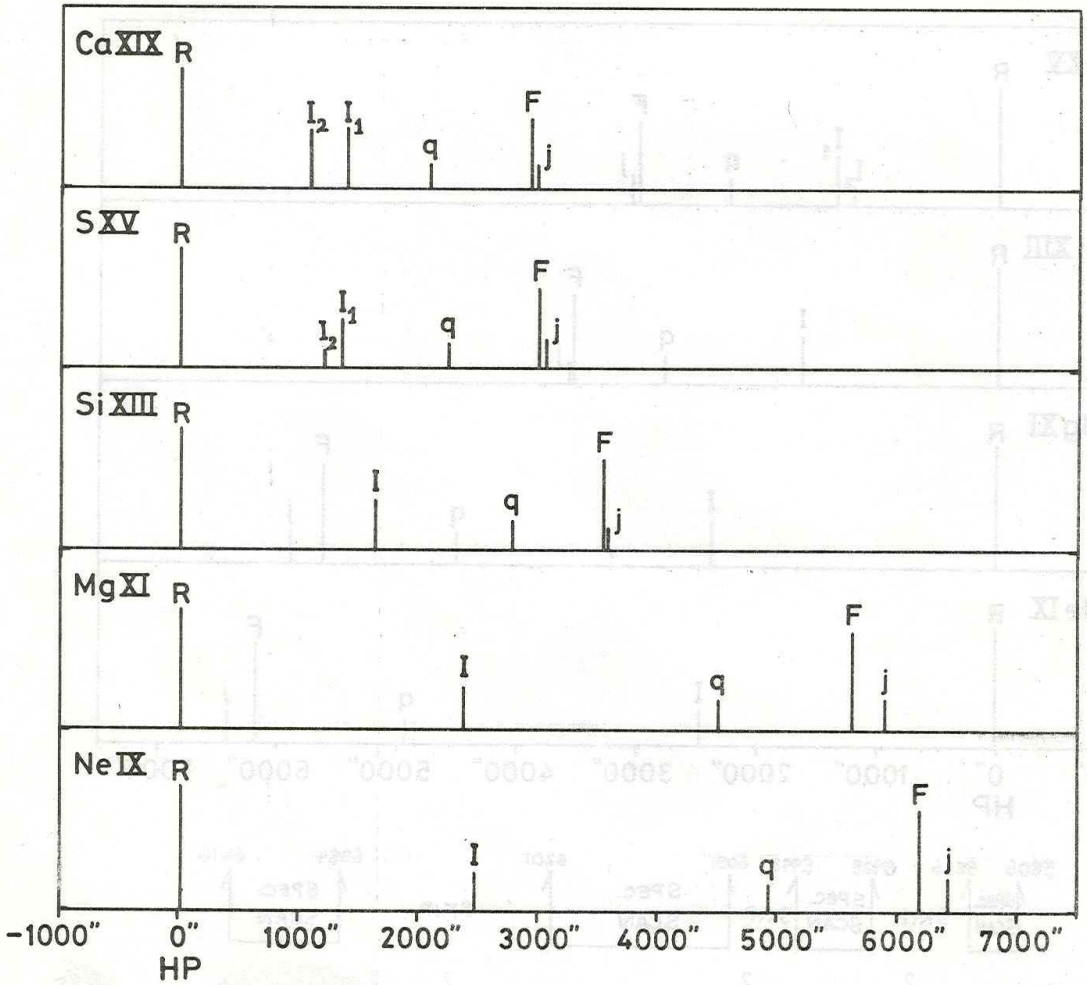

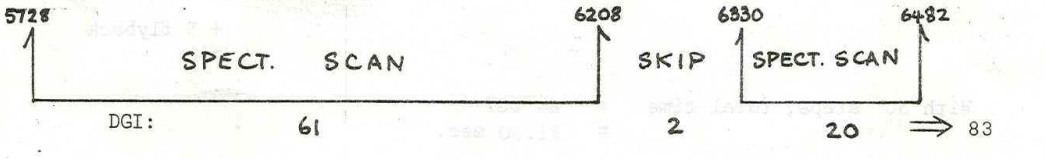

+ 5 flyback
= 88

With 80" steps, total time = 88 DGI
= 22.53 sec.

Counts/DGI at resonance line peaks of:

Ca XIX = 510; S XV = 1620; Si XIII = 3320; Mg XI = 9570;
Ne IX = 6120.

1E O VII MODE [2.0.3]

(i) Scan over O VII R, I, F lines (Active Region)
Spectroscopic scan over region 21.6-22.1Å (steps 9004-9760)
in 10" steps, 1 DGI/position. Time = 757 DGI + 5 DGI
flyback = 3m. 14.82s.

(ii) Scan over O VII R, I, F lines (Flare) [2.0.4]
Spectroscopic scan over region 21.5-22.1Å (steps 8959-9765)
in 10" steps, 1 DGI/position. Time = 807 DGI + 5 DGI
flyback = 3m. 27.87s.

(iii) O VII R, I, F lines (without continuum sample) [2.1.3]

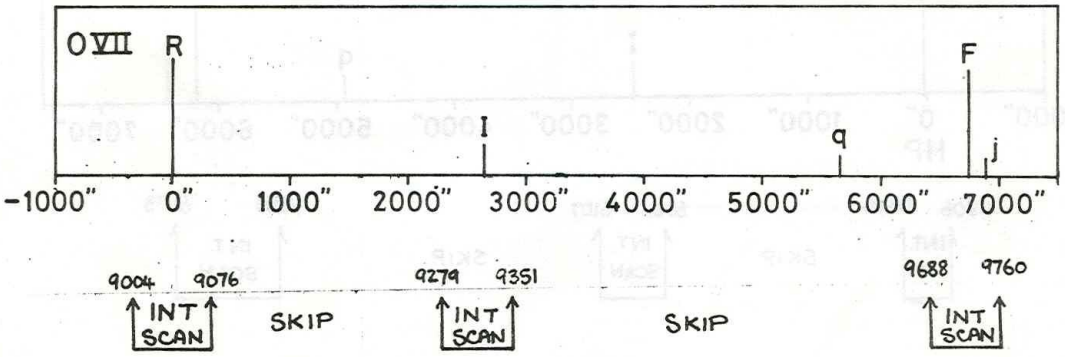

DGI: 9 3 9 3 9 ⟹ 33

+ 5 flyback
= 38

With Rate 3 (80"/DGI), total time = 38 DGI
= 9.73 sec.

Total integrated counts in O VII Resonance Line = 756.

(In diagram line positions are shown relative to O VII resonance line R at 21.602Å, step no. 9040.)

(iv) With continuum sample [2.1.4]

This mode is identical to 3E (iii) except that an integral scan of a region of the continuum between lines I and q is made. This IS will be at Rate 3 (80"/DGI) covering the step range 9004-9760 (21.887Å-21.933Å).
Time taken: 9 DGI (IS, R) + 3 (skip) + 9 (IS, I) + 2 (skip) + 9 (IS, cont.) + 2 (skip) + 9 (IS, F) + 5 (flyback) = 48 DGI = 12.29 sec.

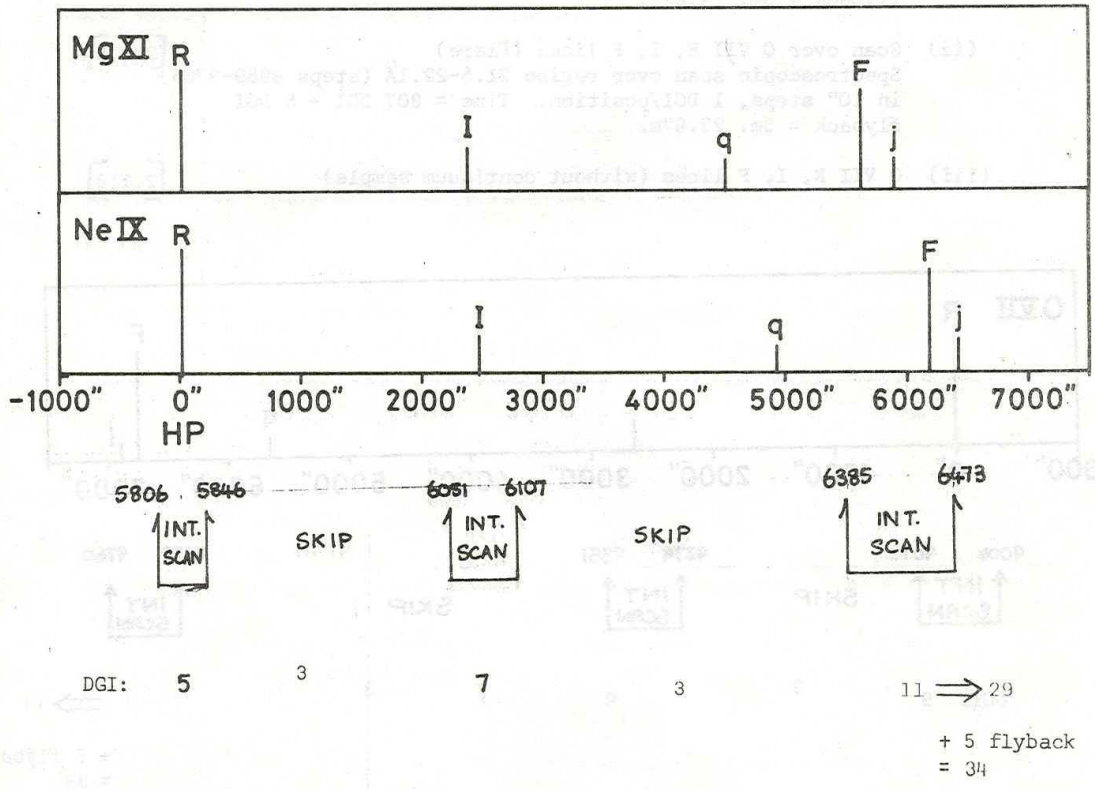

DGI: 5 3 7 3 11 ⟹ 29

+ 5 flyback
= 34

With Rate 3 (80"/DGI), total time = 34 DGI
= 8.70 sec.

Total integrated counts in resonance lines of:

Mg XI = 177; Ne IX = 147.

2. He-LIKE SATELLITES

2A.(i) ACTIVE REGION, FULL SCANS [1.0.4]

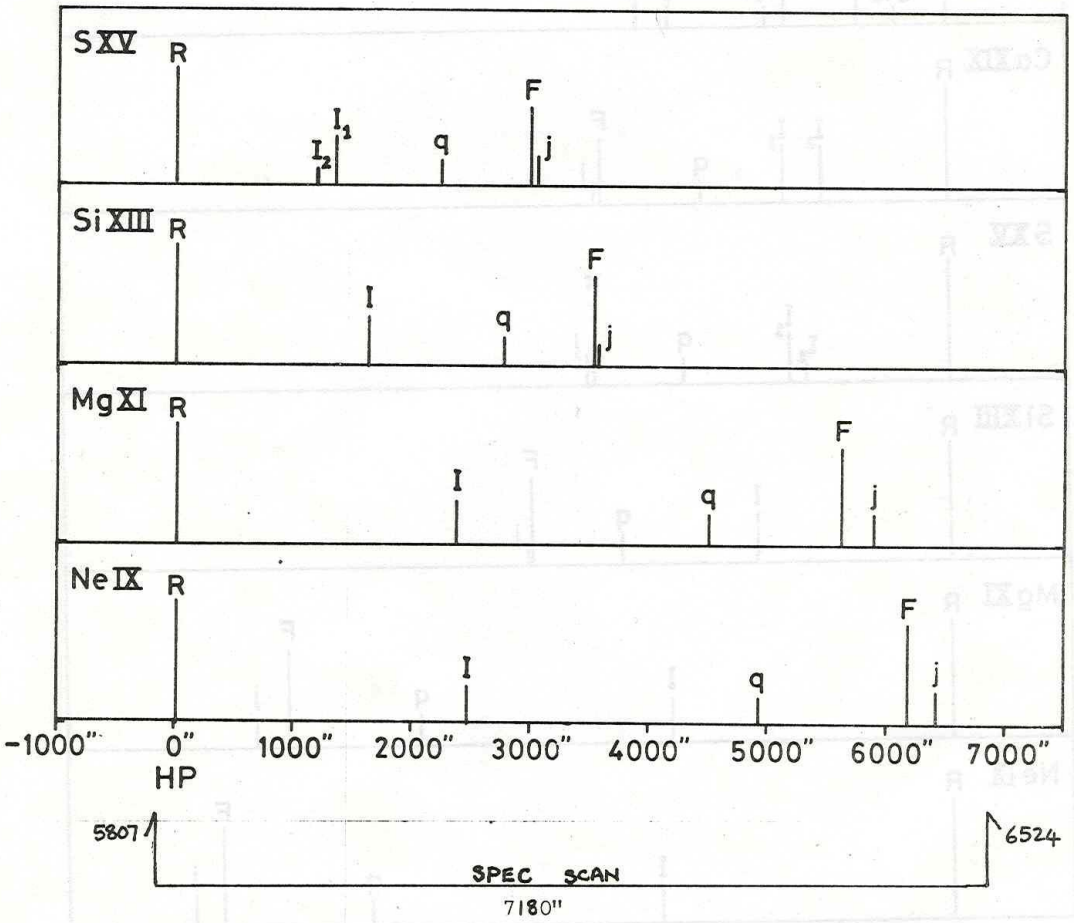

With 10" steps, total time = 718 DGI = +5 DGI flyback = 723 DGI = 3m 5.09s.

2A.(ii) PARTIAL SCAN (skip 1900" section between NeIX R and I) [1.0.5]

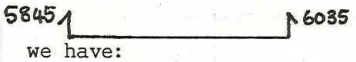

we have:

DGI: 39 2 490 ⟹ 531

+ 5 flyback
= 536

Total time = 536 DGI
= 2 min 17.22 sec.

Peak counts in resonance lines of:

S XV = 2; Si XIII = 18; Mg XI = 96; Ne IX = 61.

2B. (i) He-LIKE SATELLITES, FLARE, FULL SCAN (Ne-Fe) [1.0.6]

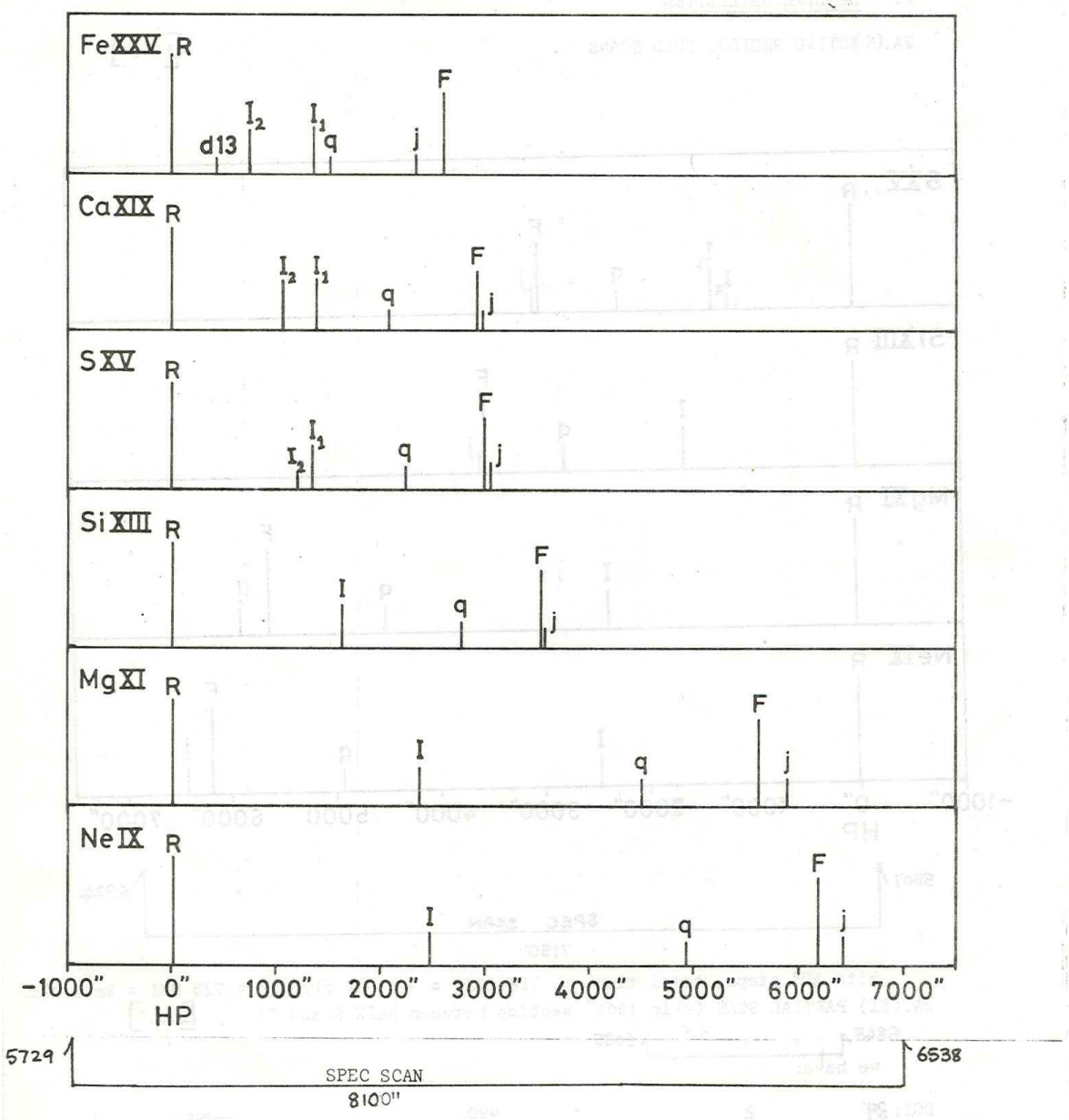

Total time (10" steps) = 810 DGI + 5 DGI flyback = 3 min 28.64 sec.

Peak counts in resonance lines of:

Fe XXV = 1540; Ca XIX = 510; S XV = 1620; Si XIII = 3320; Mg XI = 9570; Ne IX = 6120.

2B. (ii) He-LIKE SATELLITES, FLARE, FULL SCAN (Si-Fe) [1.0.7]

Spectroscopic scan over He-like lines and satellites of Si, S, Ca and Fe; some satellites of Ne and Mg not covered (see 2B(i)).
Scans steps 5729→6226 (10" steps).
Total time = 498 DGI + 4 DGI = 502 DGI = 2m. 8.51s.

2C. He-LIKE SATELLITES, FAST FLARE [1.0.8]

As 2B(ii) but scans at 40" steps.
Total time = 125 DGI + 4 DGI flyback = 129 DGI = 33.02 sec.

2D. Fe SPECTROSCOPIC SCAN [1.0.9]

Scans from steps 5688 to 6176 in 40" steps.
Total time = 123 DGI + 4 DGI flyback = 32.51 sec.
Counts/DGI at Fe XXV resonance line peak = 1540.
Mode intended for Fe XXV + Fe XXIV satellite structure (n≥2).

2E. FAST Fe DIAGNOSTIC [1.1.5]

Integral scans through R, dl3, q, j at Rate 2 (40"/DGI):

limits (steps):	5810 → 5874,	5964 → 5988,	6043 → 6067
scan range:	640" ,	240" ,	240"
IS at Rate 2, DGI:	16 ^{2}	6 ^{2}	6

⇒ 22 DGI
\+ 3 flyback
= 35 DGI

Total time = 48 DGI
= 12.29 sec.

Counts in Fe XXV R = 4820.

For $T_e = T_z = 18.5 \times 10^6$ °K, counts in Fe XXIV satellites are:

j = 3519, q = 1820, dl3 = 897.

2F. DIAGNOSTIC FOR INITIAL FLARE STAGES [3.1.1]

Integral scans through Fe Kβ transitions (not accessed by BCS), Fe XXVI Ly α and Fe XXV resonance line at Rate 4 (160"/DGI). This is a diagnostic of the presence of non-thermal electrons during the initial stages of a flare.

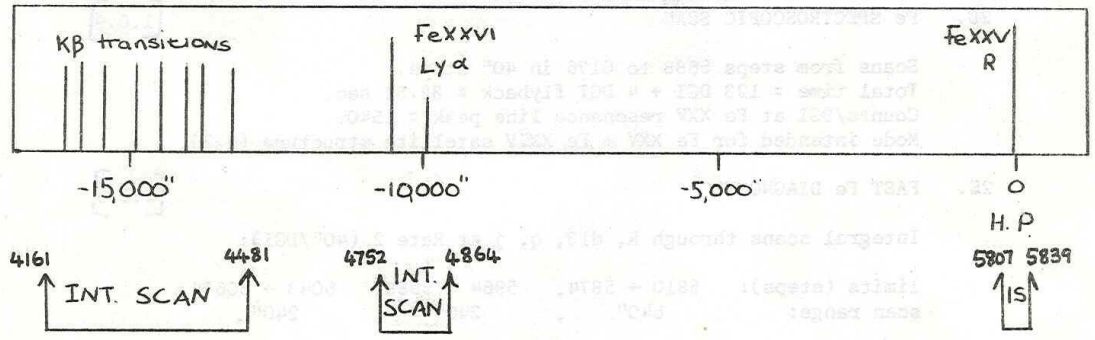

DGI: 20 3 7 5 2

⟹37

\+ 8 flyback

= 45 DGI

Total time = 45 DGI = 11.52 secs.

Counts in Fe XXV R = 600.

3. EMISSION MEASURE

3A. HOME POSITION, INTEGRAL SCAN

(i) Integral Scan, ± 160" at Rate 3 (80"/DGI), centred on Home Position Lines (steps 5809-5841). [UMMID 1.1.6]

Total time = 4 DGI + 2 DGI flyback = 1.536 sec.

Counts for Rate 3 (80"/DGI)

Ion	A.R.	Flare
O VIII	1350	
Ne IX	147	14700
Mg XI	177	17700
Si XIII	29	5400
S XV	2	1940
Ca XIX		1060
Fe XXV		2410

(ii) IS, ± 160" at Rate 4 (160"/DGI), centred on H.P. lines (counts ½ the above values). Total time = 2 DGI + 2 DGI flyback = 1.024 sec. [UMMID 1.1.7]

(iii) Identical to Mode OC. IS, ± 120" at Rate 3 (80"/DGI), centred on H.P. lines (counts as in (i)). Total time = 3 DGI + 1 DGI flyback = 1.024 sec. [UMMID 1.1.1]

(iv) IS, steps 5809-5873 at Rate 4 (160"/DGI) to account for possible Ca XIX R line misalignment. Total time = 4 DGI + 2 DGI flyback = 6 DGI = 1.536 sec. [UMMID 1.1.8]

3B. Fe IONS [UMMID 3.1.2]

Integral scan at Rate 4 (160"/DGI) over range ± 160" about prominent Fe ion lines, 11-15Å. Line widths (FWHM) are 130" for lines observed with KAP, 170" with Beryl (rocking curve >> thermal width).
Line list (in order of increasing crystal shaft rotation angle):

Ion	λ(Å)	Crystal	Steps	$T^{*}_{max}/10^{6}$	N†
Fe XIX	13.491	KAP	338- 370	8	5500
Fe XVIII	14.256	KAP	1046-1110	6.5	13500
Fe XXIV	11.174	Beryl		17	1500
Fe XXIII	11.440	Beryl	1572-1604	15	1150
Fe XVII	15.012	KAP	1753-1785	5	14500
Fe XXII	11.767	Beryl	2196-2228	14	2400
Fe XXI	12.38	Beryl	3424-3456	11	55000**
Fe XX	12.82	Beryl	4363-4395	10	7000

*Temp at which G(T) maximises
†Counts in line at Rate 4 (160"/DGI)
**Mewe's values for line flux/emission measure for this line do not agree with Neupert's OSO-5 observations, where the line is less intense than Fe XX at λ12.82Å.

3B. (Continued)

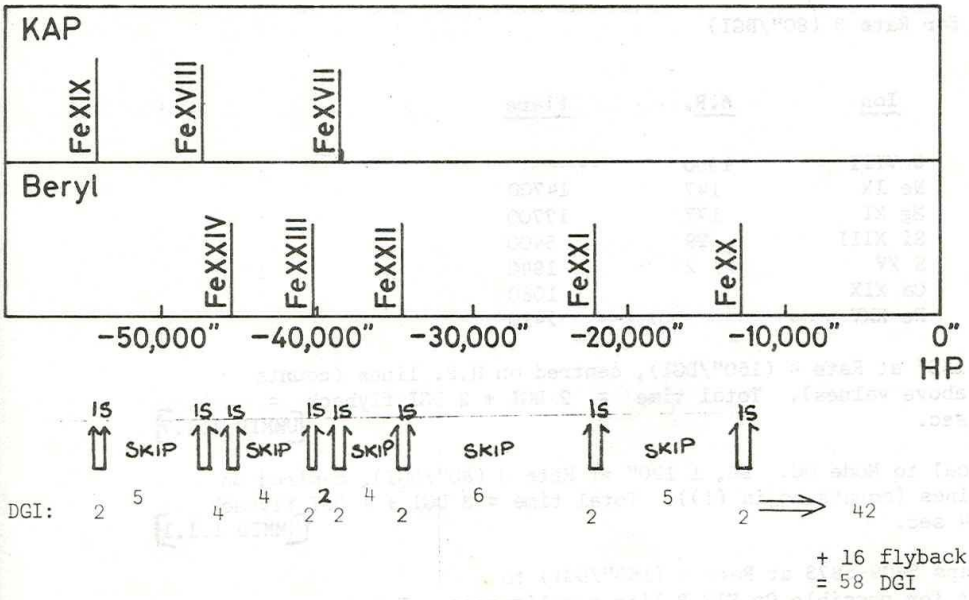

+ 16 flyback
= 58 DGI

Total time taken = 58 DGI = 14.85 sec.

[UMMID 3.1.3]

3C. BATSTONE MODE

Integral scan at Rate 3 (80"/DGI) of principal lines of H-, He- and Ne-like ions.
Line list (in order of increasing crystal shaft angle):

Ion	λ(Å)	Crystal	Steps	FWHM of line profile	Scan Over
Fe XVII	15.012	KAP	1753-1785	136"	320"
Ne X	12.13	Beryl	2910-2966	200	320
Mg XII	8.421	ADP	3180-3236	180	320
Si XIV	6.184	Qu $10\bar{1}0$	4056-4112	160	320
H.P.		All	5803-5875	Up to 240	320
O VII	21.60	KAP	9004-9076	360	640

3C. (Continued)

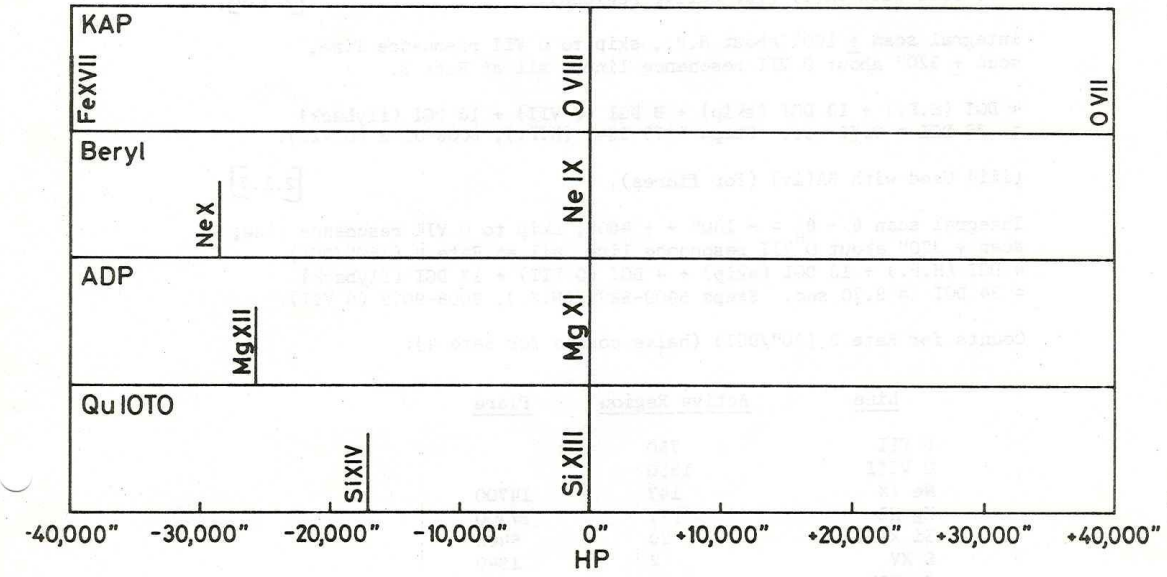

DGI: 4 6 7 3 7 5 7 8 9 13 9

Total time = 80 DGI + 27 DGI flyback = 107 DGI = 27.39 sec.

3D. NARROW G(T) MODE

Needs defining.

3E. O VII MODE

(i) Used independently of 3A. [2.1.5]

Integral scan at Rate 4 (160"/DGI) over ± 320" about O VII resonance lines (λ = 21.602Å). 4 DGI + 2 DGI flyback = 6 DGI = 1.54 sec. Counts (in A.R.) = 378. Steps 9008-9072.

(ii) Used with 3A(i) (for active regions). [2.1.6]

Integral scan ± 160" about H.P., skip to O VII resonance line, scan ± 320" about O VII resonance lines, all at Rate 3.

4 DGI (H.P.) + 13 DGI (skip) + 8 DGI (O VII) + 13 DGI (flyback) = 38 DGI = 9.73 sec. Steps 5809-5841 (H.P.), 9008-9072 (O VII).

(iii) Used with 3A(iv) (for flares). [2.1.7]

Integral scan $\theta - \theta_H$ = - 160" → + 480", skip to O VII resonance line, scan ± 320" about O VII resonance line, all at Rate 4 (160"/DGI). 4 DGI (H.P.) + 13 DGI (skip) + 4 DGI (O VII) + 13 DGI (flyback) = 34 DGI = 8.70 sec. Steps 5809-5873 (H.P.), 9008-9072 (O VII).

Counts for Rate 3 (80"/DGI) (halve counts for Rate 4):

Line	Active Region	Flare
O VII	760	
O VIII	1350	
Ne IX	147	14700
Mg XI	177	17700
Si XIII	29	5400
S XV	2	1940
Ca XIX		1060
Fe XXV		2410

3F. FAST BATSTONE MODE [3.1.4]

As 3C, omitting O VII.

At Rate 3 (80"/DGI):

Fe XVII 4 skip 6 Ne X 7 skip 3 Mg XII 7 skip 5 Si XIV 7 skip 8 H.P. 9 ⟹ 56

+ 16 DGI flyback

= 72 DGI

Total time = 72 DGI = 18.43 sec.

4. SPECTROSCOPIC ATLAS

4A. (i) Active Region. The entire spectral range cannot be observed at reasonable count rates in a time less than the time for changes in the emitting plasma. We choose to cover a limited spectral region at a time observing a single source, and to normalise these pieces of the spectrum by frequent observations at the Home Position. The program will take 3+ orbits. Each orbit should start with a 4' x 4' raster with 15" steps to find the brightest point in the Home Position line for the temperature range to be emphasised - initially O VIII.

Then a spectral scan would start with smallest crystal position thus far unobserved by this program at 4 DGIs per 10" step. Every 2 minutes, a slew would be made to the Home Position, where we perform a 2-second integral scan at Rate 1 (20"/DGI) to normalise for evolution of the source. After slewing back to the last crystal position previously scanned, the scan is continued for another 2 minutes, etc, etc.... Every fifth Home Position normalisation (∿ every 10 minutes), would be followed by a 30" x 30" brightest point find (BPF) raster, followed by a change of pointing, to correct for spatial evolution of the source. The normalisation integral scan over the Home Position would precede the resumption of the spectral scan for another 5 cycles.

The total time is thus 1 hr. 1 min 31.6 sec and 8.35° of crystal motion are covered. The number of crystal positions per SS can be modified to fit into the varying daylight portion of the orbit. Changing the number of points of the SS by 1 changes the duration by 25 seconds. The entire spectral range of 28° would be covered in 3.36 orbits. The same program with 3 DGIs per 10" could cover 11.1° per orbit and be completed easily in 3 orbits. The time-line below indicates the sequence to be used. To fit into short observing periods, between SAA and night, the program could be terminated at the arrow. [UMMID 3.0.2]

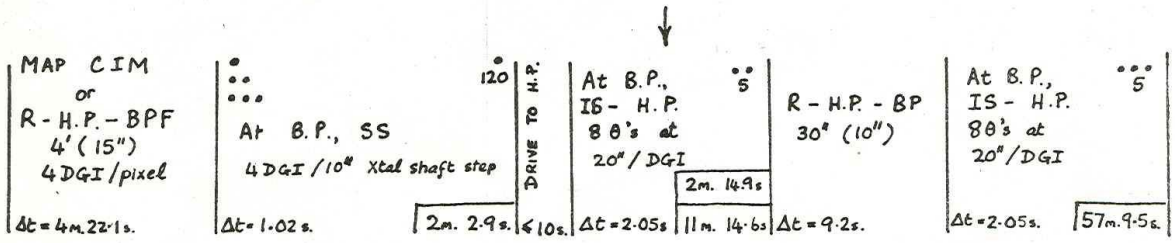

(ii) The same program should be repeated to chart the flare spectrum. In this case, the program would be initiated by the HXIS or BCS FF, and would be interrupted 4:30; before sunset to perform another "MAP". A later version of this program would stop automatically if the intensity at the H.P. during the normalisation fell below a specified minimum. [UMMID 3.0.3]

4B. SPECTROSCOPIC ATLAS - FULL SCAN [UMMID 3.0.5]

Spectroscopic scan over full (normal) range in 50" steps, 2 DGI/position (steps 0 - 10195). Time taken: 4080 DGI + 36 DGI flyback = 4116 DGI = 17 m. 33.70 s.

4C. SPECTROSCOPIC ATLAS - EXTENDED RANGE (FeXVII BRIGHT POINT) UMMID 3.0.6

Spectroscopic scan over extended range, first the lower part (steps -300 to 0) in 50" steps, 4 DGI/position; skipping the normal range (steps 0 - 10195); then scanning the upper range (steps 10195 - 13450) in 50" steps, 4 DGI/position; flying back to FeXVII 15.012Å line (KAP crystal; step 1769) and dwelling at this position for 20 DGI. Total time: 244 DGI (SS) + 36 (skip) + 2608 (SS) + 41 (FB) + 20 (dwell) = 2949 DGI = 12 m. 34.94 s. This mode will be used in early operations with an FeXVII 15.012Å raster performed to locate the bright point. (A crystal motion from this line to step -300 take 9 DGI.)

5. TEMPERATURE [3.1.5]

5A. O VIII Lyα/Lyβ

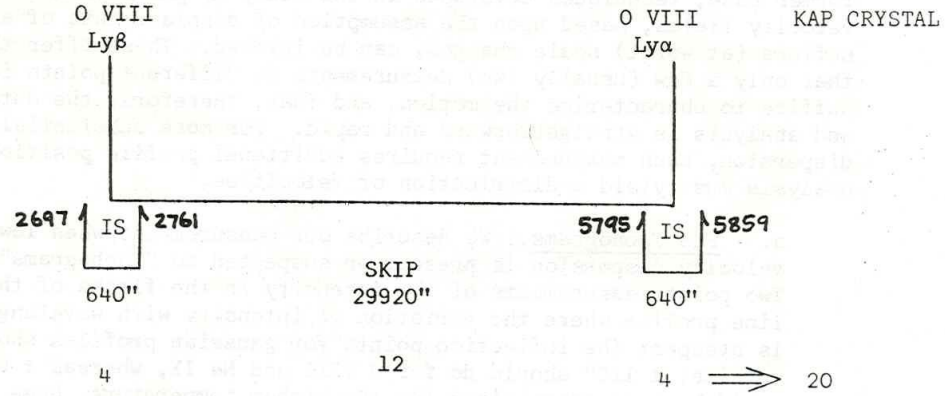

DGI: 4 12 4 ⟹ 20

+ 13 flyback
= 33 DGI

Total time = 33 DGI = 8.45 secs.

Integral scan at Rate 4 (160"/DGI) ± 320" about both lines.
For active regions, total counts in Lyα = 675, in Ly β = 70.

5B. H-LIKE : He-LIKE

5C. SATELLITES TO ls3p, ls4p

5D. Lyα SATELLITES

5E. RESONANCE LINE SATELLITES WITH n = 3, 4

6. ABUNDANCES

6A. RELATIVE ABUNDANCES

Uses lines with similar $G(T_e)$'s.

6B. ABSOLUTE ABUNDANCES

Works with line to continuum ratio. Will we see a real continuum?

7. VELOCITY MODES

Two different types of velocity measurements can be envisaged: those of plasma with a reasonably well defined mean velocity - that is differential velocities within the emitting gas significantly less than the ion thermal speed - and those for which supersonic velocities are present and for which

7. (Continued)

we can anticipate multiple components in the emission line spectrum. In the former case, techniques developed in the study of photospheric and chromospheric velocity fields, based upon the assumption of displacements of a profile which suffers (at worst) scale changes, can be invoked. These offer the advantage that only a few (usually two) measurements at different points in the profile suffice to characterise the motion, and that, therefore, the data acquisition and analysis is straightforward and rapid. For more substantial velocity dispersion, each measurement requires additional profile positions and the analysis must yield a distribution of velocities.

a. FCS Tachograms. We describe our measurements when low velocity dispersion is present or suspected as "Tachograms". Two point measurements of the intensity in the flanks of the line profile where the variation of intensity with wavelength is steepest the inflection points for gaussian profiles should suffice; ± 110" should do for O VIII and Ne IX, whereas ± 60" would be more appropriate for the higher temperature, home position lines ± 160" should do for O VII. Since we (currently) require one DGI for the crystal mechanism to stabilise after a motion of more than 150", the minimum time per pixel is 4 DGIs of which only 2 are considered clean. Therefore, we normally consider 2 DGIs per crystal position to improve the duty cycle (so a total of 6 DGI). (For the ± 60" observations, it is possible this time can be reduced.) This mode of operation is denoted 7.T.S. ("Tachogram Spectroscopic"). To be actually programmed (and analysed), we must specify θ initial, delta θ, the number of DGIs of dwell per θ, and the number of DGIs for stabilisation. For normal planning purposes, we adopt the fastest, yet most conservative, time: 6 DGI = 1.54 sec. Putting aside for the moment the ambiguity of the number of DGIs required for stabilisation of the crystal, a more complete specification of the mode is possible by appending the number of DGIs of dwell and the central crystal position; eg, 7.T.S.4 - O VII.

We can economise the time required for stabilisation between the two crystal positions for the larger angular steps by performing an integral scan. For example, a four-DGI integral scan at Rate 3 (80"/DGI) would scan ± 160". The 1 DGI flyback still appears necessary. By adding the first two and the last two DGIs, the two resulting measurements correspond to the UVSP's "dopplergram" mode. This mode is denoted: 7.T.I.N, where N can only take the values 2, 4, or 8 in the present case, and for which the time per pixel would be 4, 8, or 16 DGIs (+ 1 for the flyback, if required).

7. (Continued)

Sample tachograms for total dwell time on lines = 4 DGI
(UMMID's are for Home Position tachograms.)

Spectroscopic Scans (Mode: 7.T.S.4):

	[1.0.10]	[1.0.11]	[1.0.12]
Total spectral scan Δθ	± 60"	± 110"	± 160"
No of steps	12	22	32
Lines for which suitable	high-T Lines Res lines	O VIII, Ne IX	O VII Res line
Dwell time on line profile (DGI)	4	4	4
Total skip and flyback times (DGI)	0	1	2
Sum (DGI)	4	5	6

Integral Scans (Mode: 7.T.I.4):

	[1.1.10]	[1.1.11]
Total spectral scan Δθ	± 80"	± 160"
No of steps	16	32
DGIs on line profile	2	4
Total skip and flyback times (DGI)	1	2
Sum (DGI)	3	6

b. Higher Velocity Modes. To consider more complex velocity distributions, we consider more detailed profiles, with four spectral resolutions: "Coarse", "Low", "Medium" and "High"; each one having twice as many wavelength intervals as the preceding. For planning purposes, we restrict the many possible ranges of wavelength to two: 640" (which corresponds roughly to velocities of ± 100 km/sec in all of the channels, the "Quiet" corona) and 1280" (which we choose to deploy asymmetrically, + 100/-600 km/sec, the "Explosive corona"). As for the tachogram modes, the stabilisation time following a large crystal motion can be avoided (it appears) by performing integral scans, a series of smaller crystal motions. In addition, for "Coarse" spectral resolution programs where the step size becomes comparable to the line width, the integral scan program ensures that emission components are not missed. To make the spectroscopic scan and integral scans easily comparable, for planning purposes as well as for analysis, we choose the spectral increments for the spectroscopic scans to correspond to the interval covered by an integral scan in one DGI. The times per pixel for the various velocity modes described here are shown in the accompanying table. These modes are referred to in the JOS timelines by their resolution (C, L, M, or H) their velocity coverage (Q or E) and the type of crystal motion (I or S): eg, 7.L.E.I. takes no longer than 7.L.Q.S. because of the toll taken by the stabilisation requirement.

Finally, although we tend to concentrate on the Home Position and O VII lines when formulating observing plans, the presence of blended, temperature dependent, satellites of the Helium-like resonance will greatly complicate the use of these lines as velocity diagnostics. A fluctuation in the intensity of the satellite will be difficult to distinguish from the fluctuation in the emission at the corresponding velocity. The iron lines used in spectral program 3B may provide attractive alternatives.

7. (Continued)

RESOLUTION:	HIGH	MEDIUM	LOW	COARSE
Spectral Scan $\Delta\theta$	20"	40"	80"	160"
Stabilisation time (DGI)	0	0	1	1
Integral Scan Rate	1	2	3	4

QUIET - SUN VELOCITIES: Total θ range = 640" (vely: ± 100 km/sec)
(flyback time = 2 DGI)

No of spectral locations	33	17	9	5
Spectroscopic scan time in DGI (seconds)	35(8.96)	19(4.86)	19(4.86)	11(2.82)
UMMID	1.0.15	1.0.16	1.0.17	1.0.18
Integral scan time in DGI (seconds)	34(8.70)	18(4.61)	10(2.56)	6(1.54)
UMMID	1.1.15	1.1.16	1.1.17	1.1.18

EXPLOSIVE - TYPE VELOCITIES: Total θ range = 1280" (vely = + 100 to - 600 km/sec)
(Flyback time = 2 DGI)

No of spectral locations	65	33	17	9
Spectroscopic scan time in DGI (seconds)	67(17.15)	35(8.96)	35(8.96)	19(4.86)
UMMID	1.0.19	1.0.20	1.0.21	1.0.22
Integral scan time in DGI (seconds)	66(16.90)	34(8.70)	18(4.61)	10(2.56)
UMMID	1.1.19	1.1.20	1.1.21	1.1.22

(UMMID's are for Home Position Modes.)

8. DENSITY

8A. Fe XXI LINE RATIOS 3.0.1

A list of 15 lines, many of which are sensitive to electron densities, is given for Fe XXI at λ = 12.25-12.62Å by Mason et al. (A & A 73, 74, 1979). The wavelengths of these lines are taken from Bromage and Fawcett (M.N. 178, 605, 1977), but in some cases are not expected to have an accuracy adequate for establishing line blends in this particularly crowded region of the spectrum. This mode is designed for use early in the Mission so that the data may be analysed for detailed line identifications. After the Fe XXI lines have been positively identified, a further mode will be devised which speeds up scans between lines, so that rapid diagnoses of flare plasmas can be made.

The mode consists of a spectroscopic scan over the range 12.10-12.77Å (step nos. 2868-4269), 10" (1 step) intervals. Time taken: 1401 DGI + 7 DGI flyback = 1408 DGI = 6m. 0.45s.

8B. O VII I/F RATIO - See 1E.

8C. Ne IX AND Mg XI I/F RATIO - see 1F.

9. INSTRUMENT TESTING

9A. LOCATING HOME POSITION 1.0.23

Seventeen-point spectroscopic scan across expected home position (step 5825), 50" steps, 2 DGI/position, i.e. over steps 5785 - 5865. Time taken: 34 DGI + 2 DGI flyback = 36 DGI = 9.22 seconds.

9B. CaXIX FCS/FCS 1.0.24

Spectroscopic scan in 50" steps across expected CaXIX R position plus all satellites. Step nos. 5710 - 6410. Time taken: 141 DGI + 5 DGI flyback = 146 DGI = 37.38 secs.

9C. FeXXV FCS/BCS CROSS-CALIBRATION 1.0.25

As 9B but for FeXXV. Steps nos. 5670 - 6295. Time taken: 126 DGI + 5 DGI flyback = 131 DGI = 33.54 secs.

G(T) FUNCTIONS FOR INTENSE LINES

Date: May 2, 1978

Compiler: K. Phillips

Source: R. Mewe, Solar Phys. 22, 459 (1974).

Two plots are depicted of the function G(T), defined by:-

$$G(T) = \frac{n_{ion}}{n_{element}} \frac{e^{-W/kT}}{T^{\frac{1}{2}}} P(W/kT)$$

where W = excitation energy, $n_{ion}/n_{element}$ from ionization - equilibrium calculations, and P a slowly varying function of T defined in van Regemorter's paper (Ap. J. 136, 906, 1962). The values are from Mewe's paper.

The two plots are for:

(a) lines at the FCS home position and for the O VII line at 21.60 Å;

(b) some other intense lines in the FCS wavelength range.

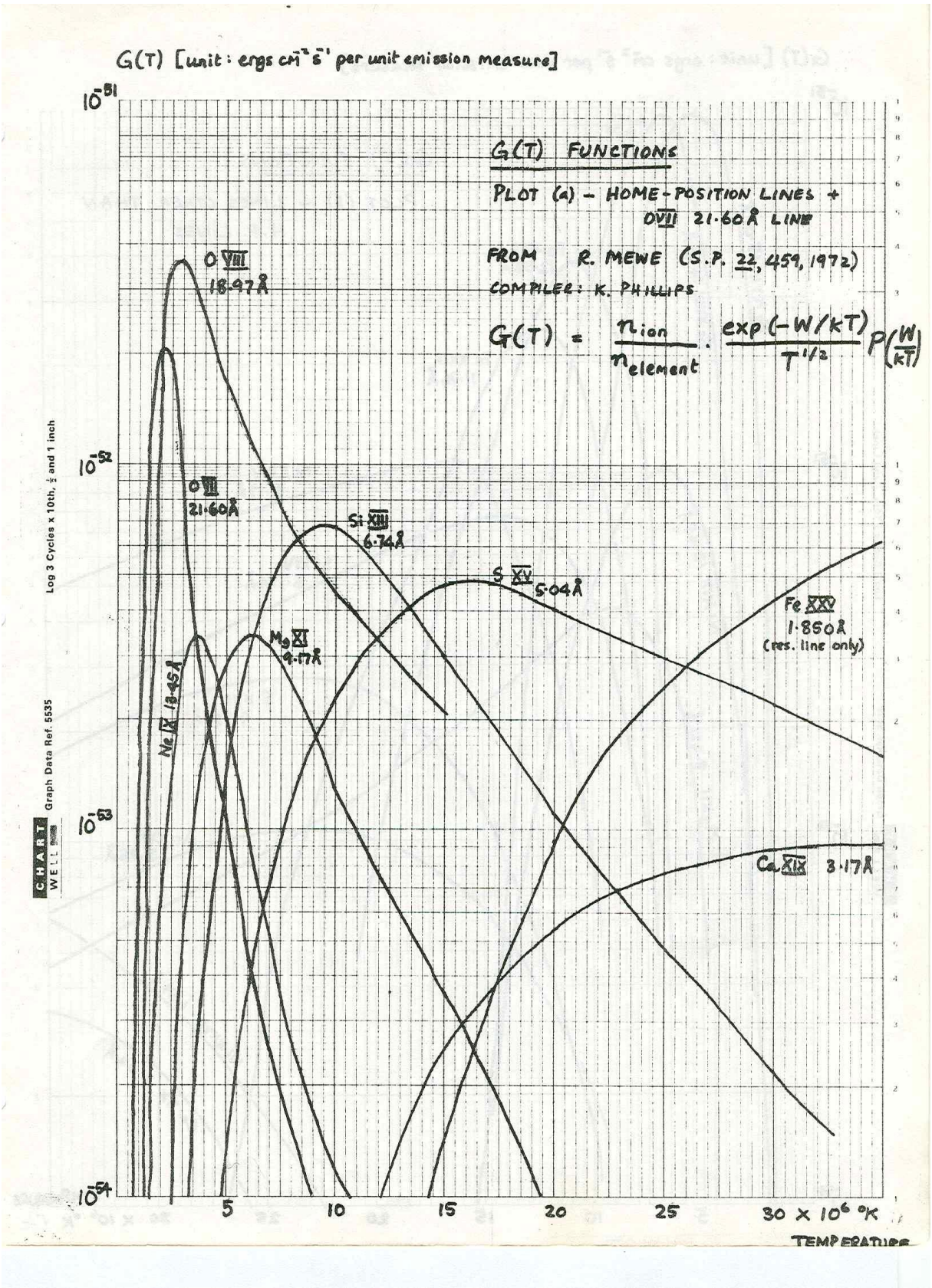
G(T) [unit: ergs cm⁻² s⁻¹ per unit emission measure]
G(T) FUNCTIONS
PLOT (a) – HOME-POSITION LINES + O VII 21·60 Å LINE
FROM R. MEWE (S.P. 22, 459, 1972)
COMPILER: K. PHILLIPS
G(T) = (n_ion / n_element) · exp(−W/kT) / T^1/2 P(W/kT)
O VIII 18·97 Å
O VII 21·60 Å
Si XIII 6·74 Å
S XV 5·04 Å
Mg XI 9·17 Å
Ne IX 13·45 Å
Fe XXV 1·850 Å (res. line only)
Ca XIX 3·17 Å
10⁻⁵¹
10⁻⁵²
10⁻⁵³
10⁻⁵⁴
5
10
15
20
25
30 × 10⁶ °K
TEMPERATURE
Log 3 Cycles x 10th, ½ and 1 inch
CHART WELL
Graph Data Ref. 5535

G(T) [unit: ergs cm^{-2} s^{-1} per unit emission measure]

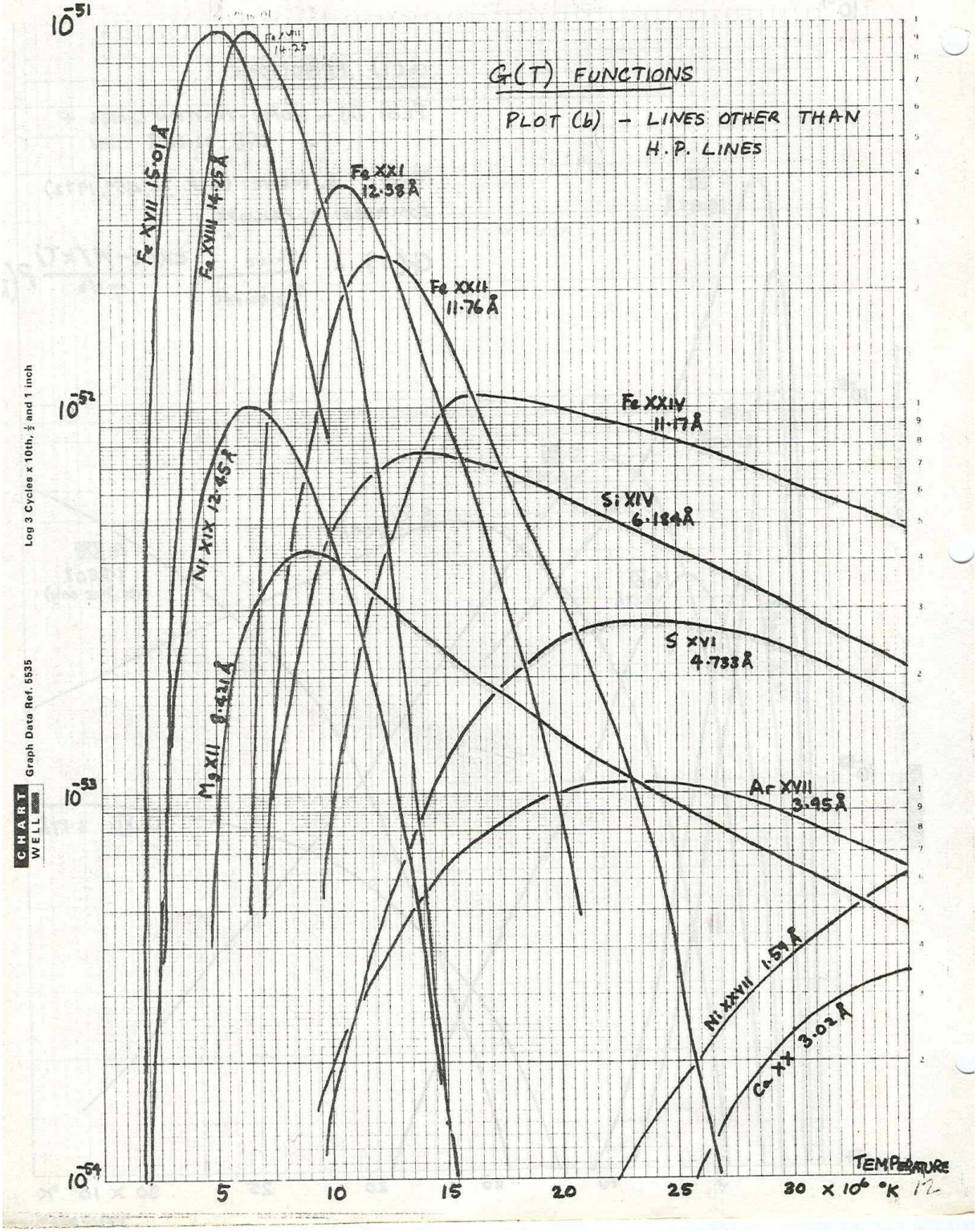

KTS 12 cm/s

O VIII

3 Cycle by 4 Cycle Log-Log

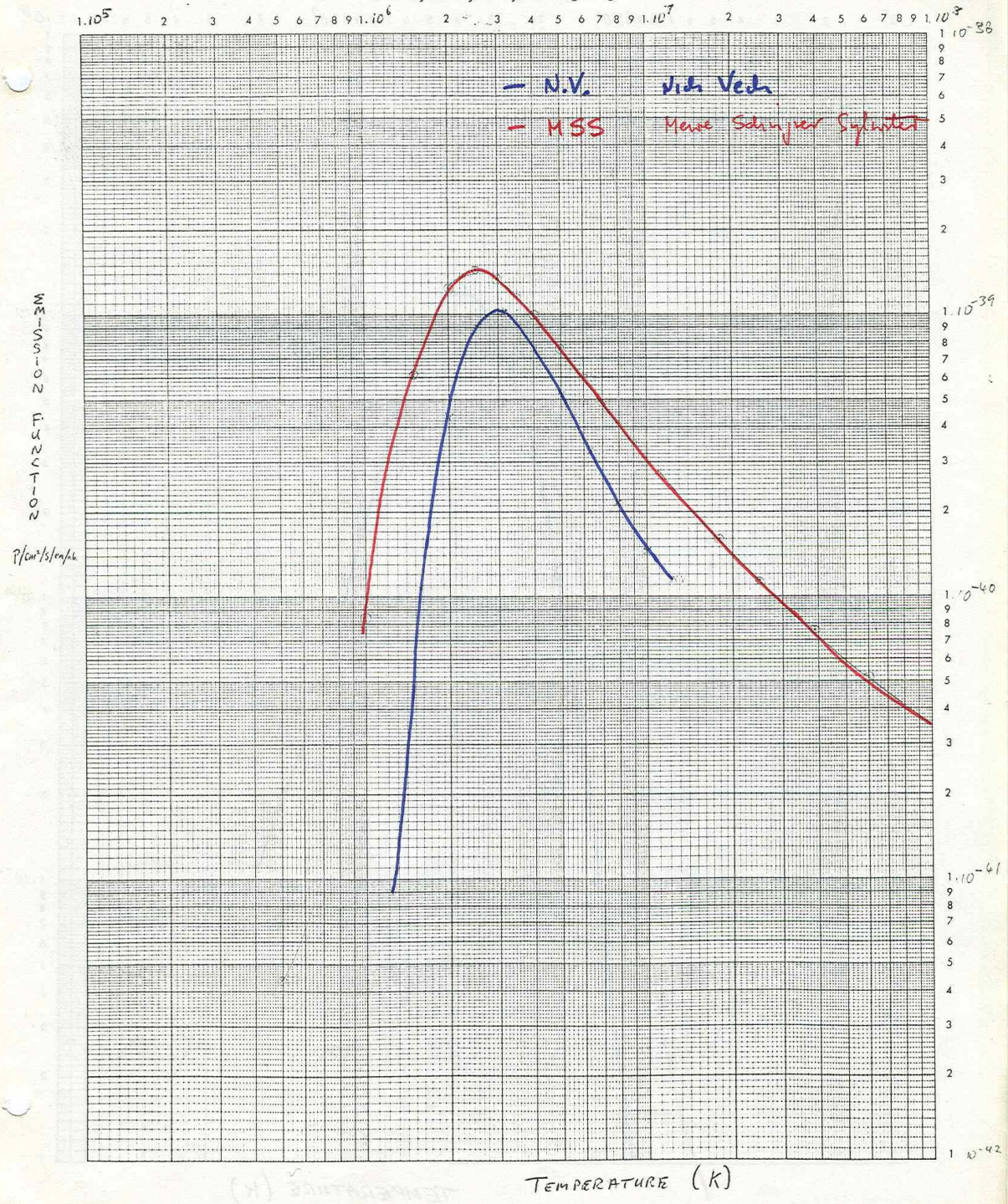

KTS, 12 JUNE 81

Ne IX

3 Cycle by 4 Cycle Log-Log

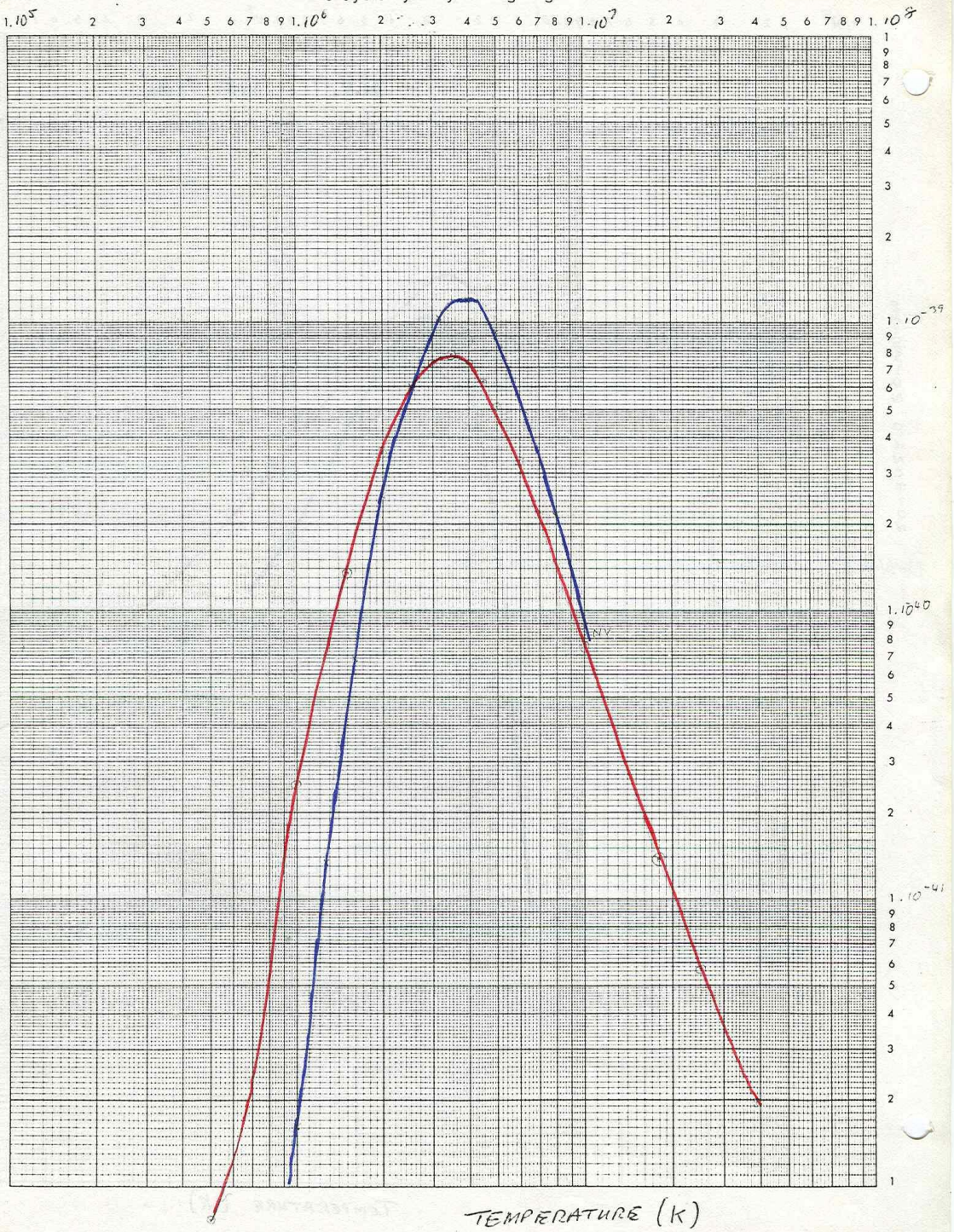

Mg XT

RTS 12 JAN 91

3 Cycle by 4 Cycle Log-Log

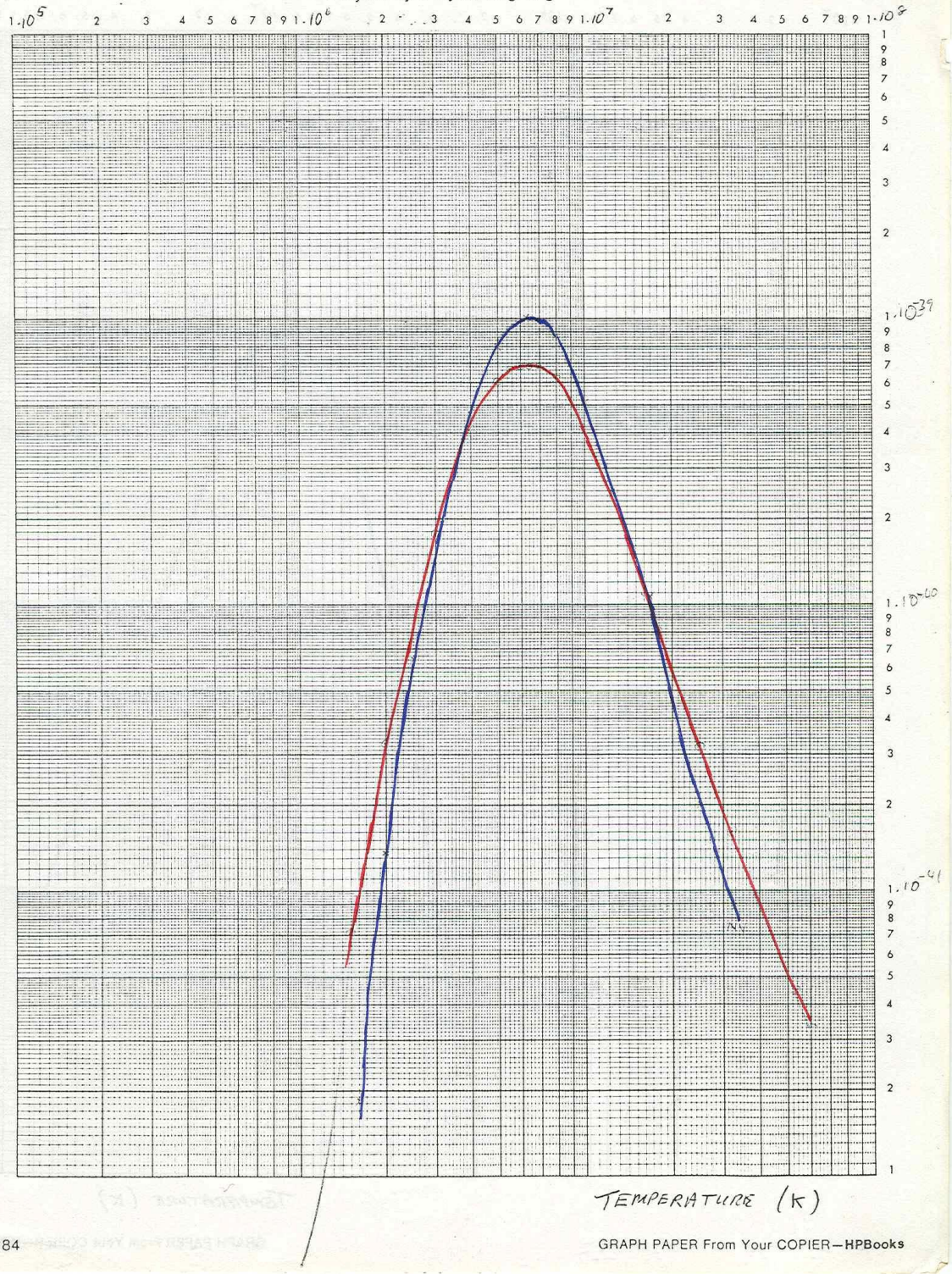

Si XIII

3 Cycle by 4 Cycle Log-Log

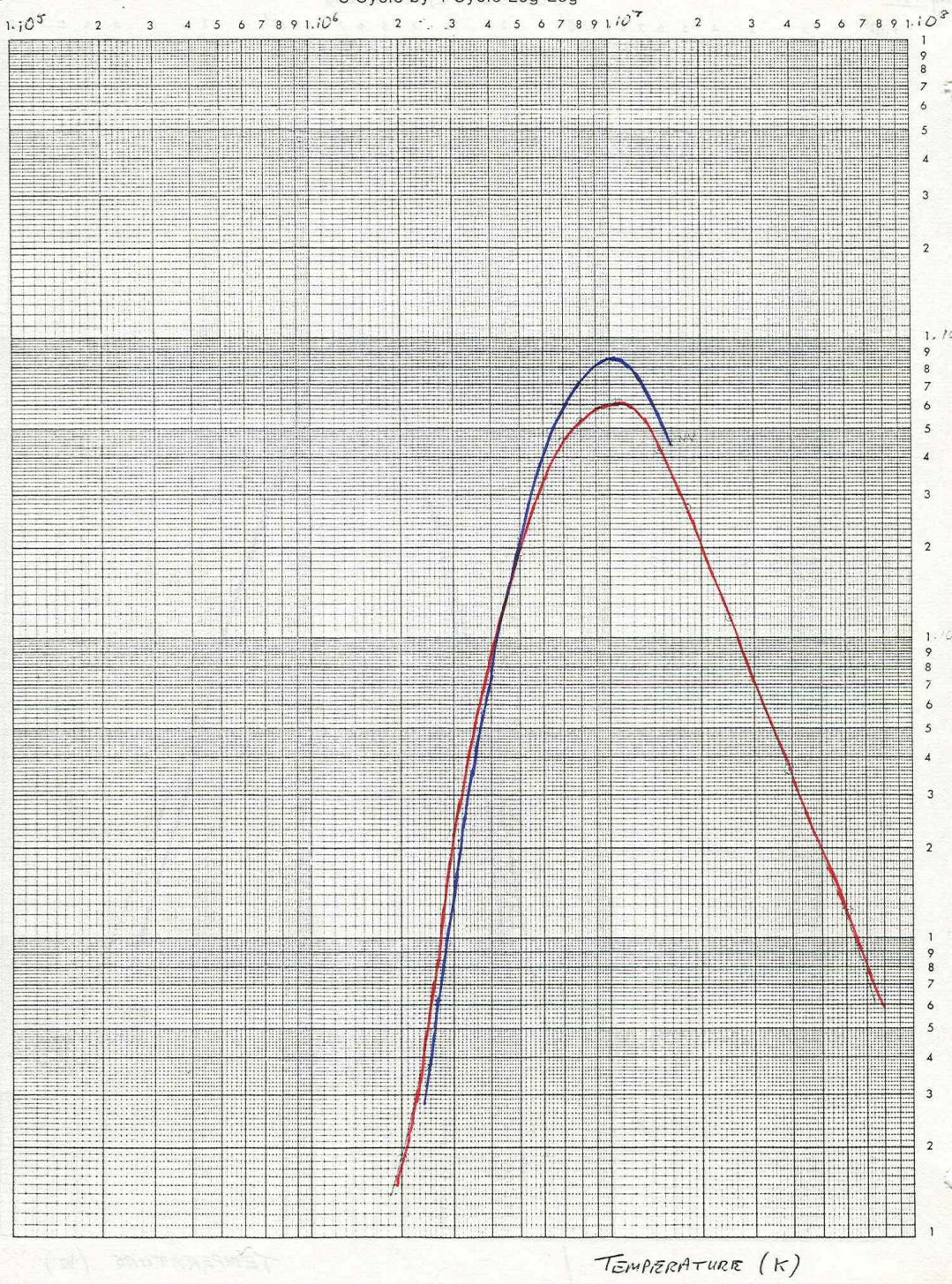

S XV

3 Cycle by 4 Cycle Log-Log

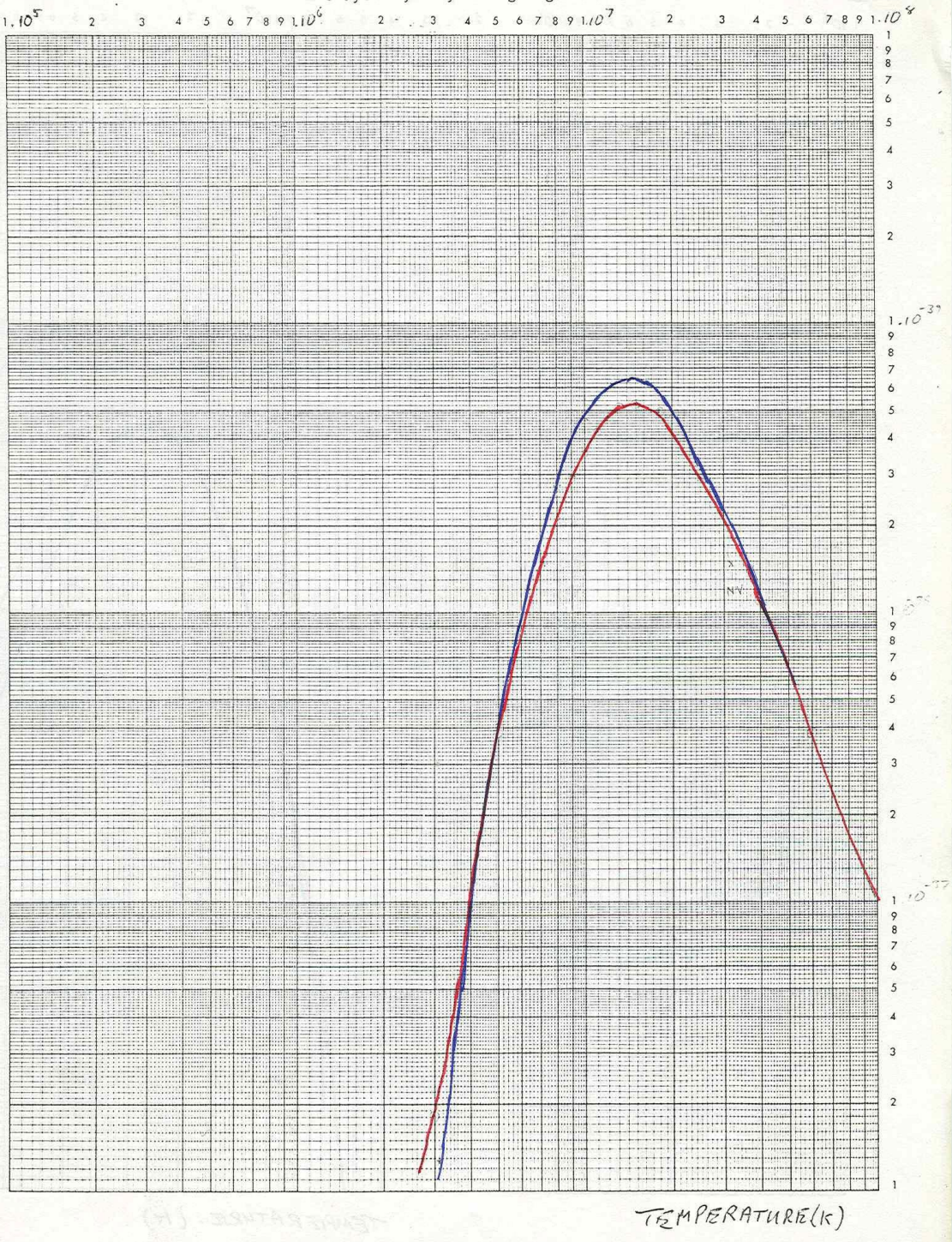

Ca XIX

3 Cycle by 4 Cycle Log-Log

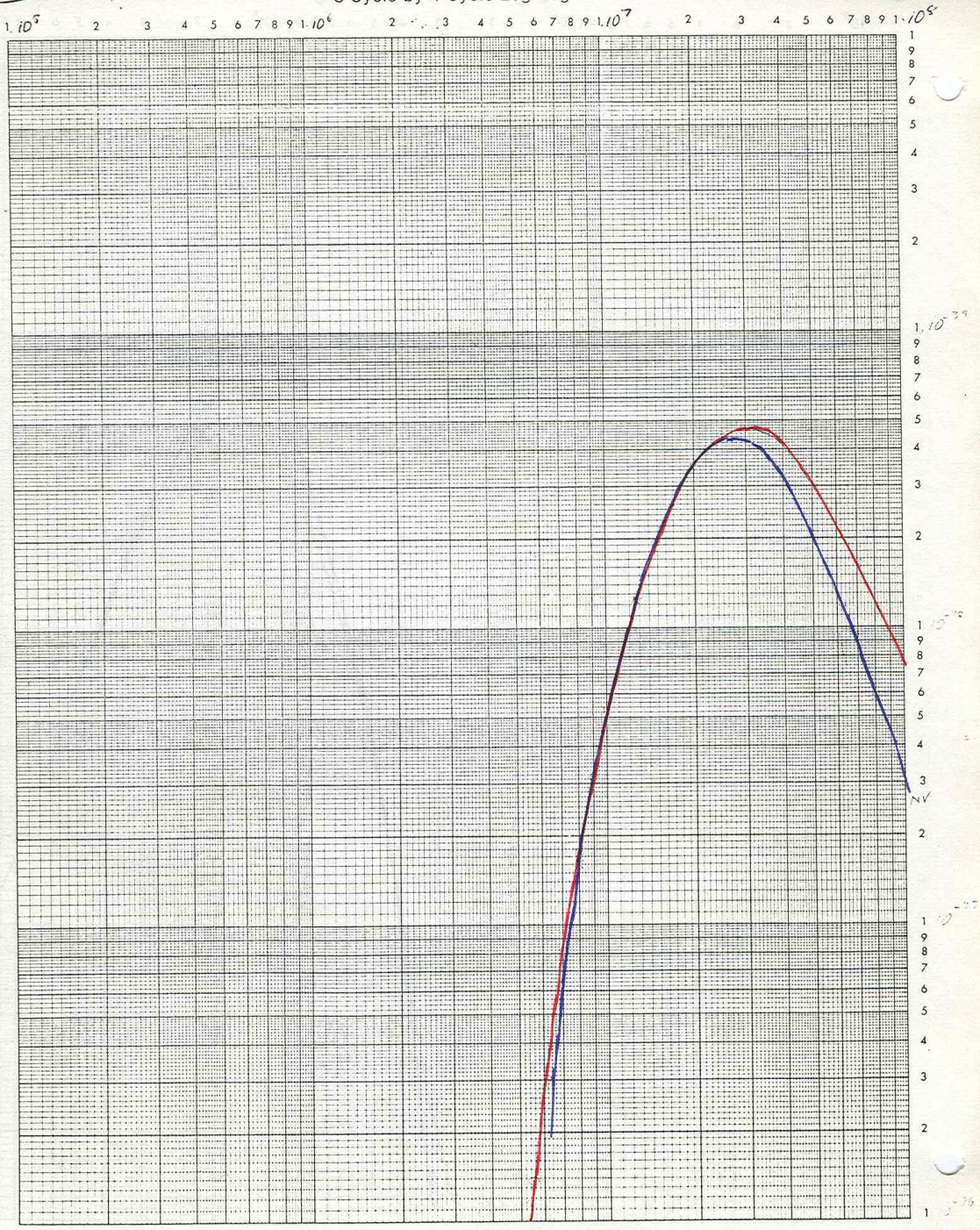

TEMPERATURE. (K)

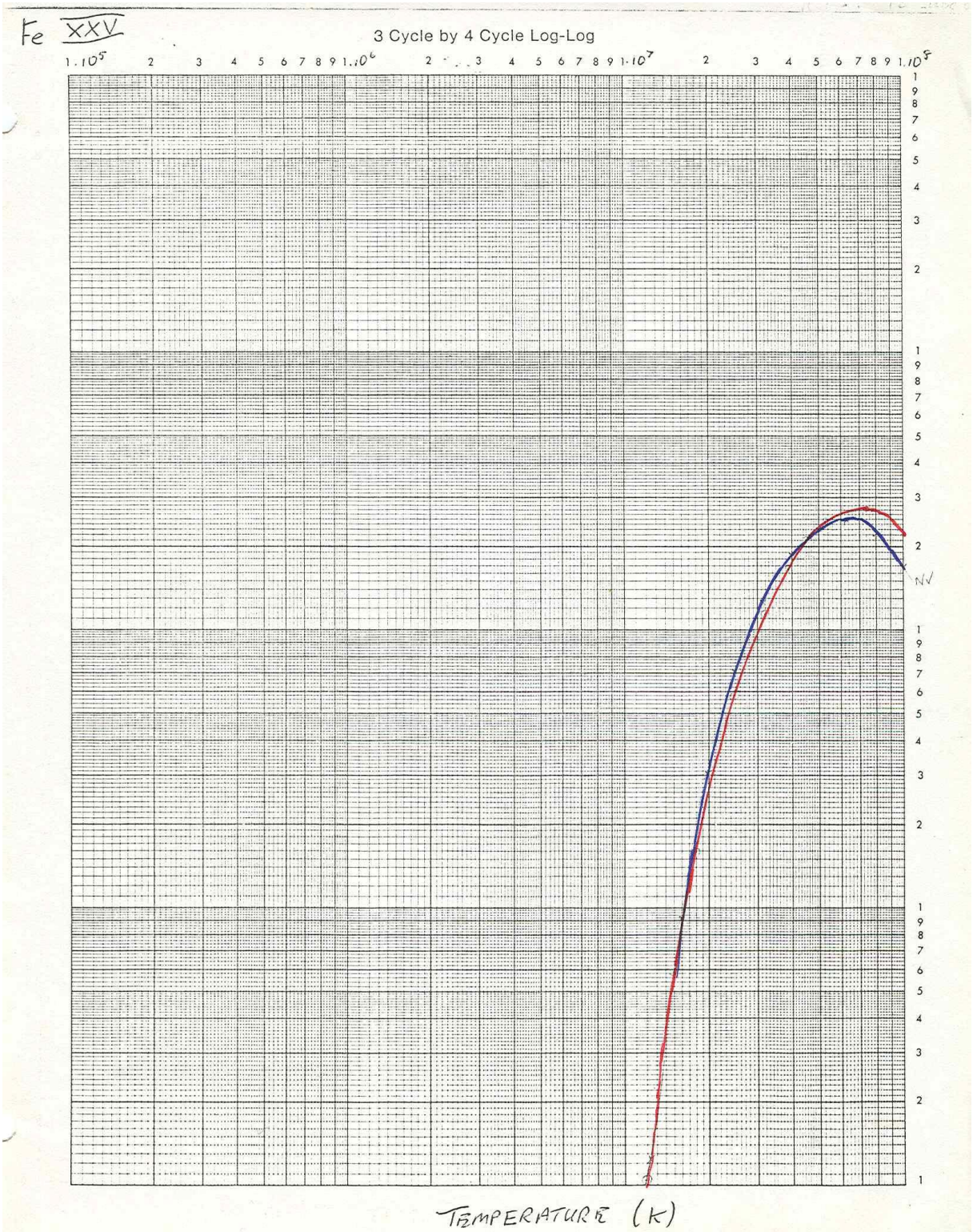
Fe XXV
3 Cycle by 4 Cycle Log-Log
1.10^5 2 3 4 5 6 7 8 9 1.10^6 2 3 4 5 6 7 8 9 1.10^7 2 3 4 5 6 7 8 9 1.10^8
1 9 8 7 6 5 4 3 2
NV
TEMPERATURE (K)

SOLAR FLARE SPECTRUM IN FCS WAVELENGTH RANGE

The diagram on the page following is a solar flare spectrum in the 6-18Å range from the OSO-5 GSFC crystal spectrometer (Neupert et al., Solar Phys. 31, 171, 1973). Identifications of principal lines shown are due to Fawcett and Hayes (M.N. 170, 185, 1975). Improved-resolution spectra in this range, comparable to the expected FCS resolution, are now available from the SOLEX instrument on the P78-1 spacecraft (McKenzie et al., Preprint, 1979).

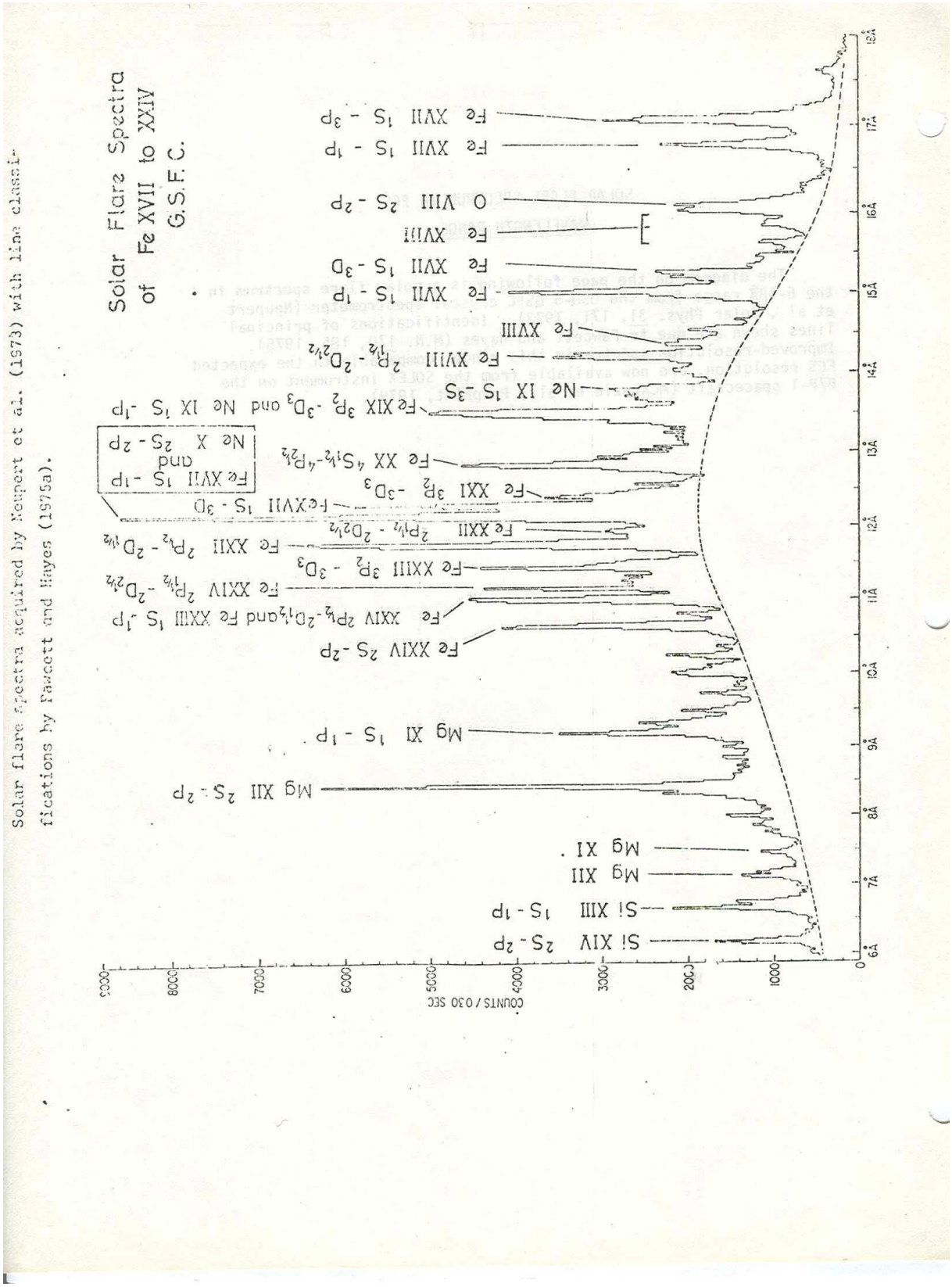

Solar flare spectra acquired by Neupert et al. (1973) with line classifications by Fawcett and Hayes (1975a).

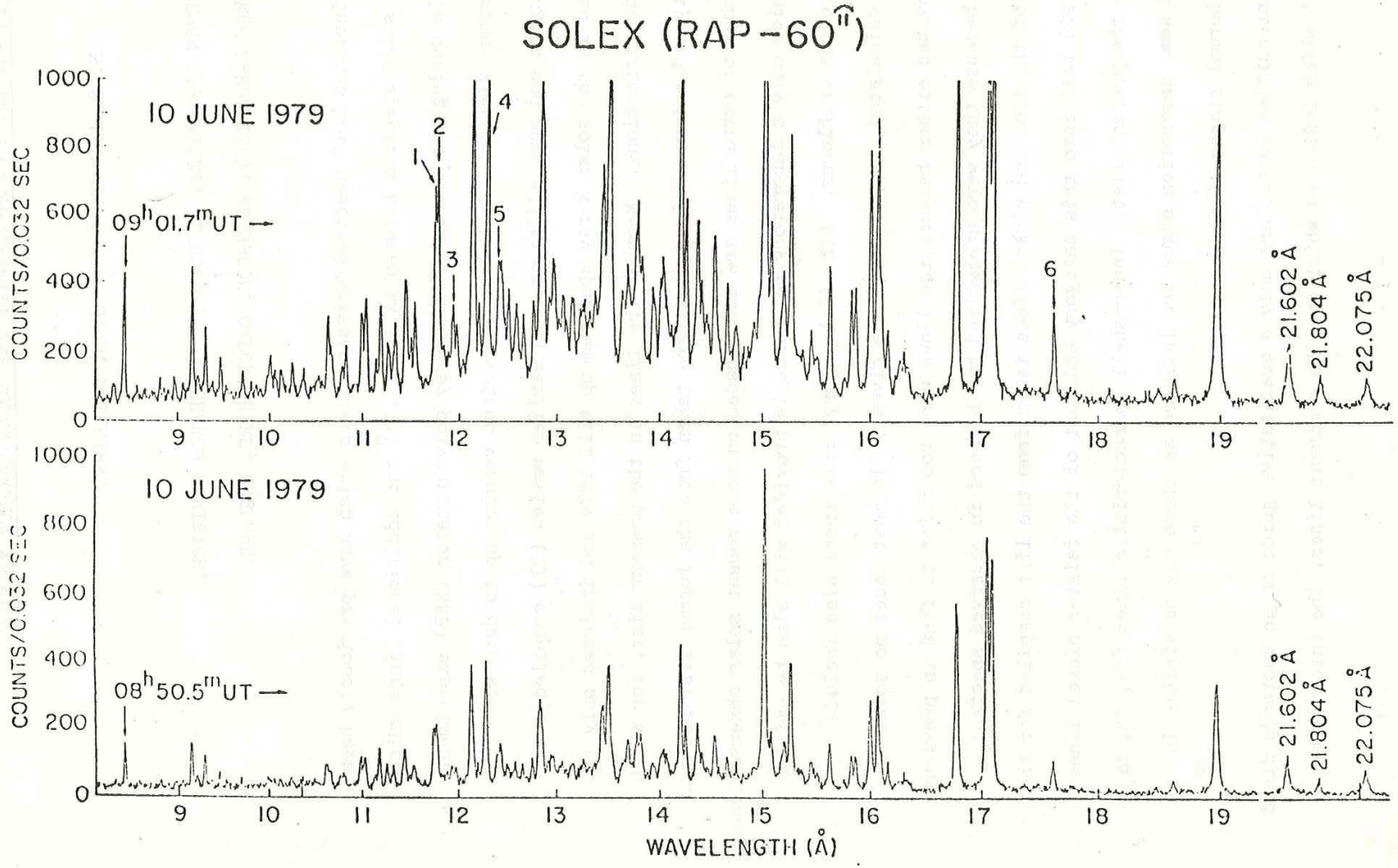
SOLEX (RAP-60")
10 JUNE 1979
09h01.7mUT
1
2
3
4
5
6
21.602 Å
21.804 Å
22.075 Å
COUNTS/0.032 SEC
10 JUNE 1979
08h50.5mUT
WAVELENGTH (Å)

WAVELENGTH LIST OF POSSIBLE SOLAR FLARE EMISSION LINES BETWEEN 1Å AND 22.11Å COMPILED FOR XRP SOLAR MAXIMUM MISSION

B. C. FAWCETT AND K. J. H. PHILLIPS

APPLETON LABORATORY, ASTROPHYSICS RESEARCH DIVISION,
CULHAM LABORATORY, ABINGDON, OXFORDSHIRE, ENGLAND.

This list includes both spectral emission lines which have previously been observed in the solar spectrum between 1Å and 22.11Å and additional lines which may be observable during the course of the X-ray polychromator (XRP) experiment on the Solar Maximum Mission. It brings a previous version up to date with improved wavelengths and some additions. An earlier review (21) compiled a list of lines observed in the solar X-ray spectrum up till 1974 and included only the most definite identifications. Most of the lines in the present list, for which a solar intensity and reference is quoted, are taken from the former list but a considerable number of extra lines are added based on more recent solar observations. The lines for which only a laboratory reference is provided will also be emitted from the solar corona or flares. (The 'Laboratory' references also include papers in which calculated energy levels are given.) In most cases no solar reference is provided either because the lines were too faint to find in previous spectrograms or because they were unresolved but blended in observed spectral features. Many of the iron and nickel lines taken from the list compiled for the SMM Newsletter (22) fall into this category and most of the fainter nickel lines are omitted from the present list. Inner-shell characteristic lines (Kα, Kβ, Lα transitions) and some absorption edges are included as these may be visible in the early, non-thermal stages of flares.

The solar intensities quoted are only a qualitative guide on an unstandardised scale from 1 to 9 which indicates which are the dominant lines. The intensities

WAVELENGTHS OF POSSIBLE SOLAR FLARE SPECTRAL EMISSION LINES

BETWEEN 1Å AND 22.11Å COMPILED FOR XRP SOLAR MAXIMUM MISSION

Wavelength(Å)	Ion	Term	J-J	Configuration	Laboratory Reference	Solar* Intensity	Solar Reference
22.11	O VI	^2P-^2D		$1s^2 2p$-$1s 2p^2$	26		
22.0975	O VII	^1S-^3S	0-1	$1s^2$-$1s 2s$	14, 26	(8)	25
22.02	O VI	^2S-$(^1S)^2P$		$1s^2 2s$-$1s 2s 2p$	26		
21.8035	O VII	^1S-^3P	0-1	$1s^2$-$1s 2p$	14, 31	(8)	25
21.6013	O VII	^1S-^1P	0-1	$1s^2$-$1s 2p$	14, 41	(9)	25
21.910	N VII	^2S-^2P		$1s$-$3p$	31		
19.826	N VII	^2S-^2P		$1s$-$4p$	31		
18.9725	O VIII	^2S-^2P		$1s$-$2p$	13		
18.9671	O VIII	^2S-^2P		$1s$-$2p$	13	(9)	25
18.6285	O VII	^1S-^1P	0-1	$1s^2$-$1s 3p$	14	(6)	25
17.768	O VII	^1S-^1P	0-1	$1s^2$-$1s 4p$	31	(4)	25
17.64	Fe XVI			$2p^6 n\ell$-$2p^5 n\ell mq$	23	(1)	39,44
17.59	Fe $L\alpha_{1,2}$			L(III)-M(IV, V)	50		
17.42	Fe XVI	^2S-^2P		$2p^6 3s$-$2p^5 3s^2$	23	(1)	39,44
17.396	O VII	^1S-^1P	0-1	$1s^2$-$1s 5p$	31	(1)	
17.200	O VII	^1S-^1P	0-1	$1s^2$-$1s 6p$	31	(1)	
17.11	Fe XVI					(1)	25
17.094	Fe XVII	^1S-^3P	0-2	$2p^6$-$2p^5 3s$			30
17.051	Fe XVII	^1S-^3P	0-1	$2p^6$-$2p^5 3s$		(9)	25,30
16.775	Fe XVII	^1S-^1P	0-1	$2p^6$-$2p^5 3s$		(9)	30
16.272	Fe XVIII	^2P-$(^3P)^4P$	$\frac{1}{2}$-$1\frac{1}{2}$	$2p^5$-$2p^4 3s$	10		
16.072	Fe XVIII	^2P-$(^3P)^4P$	$1\frac{1}{2}$-$2\frac{1}{2}$	$2p^5$-$2p^4 3s$	10		
16.026	Fe XVIII	^2P-$(^3P)^2P$	$\frac{1}{2}$-$\frac{1}{2}$	$2p^5$-$2p^4 3s$	10		
16.0059	O VIII	^2S-^2P		$1s$-$3p$	13	(7)	25,39,44
16.005	Fe XVIII	^2P-$(^3P)^4P$	$1\frac{1}{2}$-$1\frac{1}{2}$	$2p^5$-$2p^4 3s$	10,17	(1)	
15.870	Fe XVIII	^2P-$(^1D)^2D$	$\frac{1}{2}$-$1\frac{1}{2}$	$2p^5$-$2p^4 3s$	10,17	(1)	39,44
15.828	Fe XVIII	^2P-$(^3P)^2P$	$1\frac{1}{2}$-$1\frac{1}{2}$	$2p^5$-$2p^4 3s$	10		
15.766	Fe XVIII	^2P-$(^3P)^2P$	$1\frac{1}{2}$-$\frac{1}{2}$	$2p^5$-$2p^4 3s$	10		
15.625	Fe XVIII	^2P-$(^1D)^2D$	$1\frac{1}{2}$-$2\frac{1}{2}$	$2p^5 2p^4 3s$	10,17	(1)	25
15.491	Fe XVIII	^2P-$(^1S)^2S$	$\frac{1}{2}$-$\frac{1}{2}$	$3s$	10		
15.452	Fe XVII	^1S-^3P	0-1	$2p^6$-$2p^5 3d$		(3)	25,30
15.260	Fe XVII	^1S-^3D	0-1	$2p^6$-$2p^5 3d$		(7)	25,30
15.1762	O VIII	^1S-^2P		$1s$-$3p$	13, 31	(1)	15
15.172	Fe XIX	^3P-^3S	1-1	$2p^4$-$2p^3 3s$	10		
15.138	Fe XIX	^3P-^3S	0-1	$2p^4$-$2p^3 3s$			
15.012	Fe XVII	^1S-^1P	0-1	$2p^6$-$2p^5 3d$		(9)	25,30

quoted in brackets refer to lines which are emitted from the active corona (eg O VII, O VIII, Fe XVII, Fe XVIII) whereas the solar flare lines are not bracketed.

The user is recommended to consult not only the references to papers that include solar spectrograms and wavelength lists but also oscillator strengths and other atomic data. References (3, 4, 26 and 49) are of particular value to the study of satellite lines which occur near the He-like resonance lines.

October 1979

Wavelength(Å)	Ion	Term	J-J	Configuration	Laboratory Reference	Solar Intensity	Solar Reference
14.929	Fe XIX	$^3P-^3D$	1-1	$2p^4-2p^3 3s$			
14.8206	O VIII	$^2S-^2P$		1s-5p	13,31		
14.772	Fe XVIII	$^2P-(^3P)^4P$	$\frac{1}{2}-1\frac{1}{2}$	$2p^5-2p^4 3d$	10		
14.735	Fe XIX	$^3P-^3D$	2-2	$2p^4-2p^3 3s$	10		
14.668	Fe XIX	$^3P-^3D$	2-3	$2p^4-2p^3 3s$	10		
14.610	Ne $K\alpha_{1,2}$			K-L(II, III)	50		
14.610	Fe XVIII	$^2P-(^3P)^2P$	$\frac{1}{2}-1\frac{1}{2}$	$2p^5-2p^4 3d$	10		
14.581	Fe XVIII	$^2P-(^3P)^4P$	$\frac{1}{2}-\frac{1}{2}$	$2p^5-2p^4 3d$	10		
14.551	Fe XVIII	$^2P-(^3P)^4P$	$1\frac{1}{2}-1\frac{1}{2}$	$2p^5-2p^4 3d$	10		
14.534	Fe XVIII	$^2P-(^3P)^4F$	$1\frac{1}{2}-2\frac{1}{2}$	$2p^5-2p^4 3d$	10		
14.517	Fe XIX	$^3P-^3P$	1-2	$2p^4-2p^3 3s$	10		
14.486	Fe XVIII	$^2P-(^3P)^4P$	$1\frac{1}{2}-2\frac{1}{2}$	$2p^5-2p^4 3d$	10		
14.469	Fe XVIII	$^2P-(^1D)^2S$	$\frac{1}{2}-\frac{1}{2}$	$2p^5-2p^4 3d$	10		
14.453	Fe XVIII	$^2P-(^3P)^4D$	$1\frac{1}{2}-1\frac{1}{2}$	$2p^5-2p^4 3d$	10		
14.418	Fe XVIII	$^2P-(^1D)^2P$	$\frac{1}{2}-1\frac{1}{2}$	$2p^5-2p^4 3d$	10		
14.374	Fe XVIII	$^2P-(^3P)^2D$	$1\frac{1}{2}-2\frac{1}{2}$	$2p^5-2p^4 3d$	17	(1)	15
14.360	Fe XVIII	$^2P-(^1D)^2D$	$\frac{1}{2}-1\frac{1}{2}$	$2p^5-2p^4 3d$	10		
14.344	Fe XVIII	$^2P-(^1D)^2P$	$\frac{1}{2}-\frac{1}{2}$	$2p^5-2p^4 3d$	10		
14.256	Fe XVIII	$^2P-(^1D)^2S$	$1\frac{1}{2}-\frac{1}{2}$	$2p^5-2p^4 3d$	10,17		
14.203	Fe XVIII	$^2P-(^1D)^2D$	$1\frac{1}{2}-2\frac{1}{2}$	$2p^5-2p^4 3d$	10	(2)	15
14.152	Fe XVIII	$^2P-(^1D)^2D$	$1\frac{1}{2}-1\frac{1}{2}$	$2p^5-2p^4 3d$	10		
14.121	Fe XVIII	$^2P-(^1S)^2D$	$\frac{1}{2}-1\frac{1}{2}$	$2p^5-2p^4 3d$	10		
14.043	Ni XIX	$^1S-^3P$	0-1	$2p^5-2p^5 3s$	27,24	(3)	39,44
13.956	Fe XVIII	$^2P-(^1S)^2D$	$1\frac{1}{2}-1\frac{1}{2}$	$2p^5-2p^4 3d$	10		
13.890	Fe XVII	$^1S-^3P$	0-1	$2s^2 2p^6-2s2p^6 3p$		(2)	30,48
13.824	Fe XVII	$^1S-^1P$	0-1	$2s^2 2p^6-2s2p^6 3p$		(3)	30,38,48
13.797	Fe XIX	$^3P-(^2D)^3D$	2-3	$2p^4-2p^3 3d$	5		38
13.779	Ni XIX	$^1S-^1P$	0-1	$2p^6-2p^5 3s$	27,24	(3)	15,38
13.742	Fe XIX	$^3P-(^2D)^3D$	1-2	$2p^4-2p^3 3d$	5		
13.71	Ne VIII	$^2P-^2D$		$1s^2 2p-1s2p^2$	26		38,48
13.6987	Ne IX	$^1S-^3S$	0-1	$1s^2-1s2s$	14,26	4	38
13.671	Fe XIX	$^3P-(^2D)^3P$	1-1	$2p^4-2p^3 3d$	5		38
13.65	Ne VIII	$^2S-(^1S)^2P$		$1s^2 2s-1s2s2p$	26		38
13.563	Fe XIX	$^3P-(^2P)^3P$	1-2	$2p^4-2p^3 3d$	5		38
13.5529	Ne IX	$^1S-^3P$	0-1	$1s^2-1s2p$	14,16		15,38
13.521	Fe XIX	$^3P-(^2D)^3D$	2-3	$2p^4-2p^3 3d$	5,18	6	36,38
13.507	Fe XIX	$^3P-(^2D)^3P$	2-2	$2p^4-2p^3 3d$	5		38
13.491	Fe XIX	$^3P-(^2P)^3P$	0-1	$2p^4-2p^3 3d$	5		38

Wavelength(Å)	Ion	Term	J-J	Configuration	Laboratory Reference	Solar* Intensity	Solar Reference
11.650	Fe XXII	$^2P-^2P$	$\frac{1}{2}-\frac{1}{2}$	$2s^2 2p-2s2p3p$	9		
11.544	Ne IX	$^1S-^1P$	0-1	$1s^2-1s3p$	14,37	2	39,44
11.551	Fe XVIII			$2p^5-2p^4 4d$	8		
11.526	Fe XVIII			$2p^5-2p^4 4d$	8	(2)	30
11.459	Fe XXII	$^2P-^2D$	$1\frac{1}{2}-2\frac{1}{2}$	$2s^2 2p-2s2p3p$	9		
11.458	Fe XVIII			$2p^5-2p^4 4d$	8		
11.442	Fe XXII	$^2P-^2D$	$\frac{1}{2}-1\frac{1}{2}$	$2s^2 2p-2s2p3p$	9		
11.440	Fe XXIII	$^3P-^3D$	2-3	2s2p-2s3d	9,18	4	36
11.440	Fe XVIII			$2p^5-2p^4 4d$	8		
11.442	Fe XXIV	$^2P-^2S$	$1\frac{1}{2}-\frac{1}{2}$	2p-3s			
11.420	Fe XVIII			$2p^5-2p^4 4d$	8	(2)	30
11.333	Fe XXIII	$^3P-^3D$	1-2	2s2p-2s3d	9		
11.326	Fe XVIII			$2p^5-2p^4 4d$	8	(2)	30
11.318	Ni XXI	$^3P-(^2D)^3D$	2-3	$2p^4-2p^3 3d$	27		
11.298	Fe XXIII	$^3P-^3D$	0-1	2s2p-2s3d	9		
11.262	Fe XXIV	$^2P-^2S$	$\frac{1}{2}-\frac{1}{2}$	2p-3s	1,2,19		
11.253	Fe XVIII			$2p^5-2p^4 4d$	8	(3)	30
11.250	Fe XVII	$^1S-^3D$	0-1	$2p^6-2p^5 5d$		(4)	30
11.1915	Na X	$^1S-^3S$	0-1	$1s^2-1s2s$	14		
11.186	Fe XXIV	$^2P-^2D$	$1\frac{1}{2}-1\frac{1}{2}$	2p-3d	1,2,19		
11.174	Fe XXIV	$^2P-^2D$	$1\frac{1}{2}-2\frac{1}{2}$	2p-3d	1,2,18,19	4	36
11.129	Fe XVII	$^1S-^1P$	0-1	$2p^6-2p^5 5d$		(4)	30
11.0830	Na X	$^1S-^3P$	0-1	$1s^2-1s2p$	14,31		
11.041	Fe XVII	$^1S-^3P$	0-1	$2s^2 2p^6-2s2p^5 4p$		(4)	30
11.029	Fe XXIV	$^2P-^2D$	$\frac{1}{2}-1\frac{1}{2}$	$^2P-^2D$	1,2,18,19	5	36
11.025	Fe XVII	$^1S-^1P$	0-1	$2s^2 2p^6-2s2p^5 4p$		2	30
11.018	Fe XXIII	$^1S-^3P$	0-1	$2s^2-2s3p$	9	2	36
11.001	Ne IX	$^1S-^1P$	0-1	$1s^2-1s4p$	31		
11.0027	Na X	$^1S-^1P$	0-1	$1s^2-1s2p$	14,31		
10.979	Fe XXIII	$^1S-^1P$	0-1	$2s^2-2s3p$	9		
10.933	Fe XIX			$2p^4-2p^3 4d$	8	(1)	30
10.813	Fe XIX			$2p^4-2p^3 4d$	8	(2)	30
10.81	Ni XXII	$^4S-^4P$		$2p^3-2p^2 3d$	20		
10.770	Fe XIX			$2p^4-2p^3 4d$	8	(1)	30
10.685	Fe XIX			$2p^4-2p^3 4d$	8	(1)	30
10.662	Fe XXIV	$^2S-^2P$	$\frac{1}{2}-\frac{1}{2}$	2s-3p	1,2,18,14	3	36
10.658	Fe XIX			$2p^4-2p^3 4d$	8	(1)	30
10.644	Fe XIX			$2p^4-2p^3 4d$	8	(1)	30

Wavelength(Å)	Ion	Term	J-J	Configuration	Reference	Intensity	Reference
10.635	Fe XIX			$2p^4-2p^3 4d$	8	(1)	30
10.620	Fe XXIV	$^2S-^2P$	$\frac{1}{2}-1\frac{1}{2}$	2s-3p	1,2,18,19	3	36
10.617	Fe XIX			$2p^4-2p^3 4d$	8	(1)	30
10.580	Fe XIX			$2p^4-2p^3 4d$	8	(1)	30
10.564	Fe XIX			$2p^4-2p^3 4d$	8	(1)	30
10.46	Ni XXIII	$^3P-^3D$	2-3	$2p^2-2p3d$	20		
10.2389	Ne X	$^2S-^2P$		1s-3p	13,31	1	39,44
10.12	Ni XXIV	$^2P-^2D$	$1\frac{1}{2}-2\frac{1}{2}$	2p-3d	20		
10.110	Ni XIX	$^1S-^3D$	0-1	$2p^6-2p^5 4d$	27		
10.0286	Na XI	$^2S-^2P$	$\frac{1}{2}-\frac{1}{2}$	1s-2p	13,31		
10.0232	Na XI	$^2S-^2P$	$\frac{1}{2}-1\frac{1}{2}$	1s-2p	13,31		
9.977	Ni XIX	$^1S-^1P$	0-1	$2p^6-2p^5 4d$	27	1	12
9.97	Ni XXIV	$^2P-^2D$	$\frac{1}{2}-1\frac{1}{2}$	2p-3d	20		
9.8900	Mg $K\alpha_{1,2}$			K-L(II,III)		50	
9.740	Ni XXV	$^3P-^3D$	2-3	2s2p-2s3d	19		
9.7082	Ne X	$^2S-^2P$		1s-4p	13,31	1	12
9.522	Ni XXVI	$^2P-^2D$	$1\frac{1}{2}-2\frac{1}{2}$	2p-3d	19		
9.5122	Mg K			Abs Edge	50		
9.4807	Ne X	$^2S-^2P$		1s-5p	13,31		
9.385	Ni XXV	$^1S-^3P$	0-1	$2s^2-2s3p$	19		
9.374	Ni XXVI	$^2P-^2D$	$\frac{1}{2}-1\frac{1}{2}$	2p-3d	19		
9.344	Ni XXV	$^1S-^1P$	0-1	$2s^2-2s3p$	19		
9.321	Mg X	$^2P-^2D$	$1\frac{1}{2}-2\frac{1}{2}$	$1s^2 2p-1s2p^2$	26		
9.318	Mg X	$^2P-^2D$	$\frac{1}{2}-1\frac{1}{2}$	$1s^2 2p-1s2p^2$	26		
9.3141	Mg XI	$^1S-^3S$	0-1	$1s^2-1s2s$	14,26	7	48
9.286	Mg X	$^2S-(^1P)^2P$	$\frac{1}{2}-\frac{1}{2}$	$1s^2 2s-1s2s2p$	26		48
9.283	Mg X	$^2S-(^1P)^2P$	$\frac{1}{2}-1\frac{1}{2}$	$1s^2 2s-1s2s2p$	26	1	48
9.2310	Mg XI	$^1S-^3P$	0-1	$1s^2-1s2p$	14,26	3	48
9.193							
9.180							
9.1685	Mg XI	$^1S-^1P$	0-1	$1s^2-1s2p$	14,31	9	48
9.096	Ni XXVI	$^2S-^2P$	$\frac{1}{2}-\frac{1}{2}$	2s-3p	19		
9.051	Ni XXVI	$^2S-^2P$	$\frac{1}{2}-1\frac{1}{2}$	2s-3p	19		
8.614	Fe XXIII	$^3P-^3D$	2-3	2s2p-2s4d	9	1	12,36
8.547	Fe XXIII	$^3P-^3D$	1-2	2s2p-2s4d	9	1	36
8.528	Fe XXIII	$^3P-^3D$	0-1	2s2p-2s4d	9	1	36
8.4595	Na XI	$^2S-^2P$		1s-3p	13,31		
8.4246	Mg XII	$^2S-^2P$	$\frac{1}{2}-\frac{1}{2}$	1s-2p	13	9	45,46
8.4192	Mg XII	$^2S-^2P$	$\frac{1}{2}-1\frac{1}{2}$	1s-2p	13	9	45,46
8.316	Fe XXIII	$^1S-^3P$	0-1	$2s^2-2s4p$	19		

Wavelength(Å)	Ion	Term	J-J	Configuration	Laboratory Reference	Solar* Intensity	Solar Reference
8.303	Fe XXIII	$^1S-^1P$	0-1	$2s^2-2s4p$	9	4	
8.316	Fe XXIV	$^2P-^2D$	$1\frac{1}{2}-2\frac{1}{2}$	2p-4d	1,19		12,32
8.289	Fe XXIV	$^2P-^2S$	$1\frac{1}{2}-\frac{1}{2}$	2p-4s			
8.231	Fe XXIV	$^2P-^2D$	$\frac{1}{2}-1\frac{1}{2}$	2p-4d	1,19	2	12,32
8.17						1	12,32
8.08	Mg X			$1s^2 2p-1s2p3p$	31	1	12,32
8.061	Mg X			$1s^2 2p-1s2p3p$	31	1	12,32
7.992	Fe XXIV	$^2S-^2P$	$\frac{1}{2}-\frac{1}{2}$	2s-4p	1,19	5	12,32
7.984	Fe XXIV	$^2S-^2P$	$\frac{1}{2}-1\frac{1}{2}$	2s-4p	1,19	5	12,32
7.92	Al XI	$^2P-^2D$		$1s^2 2p-1s2p^2$	26		
7.8719	Al XII	$^1S-^3S$	0-1	$1s^2-1s2s$	14,26	2	45,46
7.86	Al XI	$^2S-(^1P)^2P$		$1s^2 2s-1s2s2p$	26		
7.850	Mg XI	$^1S-^1P$	0-1	$1s^2-1s3p$	31	4	45,46
7.8067	Al XII	$^1S-^3P$	0-1	$1s^2-1s2p$	14,26	1	45,46
7.7571	Al XII	$^1S-^1P$	0-1	$1s^2-1s2p$	14,31	3	45,46
7.474	Mg XI	$^1S-^1P$	0-1	$1s^2-1s4p$	31	2	45,46
7.438	Fe XXIV	$^2P-^2D$	$1\frac{1}{2}-2\frac{1}{2}$	2p-5d	1	1	36
7.370	Fe XXIV	$^2P-^2D$	$\frac{1}{2}-1\frac{1}{2}$	2p-5d	1	1	36
7.316	Mg XI	$^1S-^1P$	0-1	$1s^2-1s5p$	31	1	45,46
7.1763	Aℓ XIII	$^2S-^2P$	$\frac{1}{2}-\frac{1}{2}$	1s-2p	13,31		
7.1709	Al XIII	$^2S-^2P$	$\frac{1}{2}-1\frac{1}{2}$	1s-2p	13,31	1	45,46
7.169	Fe XXIV	$^2S-^2P$		2s-5p	1		
7.12791	Si $K\alpha_2$			K-L(II)	50		
7.12542	Si $K\alpha_1$			K-L(III)	50		
7.1062	Mg XII	$^2S-^2P$		1s-3p	13,31	3	45,46
6.7530	Si Kβ			K-M	50		
6.743	Si XII	$^2P-^2D$	$1\frac{1}{2}-2\frac{1}{2}$	$1s^2 2p-1s2p^2$	26		
6.7400	Si XIII	$^1S-^3S$	0-1	$1s^2-1s2s$	14,26	5	45,46
6.740	Si XII	$^2P-^2D$	$\frac{1}{2}-1\frac{1}{2}$	$1s^2 2p-1s2p^2$	26	1	45
6.738	Si K			Abs Edge	50		
6.7379	Mg XII	$^2S-^2P$		1s-4p	13		
6.719	Si XII	$^2S-^2P$	$\frac{1}{2}-1\frac{1}{2}$	$1s^2 2s-1s2s2p$	26	1	46
6.717	Si XII	$^2S-^2P$	$\frac{1}{2}-\frac{1}{2}$	$1s^2 2s-1s2s2p$	26	2	
6.6848	Si XIII	$^1S-^3P$	0-2	$1s^2-1s2p$	14,26		
6.6879	Si XIII	$^1S-^3P$	0-1	$1s^2-1s2p$	14,26	3	45,46
6.6477	Si XIII	$^1S-^1P$	0-1	$1s^2-1s2p$	26,14,26	8	45,46
6.635	Al XII	$^1S-^1P$	0-1	$1s^2-1s3p$	31		
6.5801	Mg XII	$^2S-^2P$		1s-5p	13		
6.314	Al XII	$^1S-^1P$	0-1	$1s^2-1s4p$	31		

Wavelength(Å)	Ion	Term	J-J	Configuration	Laboratory Reference	Solar* Intensity	Solar Reference
6.1858	Si XIV	^2S-^2P	$\frac{1}{2}$-$\frac{1}{2}$	ls-2p	13	5	45,46
6.1804	Si XIV	^2S-^2P	$\frac{1}{2}$-$1\frac{1}{2}$	ls-2p	13		45,46
6.0529	Al XIII	^2S-^2P		ls-3p	13,31		
5.815	Si XII	^2P-(^3P)^2D		$ls^2$2p-ls2p3p	31	1	45,46
5.7393	Al XIII	^2S-^2P		ls-4p	13,31		
5.686	Si XIII	^1S-^3P	0-1	ls^2-ls3p	1		45,46
5.678	Si XIII	^1S-^1P	0-1	ls^2-ls3p	14	6	45,46
5.402	Si XIII	^1S-^1P	0-1	ls^2-ls4p	31	1	45,46
5.37496	S $K\alpha_2$			K-L(II)	50		
5.37216	S $K\alpha_1$			K-L(III)	50		
5.283	Si XIII	^1S-^1P	0-1	ls^2-ls5p	31	2	
5.2172	Si XIV	^2S-^2P		ls-3p	13,31	1	45,46
5.103	S XIV	^2P-^2D	$1\frac{1}{2}$-$2\frac{1}{2}$	$ls^2$2p-ls2p^2	26	1	45
5.1012	S XV	^1S-^3S	0-1	ls^2-ls2s	14,26		45,46
5.100	S XIV	^2P-^2D	$\frac{1}{2}$-$1\frac{1}{2}$	$ls^2$2p-ls2p^2	26	2	46
5.087	S XIV	^2S-(^1P)^2P	$\frac{1}{2}$-$\frac{1}{2}$	$ls^2$2s-ls2s2p	26	1	46
5.085	S XIV	^2S-(^1P)^2P	$\frac{1}{2}$-$1\frac{1}{2}$	$ls^2$2s-ls2s2p	26	1	46
5.0629	S XV	^1S-^3P	0-2	ls^2-ls2p	14,26		
5.0662	S XV	^1S-^3P	0-1	ls^2-ls2p	14,26	1	45,46
5.0385	S XV	^1S-^1P	0-1	ls^2-ls2p	14,26	3	45,46
5.0185	S K			Abs Edge	50		
4.9469	Si XIV	^2S-^2P		ls-4p	13,31		
4.8311	Si XIV	^2S-^2P		ls-5p	13,31		
4.7328	S XVI	^2S-^2P	$\frac{1}{2}$-$\frac{1}{2}$	ls-2p	13	6	45,46
4.7274	S XVI	^2S-^2P	$\frac{1}{2}$-$1\frac{1}{2}$	ls-2p	13		45,46
4.299	S XV	^1S-^1P	0-1	ls^2-ls3p	31	1	45,46
4.19474	Ar $K\alpha_2$			K-L(II)		50	
4.19180	Ar $K\alpha_1$			K-L(III)		50	
4.104	S XV	^1S-^1P	0-1	ls^2-ls4p	31		
3.995	Ar XVI	^2P-^2D	$1\frac{1}{2}$-$2\frac{1}{2}$	$ls^2$2p-ls2p^2	26		
3.9939	Ar XVII	^1S-^3S	0-1	ls^2-ls2s	14,26,37	5	12,32,34
3.991	Ar XVI	^2P-^2D	$\frac{1}{2}$-$1\frac{1}{2}$	$ls^2$2p-ls2p^2	26		
3.9912	S XVI	^2S-^2P		ls-3p	13,31		
3.983	Ar XVI	^2S-(^1P)^2P	$\frac{1}{2}$-$\frac{1}{2}$	$ls^2$2s-ls2s2p	26		
3.981	Ar XVI	^2S-(^1P)^2P	$\frac{1}{2}$-$1\frac{1}{2}$	$2s^2$2s-ls2s2p	26		
3.9691	Ar XVII	^1S-^3P	0-1	ls^2-ls2p	14,26,37	2	34
3.9488	Ar XVII	^1S-^1P	0-1	ls^2-ls2p	14,26,37	6	12,32,34

Wavelength(Å)	Ion	Term	J-J	Configuration	Laboratory Reference	Solar Intensity	Solar Reference
3.7845	S XVI	^2S-^2P		1s-4p	13		
3.7365	Ar XVIII	^2S-^2P	$\frac{1}{2}$-1$\frac{1}{2}$	1s-2p	31,13	5	12,32,34
3.7311	Ar XVIII	^2S-^2P	$\frac{1}{2}$-$\frac{1}{2}$	1s-2p	31,13		
3.5705	K XVIII	^1S-^3S	0-1	$1s^2$-1s2s	14,26	2	12,32,34
3.5493	K XVIII	^1S-^3P	0-1	$1s^2$-1s2p	14,26	1	12,32,34
3.5316	K XVIII	^1S-^1P	0-1	$1s^2$-1s2p	14,26	3	12,32,34
3.3654	Ar XVII	^1S-^1P	0-1	$1s^2$-1s3p	37,14	1	12,32,34
3.36166	Ca $K\alpha_2$			K-L(II)		50	
3.35839	Ca $K\alpha_1$			K-L(III)		50	
3.3485	K XIX	^2S-^2P		1s-2p	31,13		
3.2108	Ca XIX	^1S-^3S	0-1	$1s^2$-1s2s	14,26	5	12,32,34
3.211	Ca XVIII	^2P-^2D	1$\frac{1}{2}$-2$\frac{1}{2}$	$1s^2$2p-1s$2p^2$	26		
3.208	Ca XVIII	^2P-^2D	$\frac{1}{2}$-1$\frac{1}{2}$	$1s^2$2p-1s$2p^2$	26		
3.203	Ca XVIII	^2S-(^1P)^2P	$\frac{1}{2}$-$\frac{1}{2}$	$1s^2$2s-1s2s2p	26		
3.1996	Ar XVII	^1S-^1P	0-1	$1s^2$-1s4p	31,14		
3.201	Ca XVIII	^2S-(^1P)^2P	$\frac{1}{2}$-1$\frac{1}{2}$	$1s^2$2s-1s2s2p	26		
3.1925	Ca XIX	^1S-^3P	0-1	$1s^2$-1s2p	14,26	4	12,32
3.1889	Ca XIX	^1S-^3P	0-2	$1s^2$-1s2p	14,26		
3.1769	Ca XIX	^1S-^1P	0-1	$1s^2$-1s2p	11,14,26	7	12,32,34
3.1506	Ar XVIII	^2S-^2P		1s-3p	31,13		
3.0897	Ca $K\beta_{1,3}$			K-M(II,III)	50		
3.0746	Ca $K\beta_5$			K-M(IV, V)	50		
3.0703	Ca K			Abs Edge	50		
3.0239	Ca XX	^2S-^2P	$\frac{1}{2}$-$\frac{1}{2}$	1s-2p	31,14	3	12,32,34
3.0185	Ca XX	^2S-^2P	$\frac{1}{2}$-1$\frac{1}{2}$	1s-2p	14		
2.9875	Ar XVIII	^2S-^2P		1s-4p	13		
2.706	Ca XIX	^1S-^1P	0-1	$1s^2$-1s3p	31	1	12,32,34
2.573	Ca XIX	^1S-^1P	0-1	$1s^2$-1s4p	31		
2.5494	Ca XX	^2S-^2P		1s-3p	13,31		
2.4174	Ca XX	^2S-^2P		1s-4p	13		
2.3609	Ca XX	^2S-^2P		1s-5p	13		
2.1817	Cr XXIII	^1S-^1P	0-1	$1s^2$-1s2p	11,14	1	12,32,34
2.0059	Mn XXIV	^1S-^1P	0-1	$1s^2$-1s2p	11,14	1	12,32,34
1.939980	Fe $K\alpha_2$			K-L(II)	40,50		
1.936042	Fe $K\alpha_1$			K-L(III)	40,50		
1.8680	Fe XXV	^1S-^3S	0-1	$1s^2$-1s2s	14,26,40	3	28,29,43
1.8657	Fe XXIV	^2P-^2D	1$\frac{1}{2}$-2$\frac{1}{2}$	$1s^2$2p-1s$2p^2$	26,40	4	28,29,43
1.8635	Fe XXIV	^2S-(^1P)^2P	$\frac{1}{2}$-$\frac{1}{2}$	$1s^2$2p-1s2s2p	26,40		28,29,43
1.8631	Fe XXIV	^2P-^2D	$\frac{1}{2}$-1$\frac{1}{2}$	$1s^2$2p-1s$2p^2$	26,40	4	28,29,43

Wavelength(Å)	Ion	Term	J-J	Configuration	Reference	Intensity	Reference
1.8604	Fe XXIV	$^2S-(^1P)^2P$	$\frac{1}{2}-1\frac{1}{2}$	$1s^2 2s-1s2p2s$	26,40	3	28,29,43
1.8593	Fe XXV	$^1S-^3P$	0-1	$1s^2-1s2p$	26,40		28,29,43
1.8553	Fe XXV	$^1S-^3P$	0-2	$1s^2-1s2p$	14,26,40	1	28,29,43
1.8528	Fe XXIV	$^2P-(^1P)^2D$	$1\frac{1}{2}-2\frac{1}{2}$	$1s^2 3p-1s2p3p$	3		29
1.8502	Fe XXV	$^1S-^1P$	0-1	$1s^2-1s2p$	11,14,26	9	28,29,43
1.7917	Fe XXV	$^1P-^1D$	1-2	$1s2p-2p^2$			49
1.7861	Fe XXV	$^1S-^1P$	0-1	1s2p-2s2p			49
1.7835	Fe XXVI	$^2S-^2P$	$\frac{1}{2}-\frac{1}{2}$	1s-2p	13	1	34
1.7780	Fe XXVI	$^2S-^2P$	$\frac{1}{2}-1\frac{1}{2}$	1s-2p	13	1	34
1.75661	Fe $K\beta_{1,3}$			K-M(II,III)	40,50		
1.7442	Fe $K\beta_5$			K-M(IV,V)	40,50		
1.74346	Fe K			Abs Edge	50		
1.6034	Ni XXVII	$^1S-^3S$	0-1	$1s^2-1s2s$	26,14		
1.6007	Ni XXVI	$^2P-^2D$	$1\frac{1}{2}-2\frac{1}{2}$	$1s^2 2p-1s2s^2$	26		
1.5963	Ni XXVII	$^1S-^3P$	0-1	$1s^2-1s2p$	11,14	3	34
1.5922	Ni XXVII	$^1S-^3P$	0-2	$1s^2-1s2p$	14		
1.5883	Ni XXVII	$^1S-^1P$	0-1	$1s^2-1s2p$	14		
1.5730	Fe XXV	$^1S-^1P$	0-1	$1s^2-1s3p$	14		
1.5028	Fe XXVI	$^2S-^2P$		1s-3p	13		
1.4945	Fe XXV	$^1S-^1P$	0-1	$1s^2-1s4p$	31,14		
1.4251	Fe XXVI	$^2S-^2P$		1s-4p	13		

*Solar intensities are not relative but only indicate strong or weak previously observed line. Those in brackets appear in active sun spectra.

REFERENCES

1. Boiko, V. A., Faenov, A. Ya. & Pikuz, S. A., 1978. J. quant. Spectr. rad. Trans. 19, 11.

2. Boiko, V. A., Pikuz, S. A., Safranova, U. I. & Faenov, A. Ya., 1977. J. Phys. B. Atom. Molec. Phys., 10, 1253.

3. Bely-Dubau, F., Gabriel, A. H., Volonté, S., 1979. Mon. Not. Roy. astr. Soc. 186, 405 and Gabriel, A. H., Phillips, K. J. H. (ibid) (In the Press).

4. Bhalla, C. P., Gabriel, A. H. Presnykov, L. P. 1975. Mon. Not. R. astr. Soc. 181, 107.

5. Bromage, G. E., Fawcett, B. C., 1977a. Mon. Not. R. astr. Soc. 178, 591-598.

6. Ibid 1977b, 179, 683-689.

7. Ibid 1977c. 178, 605-610.

8. Bromage, G. E., Fawcett, B. C., Cowan, R. D., 1977a, Mon. Not. R. astr. Soc. 178, 599-604.

9. Bromage, G. E., Cowan, R. D., Fawcett, B. C., Ridgeley, A. 1977b, J. Opt. Soc. Am 68, 48-51.

10. Bromage, G. E., Cowan, R. D., Fawcett, B. C., Gordon, H., Hobby, M. G., Peacock, N. J., Ridgeley, A. 1978b. Culham Laboratory Report CLM-R170, (HMSO).

11. Cohen, L., Feldman, U., Swartz, M., and Underwood, J. H. (1968b). J. Opt. Soc. Amer. 58, 843.

12. Doschek, G. A., Meekins, J. F., and Cowan, R. D. (1973b). Sol. Phys. 29, 125.

13. Erickson, G. W., 1977. J. Phys. Chem. Ref. Data 6, 831.

14. Ermolaev, A. M., Jones, M. 1973. J. Phys. B. 6, 1.

15. Evans, K., and Pounds, K. A. (1968). Astrophysics J. 152, 319.

16. Fawcett, B. C., Gabriel, A. H., Jones, B. B., and Peacock, N. J. (1964). Proc. Phys. Soc., London 84, 257 (C1).

17. Fawcett, B. C. Gabriel, A. H., and Saunders, P. A. H. (1967a). Proc. Phys. Soc., London 90, 863, (C1).

18. Fawcett, B. C., Cowan, R. D., and Hayes, R. W. (1974a). Astrophys. J. 187, 377.

19. Fawcett, B. C., Ridgeley, A., Hughes, T. P., 1979. Mon. Not. Roy. astr. Soc. (In the Press.)

20. Fawcett, B. C., Hayes, R. W. 1975. Mon. Not. R. astr. Soc. 170. 185-197.

21. Fawcett, B. C., 1974. Advances in Atomic and Molecular Physics 10, 223-293.

22. Fawcett, B. C., 1979. SMM Newsletter, No.5.

23. Feldman, U., and Cohen, L. (1968). Astrophys. J. 151, L.55 (C1) and JOSA 1967, 57, 1128.

24. Feldman, U., Cohen, L., and Swartz, M. (1976b). Astrophys. J. 148, 585 (C1).

25. Freeman, F. F., and Jones, B. B. (1970). Sol. Phys. 15, 288.

26. Gabriel, A. H. (1972). Mon. Notic. Roy. astr. Soc. 160, 90: (See also Ref's. 3 and 4).

27. Gordon, H., Hobby, M. G., Peacock, N. J. (1978). J. Phys. B. (To be Submitted).

28. Grineva, Yu. I., Karev, V. I., Korneev, V. V., Krutov, V. V., Mandelshtam, S. L., Vainshtein, L. A., Vasiljev, B. N. and Zitnik, I. A. (1971). COSPAR Conf. Proc., 14th 1972, p. 1553.

29. Grineva, Y. I., Karev, V. I., Korneev, V. V., Krutov, V. V., Mandelshtam, S. L., Vainshtein, L. A., Vasiljev, B.N., and Zitnik, I. A. (1973). Sol. Phys. 29, 441.

30. Hutcheon, R. J., Pye, J. P., Evans, K. D. (1976). Astron. Astrophys. 51, 451-450 and (1976) Mon. Not. Roy. Soc. 175, 489.

31. Kelly, R. L., Palumbo, L. J. (1973). NRL. Rep. No. 7599. US. Govt. Printing Office, Washington, D.C.

32. Meekins, J. F., Doschek, G. A., Friedman, H., Chubb, T. A., and Kreplin, R. W. (1970). Sol. Phys. 13, 198.

33. Mason, H. E. Doschek, G. A., Feldman, U., Bhatia, A. K., 1978. Astronomy and Astrophysics.

34. Neupert, W. M., (1970). Proc. NATO Conf. Sol. Corona, 1971. p.237.

35. Neupert, W. M., Gates, W., Swartz, M., Young, R., 1967. Astrophys. J. Lett. 149, L79.

36. Neupert, W. M., Swartz, M., Kastner, S. O., 1973. Sol. Phys. 31, 171.

37. Peacock, N. J., Speer, R. J., and Hobby, M. G. (1969). Proc. Phys. Soc., London (At. Mol. Phys.) 2, 798 (C1).

38. Pye, J. P., Evans, K. D., Hutcheon, R. J., 1977. Mon. Not. Roy. astr. Soc. 178, 611-618.

39. Rugge, H. R., and Walker, A. B. C. (1968). Space Res. 8, 439.

40. Schwob, J. L. and Fraenkel, B. S. (1972). Phys. Lett. A 40, 83.

41. Svensson, L. A. 1970: Physica Scripta, 1, 246.

42. Traebert, E., Fawcett, B. C., 1979. J. Phys. B. (In the Press).

43. Vasilyev, B. N., Grineva, Yu. I., Zhitnik, I. A., Karev, V. I., Koneev, V. V., Krutov, V. V., and Mandelshtam, S. L. (1972). "Short Communications in Physics," Vol. 3, p.29. Lebedev Institute, Academy of Sciences, U.S.S.R.

44. Walker, A. B. C., and Rugge, H. R. (1969). "Solar Flares and Space Research", Vol. 3. p.29. Lebedev Institute, Academy of Sciences, U.S.S.R.

45. Walker, A. B. C., and Rugge, H. R. (1970). Astron. Astrophys. 5, 4.

46. Walker, A. B. C., and Rugge, H. R. (1971). Astrophys. J. 164, 181.

47. Widing, K. G., Sandlin, G. D., and Cowan, R. D. (1971). Astrophys. J. 169, 405 (C1).

48. Parkinson, J. H. (1972). Nature, Phys. Sci. 236, 68; 233, 38.

49. Dubau, J., Gabriel, A. H., Loulergue, M., Steenman-Clarke, L., Volonté, S. MNRAS in preparation.

50. Bearden, J.A. (1967), Rev. Mod. Phys. 39, 78.

Gabriel et. al. Notation for He-like ion satellites

Date: February 12, 1980

The following table gives the notation used in various papers by A. H. Gabriel and others for satellite lines near the He-like ion resonance line. Expanded lists are given in:

A. H. Gabriel, M.N. 160, 99(1972)

F. Bely-Dubau, A. H. Gabriel, S. Volonté, M. N. 189, 801(1979).

w		$1s^2$	$^1S_0$	- $1s2p\ ^1P_1$	He-like ion
x		$1s^2$	$^1S_0$	- $1s2p\ ^3P_2$	"
y		1s2	$^1S_0$	- $1s2p\ ^3P_1$	"
z		$1s^2$	$^1S_0$	- $1s2s\ ^3S_1$	"
j	$1s^2 2p$		$^2P_{3/2}$	- $1s2p^2\ ^2D_{5/2}$	Li-like ion
r	$1s^2 2P$		$^2S_{1/2}$	- $1s2p(^1P)2s\ ^2P_{1/2}$	"
k	$1s^2 2p$		$^2P_{1/2}$	- $1s2p^2\ ^2D_{3/2}$	"
q	$1s^2 2s$		$^2S_{1/2}$	- $1s2p(^1P)2s\ ^2P_{3/2}$	"
d13	$1s^2 3p$		$^2P_{3/2}$	- $1s2p(^1P)3p\ ^2D_{5/2}$	"

CHIEF LINES IN FCS WAVELENGTH RANGES

Date: February 12, 1980

Source: Fawcett and Phillips Line List (q.v.)

The FCS crystal ranges are displayed with home position lines aligned. Wavelengths at the sides indicate the minimum and maximum wavelengths in the 'normal' range.

LINES IN BCS WAVELENGTH RANGES

Date: February 12, 1980

Source: XRP 'Solar Physics' paper

Solar and laboratory Fe lines are indicated for BCS channels 2-8. They are based on the following references:

Schwob and Fraenkel, Space Sci. Rev. 13, 589
Grineva et. al., Solar Phys. 29, 441
plus theoretical papers referred to by Gabriel (M. N. 160, 99). Better wavelengths for FeXXV lines, the FeXXIV satellites and $K\alpha$ transitions now exist (see Fawcett and Phillips line list).

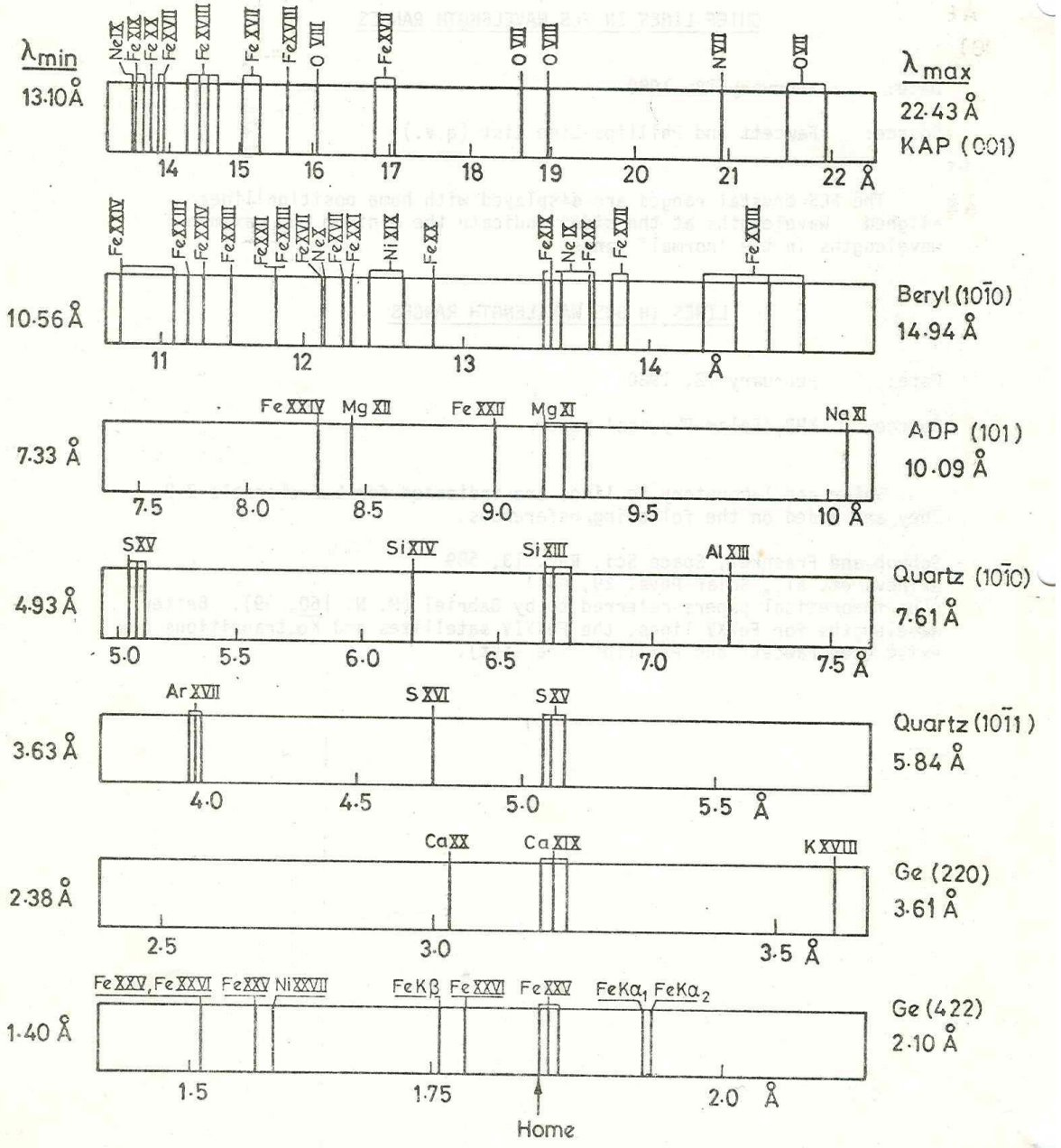
λmin
13.10Å
λmax
22.43 Å
KAP (001)
Beryl (10$\bar{1}$0)
14.94 Å
10.56 Å
ADP (101)
10.09 Å
7.33 Å
Quartz (10$\bar{1}$0)
7.61 Å
4.93 Å
Quartz (10$\bar{1}$1)
5.84 Å
3.63 Å
Ge (220)
3.61 Å
2.38 Å
Ge (422)
2.10 Å
1.40 Å
Home

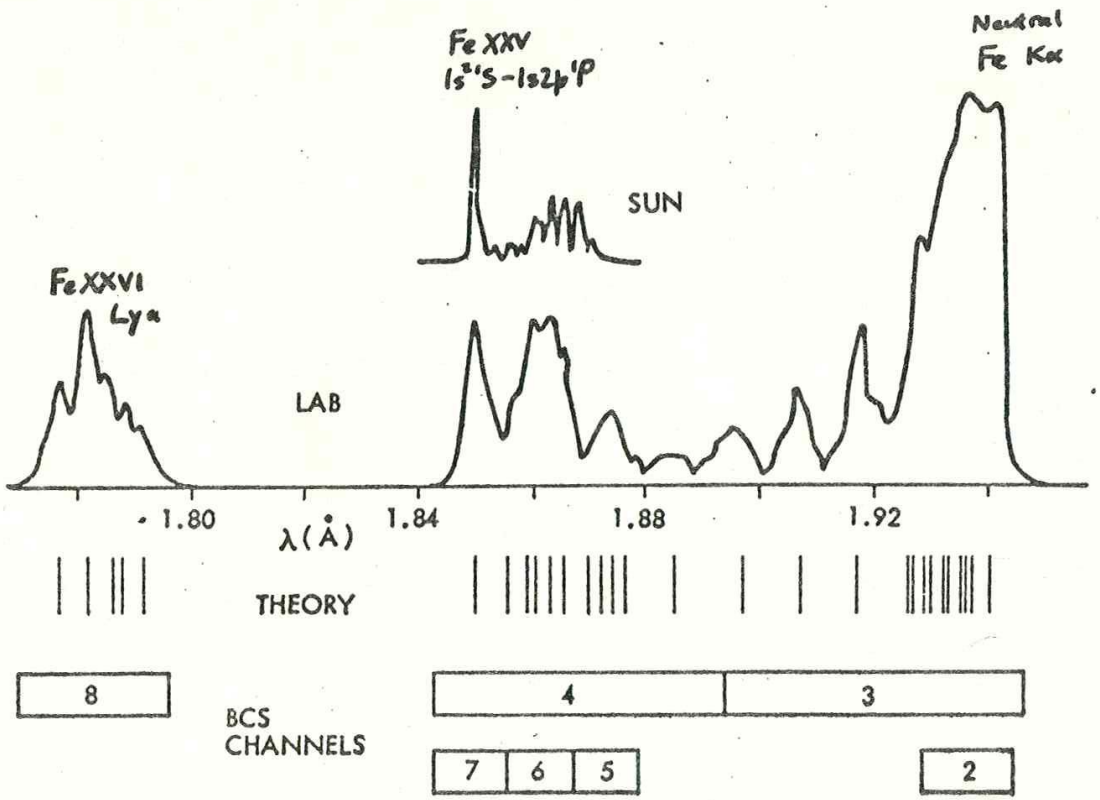
Fe XXV
$1s^2\,{}^1S - 1s2p\,{}^1P$
Neutral
Fe Kα
SUN
Fe XXVI
Lyα
LAB
1.80
1.84
1.88
1.92
λ(Å)
THEORY
8
4
3
BCS
CHANNELS
7
6
5
2